THE EFFECT OF ARCHITECTURE AND MOLECULAR WEIGHT ON CELL UPTAKE AND INTRACELLULAR DISTRIBUTION OF POLY(ETHYLENE GLYCOL)

A Thesis Submitted to
the Graduate School of Engineering and Sciences of
İzmir Institute of Technology
in Partial Fulfillment of the Requirements for the Degree of

MASTER OF SCIENCE

in Biotechnology

by
İmran ÖZER

January 2014
İZMİR

We approve the thesis of **İmran ÖZER**

Examining Committee Members:

_____

Prof. Dr. Volga BULMUŞ
Department of Chemical Engineering
İzmir Institute of Technology

_____

Prof. Dr. Sacide ALSOY ALTINKAYA
Department of Chemical Engineering
İzmir Institute of Technology

_____

Assoc. Prof. Dr. Devrim PESEN OKVUR
Department of Molecular Biology and Genetics
İzmir Institute of Technology

6 January 2014

_____

Prof. Dr. Volga BULMUŞ
Supervisor, Department of Chemical Engineering
İzmir Institute of Technology

_____

Assoc. Prof. Dr. Yusuf BARAN
Co-Supervisor, Department of Molecular Biology and Genetics
İzmir Institute of Technology

_____

Prof. Dr. Volga BULMUŞ
Head of the Department of Biotechnology and Bioengineering

_____

Prof. Dr. R. Tuğrul SENGER
Dean of the Graduate School of Engineering and Sciences

ACKNOWLEDGMENTS

Firstly, I would like to express my deep and sincere gratitude to my supervisor Prof. Dr. Volga BULMUŞ for her supervision, encouragements and guide throughout my M.Sc. study.

I also would like to express special thanks to my co-supervisor Assoc. Prof. Dr. Yusuf BARAN and Assist. Prof. Dr. Hadi ZAREİE for his academic support.

I would like to thank The Scientific and Technological Research Council of Turkey (TÜBİTAK/BIDEB/2210) to fund me throughout my M.Sc. study.

I am grateful to Dr. Gizem AYNA DURAN for her kind help and friendship throughout the intracellular distribution experiments. I am thankful to Fırat ZİYANAK and Murat TOPUZOĞULLARI for their help throughout the NMR and GPC experiments. I would like to extend my thanks to staff of Biotechnology and Bioengineering Research and Application Center; specialist Özgür OKUR for her helps and supports throughout the flow cytometry analyses.

I warmly express my special thanks to my co-workers, Esra AYDINLIOĞLU, Damla TAYKOZ, Ekrem ÖZER, Vildan GÜVEN and Deniz UĞUR for their help, support and friendships. Grateful thanks go to Mehmet Özgün ÖZEN, for his logical scientific approaches, endless care and kind love.

Finally, I would like to express special thanks to my family. I am grateful for their endless love, support and patience of my father Mecit ÖZER, my sister Kevser ÖZER and my mother Muzaffer ÖZER to whom I dedicate this thesis for their never ending love, support and encouragements during my all life.

ABSTRACT

THE EFFECT OF ARCHITECTURE AND MOLECULAR WEIGHT ON CELL UPTAKE AND INTRACELLULAR DISTRIBUTION OF POLY(ETHYLENE GLYCOL)

The aim of this thesis was to investigate interactions of comb-type poly(polyethylene glycol) methyl ether methacrylate (p(PEG-MA)) with *in vitro* cultured cells and compare to linear PEG counterparts.

For this purpose, p(PEG-MA) polymers were at different molecular weights (10,000 g/mol (10K) and 20,000 g/mol (20K)) were synthesized via reversible addition fragmentation chain transfer (RAFT) polymerization. Characterizations of polymers were performed via NMR, GPC and DLS.

The effects of polymers on *in vitro* cultured cells were investigated using cancerogenic A549 and healthy BEAS-2B human lung cell lines. Cytotoxicity of polymers was investigated via MTT assay. Comb-type p(PEG-MA) and linear PEG decreased the cell viability in a dose-dependent manner. However, the lowest cell viability was above 50% indicating no significant cytotoxic effect of both types of polymers. LDH assay was performed to determine the effect of polymers on cell membrane integrity. Both polymers enhanced membrane permeability in a dose-dependent manner. The highest LDH release was less than 2% indicating no significant effect on cell membrane integrity.

Cellular uptake of both types of polymers completely diminished at $4^{o}C$ suggesting energy-dependent internalization mechanism of polymers. Comb-type polymers were found to be taken up more by A549 cells. Comb-type polymers were internalized by A549 cells mainly via actin-dependent pathway, while BEAS-2B cells took up the all polymers via microtubule-dependent pathway. Linear 20K PEG was internalized by A549 cells via dominantly actin and also microtubule-dependent pathways while linear 10K PEG was taken up via actin-dependent pathway. Both comb-type and linear polymers were found to be localized in endocytic vesicles and cytosol.

Consequently, comb-type PEG may offer an alternative to linear PEG with better cellular uptake properties and possess different uptake mechanisms in normal and cancer cells that may provide a potential for selective targeting strategies.

ÖZET

POLİETİLEN GLİKOL'ÜN MİMARİSİ VE MOLEKÜL AĞIRLIĞININ HÜCRE ALIMINA VE HÜCRE İÇİ DAĞILIMINA ETKİSİ

Bu tezin amacı, farklı molekül ağırlığındaki tarak-tipi polietilen glikol metil eter metakrilat (p(PEG-MA)) polimerlerinin *in vitro* ortamda hayvan hücreleri ile etkileşimlerinin belirlenmesi ve lineer eşlenikleri ile karşılaştırılmasıdır.

Bu amaçla, farklı moleküler ağırlıklardaki tarak-tipi p(PEG-MA) (10,000 g/mol (10K) and 20,000 g/mol (20K)) polimerleri, tersinir katılma ayrışma zincir transfer (RAFT) polimerizasyonu ile sentezlendi ve karakterizasyonları NMR, GPC ve DLS yöntemleri ile gerçekleştirildi.

Polimerlerin *in vitro* ortamdaki özellikleri kanserojenik A549 ve sağlıklı BEAS-2B insan akciğer hücreleri kullanılarak gerçekleştirildi. Polimerlerin sitotoksisitesi MTT metodu ile belirlendi ve hem tarak hem de lineer PEG polimerlerinin doza bağımlı olarak canlılığı düşürdüğü tespit edildi. Buna karşılık, en düşük hücre canlılığı % 50'nin üzerinde belirlendiğinden, polimerlerin sitotoksik özellik taşımadığı sonucuna varıldı. Polimerlerin hücre membran bütünselliğine olan etkisi LDH ölçüm metodu ile belirlendi. LDH salımının doza bağımlı olarak arttığı fakat en yüksek LDH salımının %2'den daha az olması sebebiyle, polimerlerin hücre membran bütünlüğüne bir etkisinin olmadığı sonucuna varıldı.

4^{o}C'de hücre içi alım gerçekleşmediği tespit edildikten sonra polimerlerin hücre içine enerjiye bağımlı yöntemler ile alındığı sonucuna varıldı. Tarak-tipi polimerlerin A549 hücreleri tarafından lineer polimerlere göre daha fazla alındığı ve alımda aktin-bağımlı yolağın aktif olduğu belirlendi. Lineer 10K PEG aktin-bağımlı yolak ile alınırken, lineer 20K polimerin hücreye alımında ek olarak miktobül-bağımlı yolağında aktifleştiği sonucuna varıldı. Buna karşılık tarak-tip ve lineer polimerlerin tamamının BEAS-2B hücreleri tarafından mikrotübül-bağımlı yolak ile hücre içine alındığı tespit edildi. Lineer ve tarak-tip PEG polimerlerinin endositoz-ilişkili veziküllerde ve sitozolde lokalize olduğu belirlendi.

Sonuç olarak, tarak-tipi PEG polimerlerinin lineer PEG'e göre daha iyi hücre içi alım profiline sahip olduğu ve normal-kanserli hücreler arasında seçici hedeflemeyi sağlayabilecek farklı metotlar ile hücre içi alımının gerçekleştirildiği tespit edildi.

TABLE OF CONTENTS

LIST OF FIGURES viii

LIST OF TABLES xi

CHAPTER 1. INTRODUCTION 1

CHAPTER 2. LITERATURE REVIEW 3

2.1 Effects of PEGylation on Pharmacokinetic and Pharmacodynamic Properties 5

2.1.1 Advantages of PEGylation 5

2.1.2 Limitations of PEGylation 10

2.2 Types of PEG Architectures 12

2.2.1 Comb-Type PEG Conjugates 15

CHAPTER 3. MATERIALS AND METHODS 19

3.1 Materials 19

3.2 Methods 20

3.2.1 Synthesis of Poly(Polyethylene glycol) Methyl Ether Methacrylate p(PEG-MA) 20

3.2.2 Physicochemical Characterization of Polymers 21

3.2.2.1 Nuclear Magnetic Resonance (NMR) Analysis 21

3.2.2.2 Gel Permeation Chromatography (GPC) Analysis 21

3.2.2.3 Dynamic Light Scattering (DLS) Analysis 22

3.2.3 End Group Modifications 23

3.2.3.1 Removal of RAFT End-Group and Deactivation of Thiol End-Group 23

3.2.3.3 Fluorescent Dye Labelling 24

3.2.4 Cell Culture Experiments 25

3.2.4.1 Determining the Effect of Polymers on Cell Viability via MTT Assay 25

3.2.4.2 Determining Membrane Integrity via Lactate Dehydrogenase (LDH) Assay 26

3.2.4.3 Cell Uptake of Polymers 27
3.2.4.4 Intracellular Distribution of Polymers 28

CHAPTER 4. RESULTS AND DISCUSSION 30
4.1 Synthesis of Poly(Polyethylene Glycol) Methyl Ether Methacrylate (p(PEG-MA)) 30
4.2 Characterization of Poly(Polyethylene Glycol) Methyl Ether Methacrylate (p(PEG-MA)) 30
4.2.1 Chemical Structure and Molecular Weight Characterization 30
4.2.2 Hydrodynamic Size of Polymers 33
4.3 End Group Modifications 34
4.3.1 Removal of RAFT End-Group of Comb-Type Polymers and Deactivation of Thiol End-Group 34
4.3.2 Fluorescent Dye Labelling 37
4.3 Effect of Polymers on Cell Viability 38
4.4. Effect of Polymers on Membrane Integrity 42
4.5. Cell Uptake of Polymers 44
4.5.1 Energy Dependence of Polymer Uptake 44
4.5.2 The Effect of Polymer Concentration and Incubation Time on Cellular Uptake of Polymers 46
4.5.3 The Effect of Transport Inhibitors on Cellular Uptake of Polymers 47
4.5.3.1 Cellular Toxicity of Transport Inhibitors 48
4.5.3.2 Cell Uptake Pathway of Polymers 50
4.6. Intracellular Localization of Polymers 53

CHAPTER 5. CONCLUSION 57

REFERENCES 60

APPENDICES
APPENDIX A. POLYMER CHARACTERIZATION 67
APPENDIX B. CELL VIABILITY AND MEMBRANE INTEGRITY ANALYSES 72
APPENDIX C: CELL UPTAKE ANALYSIS 74

LIST OF FIGURES

Figure **Page**

Figure 2.1. PEG-drug conjugate…… ... 3

Figure 2.2. Advantages and drawbacks of pegylation…….. ... 6

Figure 2.3. Steric hindrance of branched and linear PEG…….…. .. 9

Figure 2.4. The enhanced permeability and retention (EPR) effect…….. . 10

Figure 2.5. Chemical structure of comb-type PEG……..... 14

Figure 2.6. Structures of tertiary amine methacrylate polymers……..... 18

Figure 3.1. Polymerization reaction scheme for synthesis of poly(polyethylene glycol) methyl ether methacrylate p(PEGMA)……21

Figure 3.2. Removal of raft end-group of comb-type polymers p(PEG-MA)via aminolysis reaction……....23

Figure 3.3. Deactivation of thiol end-group of comb-type polymers (p(PEG-MA)) by addition of OEGMA monomeric unit…… . 24

Figure 4.1. ^{1}H-NMR spectrum of purified p(PEG-MA)- (10K) synthesized using a [OEGMA]/[CPADB]/[AIBN] mol ratio of 50/1/0.25. 31

Figure 4.2. ^{1}H-NMR spectrum of purified p(PEG-MA)- (20K) synthesized using a [OEGMA]/[CPADB]/[AIBN] mol ratio of 50/1/0.25. 32

Figure 4.3. ^{1}H-NMR spectrum of RAFT end-group removed comb-type 20K p(PEG-MA) polymer after removal of the RAFT end-group. 36

Figure 4.5. The UV-Vis spectra of Oregon Green Maleimide® labeled polymers at 33 μM polymer concentration. 38

Figure 4.6. Cell number- absorbance calibration curve obtained from MTT assays of BEAS-2B and A549 cell lines. 39

Figure 4.7. The percent cell viability of A549 cell line after incubation with polymers for 24 hours. 40

Figure 4.8. The percent cell viability of A549 cell line after incubation with polymers for 72 hours. 40

Figure 4.9. The percent cell viability of BEAS-2B cell line after incubation with polymers for 24 hours. 41

Figure 4.10. The percent cell viability of BEAS-2B cell line after incubation with polymers for 72 hours. 41

Figure 4.11. The percent LDH release of A549 cells after incubation with polymers for 24 or 72 h. 42
Figure 4.12. The percent LDH release of BEAS-2B cells after incubation with polymers for 24 or 72 h. 43
Figure 4.13. Polymer uptake profile of A549 cells at 37^{o}C and 4^{o}C 45
Figure 4.14. Polymer uptake profile of BEAS-2B cells at 37^{o}C and 4^{o}C 45
Figure 4.15. Polymer uptake profile of A549 cell line at 12.5 and 25 μM for 1h and 3h 46
Figure 4.16. Polymer uptake profile of BEAS-2B cell line at 12.5 and 25 μM for 1h and 3h. 47
Figure 4.17. Viability of A549 and BEAS-2B cells after exposure to varying concentrations of nocodazole for 3 hours. 49
Figure 4.18. Viability of A549 and BEAS-2B cells after exposure to varying concentrations of cytochalasin D for 3 hours. 49
Figure 4.19. Viability of A549 and BEAS-2B cells after exposure to 20 μM nocodazole and 10 μM cytochalasin D for 3 hours. 50
Figure 4.20. Uptake of comb-type 10K PEG by A549 and BEAS-2B cells.. 51
Figure 4.21. Uptake of comb-type 20K PEG by A549 and BEAS-2B cells.. 51
Figure 4.22. Uptake of linear 10K PEG by A549 and BEAS-2B cells 52
Figure 4. 23. Uptake of linear 20K PEG by A549 and BEAS-2B cells. 53
Figure 4.24. Fluorescence micrographs of A549 cells after incubation with Oregon green labeled comb-type 10K PEG at 40X magnification a) Nucleus staining by DAPI b) Oregon green stained comb-type 10K polymers c) Merge of a and b. 53
Figure 4.25. Fluorescence micrographs of A549 cells after incubation with Oregon green labeled comb-type 20K PEG at 40X magnification a) Nucleus staining by DAPI b) Oregon green stained comb-type 10K polymers c) Merge of a and b.. 54
Figure 4.26. Fluorescence micrographs of A549 cells after incubation with Oregon green labeled linear 10K PEG at 40X magnification a) Nucleus staining by DAPI b) Oregon green stained comb-type 10K polymers c) Merge of a and b.. 54

Figure 4.27. Fluorescence micrographs of A549 cells after incubation with Oregon green labeled comb-type 10K PEG at 40X magnification a) Nucleus staining by DAPI b) Oregon green stained comb-type 10K polymers c) Merge of a and b. 54
Figure 4.28. Fluorescence micrographs of BEAS-2B cells after incubation with Oregon green labeled comb-type 10K PEG at 40X magnification a) Nucleus staining by DAPI b) Oregon green stained comb-type 10K polymers c) Merge of a and b.. 55
Figure 4.29. Fluorescence micrographs of BEAS-2B cells after incubation with Oregon green labeled comb-type 20K PEG at 40X magnification a) Nucleus staining by DAPI b) Oregon green stained comb-type 10K polymers c) Merge of a and b.. 55
Figure 4.30. Fluorescence micrographs of BEAS-2B cells after incubation with Oregon green labeled linear 10K PEG at 40X magnification a) Nucleus staining by DAPI b) Oregon green stained comb-type 10K polymers c) Merge of a and b. 55
Figure 4.31. Fluorescence micrographs of BEAS-2B cells after incubation with Oregon green labeled linear 20K PEG at 40X magnification a) Nucleus staining by DAPI b) Oregon green stained comb-type 10K polymers c) Merge of a and b.. 56

LIST OF TABLES

Table **Page**

Table 2.1. The PEGylated therapeutics that are currently on the market. 4

Table 3.1. Refractive index and viscosity values of different dispersants. 22

Table 4.1. Properties of comb-type p(PEG-MA) polymers synthesized throughout the study 32

Table 4.2. Mean number average diameter of polymers determined by Dynamic Light Scattering (DLS) (nm). 33

Table 4.3. The fluorescence labeling degree of comb-type and linear PEG polymers. 38

CHAPTER 1

INTRODUCTION

Polyethylene glycol (PEG) has an overwhelming use in biomedical applications because of its amphiphilic, water- soluble, inert, non-immunogenic and low cytotoxic nature. (Hamidi, Azadi et al. 2006; Knop, Hoogenboom et al. 2010).

In 1970s, Davis and Abuchowsky proposed PEGylation that involves modification of molecules by addition of PEG moieties. Since then, PEGylation has become one of the most widely used technologies in pharmaceutical industry not only for the modification of biomolecules but also the surface enhancement of liposomes and nanoparticles (Veronese and Pasut 2005; Hamidi, Azadi et al. 2006).

PEGylation provides improvements in terms of pharmacological and physiological properties of molecules. PEGylation is applied to prolong the blood circulation half-life of molecules, reduce the immunogenicity by masking the molecules with a hydrated polymeric cloud and alter the biodistribution profile (Duncan 2003; Hamidi, Azadi et al. 2006; Knop, Hoogenboom et al. 2010) and diminish the enzymatic degradation (Molineux 2002; Werle and Bernkop-Schnurch 2006).

Besides its advantages, there are also several limitations of PEGylation technology. PEG is a synthetic polymer and obtained by chemical synthesis. Although it is quite narrow, there is distribution in molecular weight of PEG chains. The synthetic protocols also lead to the formation of bifunctional polymer chains all these constitute major problems that lead to non-uniform conjugates of PEG (Veronese and Pasut 2005; Ryan, Mantovani et al. 2008; Bouladjine, Al-Kattan et al. 2009). PEG chains display steric hindrance effect to the molecules that they are conjugated to this effect results in masking recognition sites, causing poor cellular uptake of PEG or its conjugates (Caliceti and Veronese 2003; Kunath, Merdan et al. 2003). Non-biodegradable structure is also a limitation for PEG. Particularly, PEG with molecular weight higher than the renal filtration threshold results in the accumulation of PEG in liver (Bailon, Palleroni et al. 2001; Knop, Hoogenboom et al. 2010). Another drawback of PEGylation is loss of biological activity of biomolecule during conjugation. Alternative conjugation strategies have been developed to overcome this problem (Bailon, Palleroni et al. 2001).

The molecular architecture of polymer therapeutics affects the pharmacokinetic properties to biomolecules. Ethylene glycol based polymers can be synthesized in a variety of architectures such as linear, branched or block copolymers (Duncan 2003). Comb-type PEGs are one of the emerging architectures that consist of poly(meth)acrylate backbone and a number of linear polymer chains grafted to the backbone (Sayers, Mantovani et al. 2009). Comb-type PEGs are susceptible of hydrolyses because of ester bonds thus they can degrade biologically. This feature is very promising for drug delivery applications to prevent PEG from accumulation in liver (Sayers, Mantovani et al. 2009). Moreover, comb-type PEGs can be synthesized by controlled radical polymerization techniques (CRP) such as reversible addition fragmentation chain transfer (RAFT) that allow narrow polydispersity, predefined molecular weight and chain-end functionality.

The aim of this master thesis is to investigate *in vitro* effects of comb-type poly(polyethylene glycol) methyl ether methacrylate (p(PEG-MA)) at varying molecular weights and compare to linear PEG counterparts. For this aim, Comb-type PEGs were synthesized at 10000 g/mol and 20000 g/mol molecular weights via RAFT polymerization while linear PEGs at the same molecular weight were purchased. Nuclear Magnetic Spectroscopy (NMR), Gel Permeation Chromatography (GPC) and Dynamic Light Scattering (DLS) were used to characterize all types of polymers. Afterwards, effects of polymers on membrane integrity and cytotoxicity were determined via LDH and MTT assays using human lung adenocarcinoma epithelial cell line (A549) and its noncancerous counterpart - BEAS-2B cells, respectively. Intracellular distribution experiments were performed via fluorescence microscopy. Cellular uptake, uptake mechanisms and effects of polymers on cell cycle were determined via flow cytometry analyses. Literature review, experimental procedures and results of the study are presented in Chapter 2, 3 and 4, respectively.

CHAPTER 2

LITERATURE REVIEW

Modern approaches in drug delivery include the use of nanoparticles, liposomes and polymer therapeutics. Polymer therapeutics is a term used to describe nanometer scale, soluble or dispersible polymer-based carriers and conjugates developed for gene and drug delivery. Synthetic chemistry allows polymer therapeutics to have biomimetic and bio-responsive properties, defined three-dimensional architecture, chemical composition and tailored molecular weight. Polymer therapeutics have been approved to use in clinical conditions and polyethylene glycol (PEG) is the one of the most widely used polymer in that area (Duncan 2003; Veronese and Pasut 2005; Hamidi, Azadi et al. 2006).

PEGylation defines a process that includes modification of molecules by the linking of one or more polyethylene glycol (PEG) chains (Figure 2.1). Davis and Abuchowsky proposed PEGylation in the 1970s and this technology has gained importance over time (Veronese and Pasut 2005; Hamidi, Azadi et al. 2006).

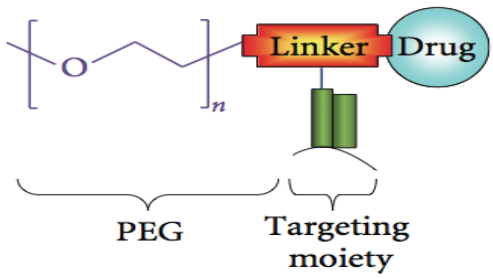

Figure 2.1.PEG-drug conjugate
(Source: Banerjee et al. 2012)

The properties that account for the overwhelming use of PEG in biomedical applications are its amphiphilic, water-soluble, inert and polar structure consisting of ethylene oxide repetitive units (Veronese 2001; Hamidi, Azadi et al. 2006; Ryan, Mantovani et al. 2008; Knop, Hoogenboom et al. 2010). These properties provide low cytotoxicity, low protein adsorption, non-immunogenicity, prolonged life span in blood circulation and altered bio-distribution profile to the conjugated or entrapped drug (Duncan 2003; Hamidi, Azadi et al. 2006; Knop, Hoogenboom et al. 2010).

The first approved PEGylated product that was polyethylene glycol (PEG)-adenosine deaminase has been on the market since March 1990 (Duncan 2003; Knop, Hoogenboom et al. 2010). The PEGylated therapeutics currently on the market are listed in the Table 2.1:

Table 2.1. The PEGylated therapeutics that are currently on the market.

Conjugate and Name	**Year of Approval**	**Type of PEGylation**	**Indication**	**Reference**
PEG-Adenosine Deaminase (Adagen®)	1990	Random, Linear PEG 11-17x5 kDa	Severe combined immunodeficiency disease (SCDI)	(Duncan 2003)
PEG-Asparaginase (Oncaspar®)	1994	Random, Linear PEG 5 kDa	Acute lymphoblastic leukemia	(Veronese and Pasut 2005)
Liposomal Doxorubicin Doxil/Caelyx	1995	Random, Linear PEG	Kaposi's sarcoma, ovarian cancer, breast cancer,	(Knop, Hoogenboom et al. 2010)
Doxorubicin HCl Liposome (Doxil/ Caelyx ®)	1999	Random, Linear PEG 2kDa	Kaposi's sarcoma, ovarian cancer, breast cancer and multiple myeloma	(Charrois and Allen 2004)
PEG-interferon-α2b (PegIntron®)	2000	Random, Linear PEG 2-20 kDa	Hepatitis C	(Knop, Hoogenboom et al. 2010)
PEG-interferon-α2a (Pegasys®)	2002	Random, Branched PEG 40 kDa	Hepatitis C	(Duncan 2003; Veronese and Pasut 2005)
PEG- HG receptor antagonist (Pegvisomant, Somavert®)	2002	Random, Linear PEG 4-6 x 5 kDa	Acromegaly	(Knop, Hoogenboom et al. 2010)
PEG-G-GCSF (Pegfilgrastim, Neulasta®)	2002	Selective, Linear PEG 20 kDa	Prevention of neutropenia during chemotherapy	(Duncan 2003; Vicent and Duncan 2006)
PEG-anti-VEGF aptamer (Pegaptanib, Macugen^{TM})	2004	Selective, Branched PEG 40 kDa	Macular degeneration (age-related)	(Veronese and Pasut 2005)

(Cont. on next page)

Table 2.1. (Cont.)

Conjugate and Name	Year of Approval	Type of PEGylation	Indication	Reference
Methoxypolyethylene glycol epoetin beta (Mircera®)	2007	Selective Linear 30 kDa	Anemia	(Curran and McCormack 2008)
Certolizumab pegol anti-TNFα (Cimzia®)	2008	Selective Linear PEG 2x40 kDa	Crohn's disease, Rheumatoid arthritis	(Schreiber, Khaliq-Kareemi e al. 2007)
Pegloticase (Krystexxa®)	2010	Selective Linear PEG 10 kDa	Refractory chronic gout	(Schlesinger, Yasotha et al. 2011)
Peginesatide (Omontys®)	2012-2013 (recalled)	Selective Branched PEG 2x20 kDa	Treatment of anemia of chronic renal failure	(Doss and Schiller 2010; Woodburn, Holmes et al. 2012)

HG: Human Growth, GCSF: Granulocyte colony stimulating factor, VEGF: Vascular endothelial growth factor, TNFα: Tumor necrosis factor

2.1 Effects of PEGylation on Pharmacokinetic and Pharmacodynamic Properties

2.1.1 Advantages of PEGylation

Attachment of polyethylene glycol (PEG) results in pharmacokinetic alterations in the therapeutic molecules that have very limited blood circulation time. The conjugation or entrapment of therapeutic molecules with polyethylene glycol (PEG) increases the molar mass, causes reduced renal clearance and results in prolonged plasma half- life, thus provides an enhanced bioavailability (Duncan 2003; Hamidi, Azadi et al. 2006; Knop, Hoogenboom et al. 2010). Several advantages of PEGylation is represented in the Figure 2.2 (Duncan 2003).

Polyethylene glycol (PEG) has the ability of shielding of conjugated or entrapped molecules by masking with hydrated polymeric cloud and thus, non- specific interactions with the cells of reticuloendothelial system (RES) are reduced and complement system is not activated. Shielding of molecules avoids rapid clearance

from the body that is known as the stealth effect (Duncan 2003; Hamidi, Azadi et al. 2006; Knop, Hoogenboom et al. 2010).

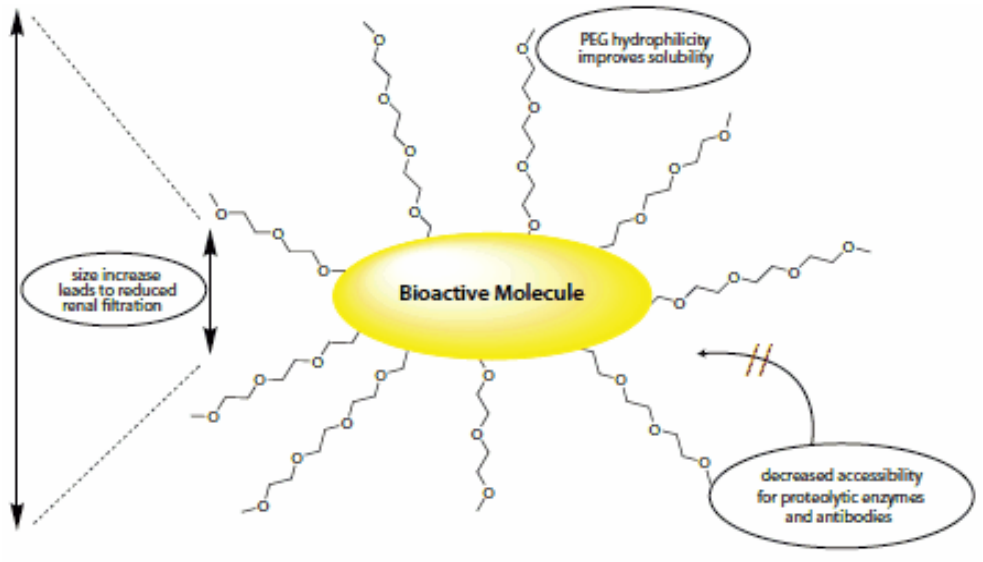

Figure 2.2. Advantages and drawbacks of PEGylation
(Source: Duncan, 2003)

Many studies indicated the enhancement in plasma half-life of drug molecules as a result of PEGylation. In general, smaller therapeutic materials are conjugated with higher molecular weight PEG (2–50 kDa) to prevent excretion by the kidneys and maintain a high blood concentration for longer periods of time while nanoparticles are coated with smaller lengths of PEG (3.4–10 kDa) because further increases in hydrodynamic radius could shorten $t_{1/2}$ (Jokerst, Lobovkina et al. 2011).

Lee et al. reported that the serum half-life of PEGylated sFv conjugates significantly increased from 2.6- fold up to 20.3- fold compared to the plasma half-life of unmodified sFv protein that is 0.7 ± 0.4 h. The researchers also revealed that PEGylated sFv conjugates, that have similar repetitive PEG numbers and molecular weight, had similar blood circulation times and the sFv molecules grafted with longer PEG chains had longer life span in bloodstream than molecules grafted with shorter PEG chains even though both conjugates have similar molecular weight (Lee, Conover et al. 1999).

Turecek et al. reported that PEGylation does not influence the homeostatic function of human recombinant FVIII (rFVIII) *in vitro* and *in vivo*. However, pharmacokinetic properties of the molecule demonstrated improvements. For instance, (rFVIII) had greater plasma half- life when conjugated with PEG. The human

recombinant FVIII (rFVIII) was measurable up to 18 hours after administration whereas PEGylated form (BAX 855) was detected in the bloodstream even 32 hours after injection. The mean residicence time of PEGylated protein also increased to 7.9 hours while rFVIII had a mean residence time of 4.9 hours. In macaques, the mean residence time was determined as 15.4 hours compared to 10.7 hours for rFVIII (Turecek, Bossard et al. 2012).

Kaul and Amiji investigated the comparative pharmacokinetic properties and biodistribution profiles of gelatin and PEGylated gelatin nanoparticles in Lewis lung carcinoma (LLC)-bearing female C57BL/6J mice. PEG conjugated gelatin nanoparticles had higher blood circulation times than native gelatin due to the steric repulsion effect of the attached PEG chains. Additionally, PEG attached gelatin nanoparticles was found 4-5% of the initial value in the tumor mass for up to 12 hours. As a result of this study, it was revealed that PEGylated gelatin nanoparticles had altered biodistribution profile and distributed in the tumor mass after systemic delivery (Kaul and Amiji 2004).

Several studies reported that increasing molecular weight of PEG moiety or number of conjugated polymer chains could decrease immunogenicity and antigenicity. It is also demonstrated that branched polymers could be more effective compared to linear polymers due to their umbrella- like structure (Caliceti and Veronese 2003). Caliceti et al. reported that attachment of 10 kDa branched PEG moiety to uricase more efficiently suppressed the immunogenicity than 5kDa linear counterpart does (Caliceti, Schiavon et al. 2001).

Stewart et al. investigated the effects of PEGylation on the cellular recognition of drug-loaded liposomes (liposomal doxorubicin) and pharmacokinetic properties as a Phase III study. The incorporation of PEG chains to the liposome triggers a hydrated shell around the liposome and provides protection from plasma proteins and lipoproteins. As a result of this, liposomes modified with PEG had decreased cellular recognition by the cells of reticuloendothelial system (RES) and increased plasma half-life compared to unmodified liposomes. Consequently, PEGylated liposomal doxorubicin was found as an effective treatment for HIV- related Kaposi's sarcoma (Stewart, Jablonowski et al. 1998).

Ozcan et al. investigated the effects of PEG attachment to poly(γ-benzyl-L-glutamate) (PBLG) nanoparticles on recognition by mononuclear phagocyte system and biodistribution profiles. As a result of the study, there was slight yellow fluorescence in

liver and spleen tissues after injection of PEG attached nanoparticles that suggested that PBLG nanoparticles were useful for avoiding capture by the mononuclear phagocyte system (MPS). Additionally, significantly altered biodistribution profiles were determined in liver and spleen. 24 hours after the IV injection to rats, there was only slight fluorescence that belonged to PEGylated nanoparticles in the liver and spleen compared to the nonPEGylated ones. As a result of this study, it was revealed that outer PEG coating provided stealth shield to PBLG nanoparticles (Ozcan, Segura-Sanchez et al. 2010).

Polyethylene glycol (PEG) molecules also provide steric hindrance (Figure 2.3) to the molecules and nanoparticles. This results in decreasing the enzymatic degradation of conjugated biomolecules. (Molineux 2002; Werle and Bernkop-Schnurch 2006). Monfardini and colleagues reported that attachment of linear or branched PEG chains reduced the degradation of asparaginase by trypsin. After 50 minutes incubation with trypsin enzyme, the residual activity of native, linear PEG conjugated and branched PEG conjugated enzymes were 5, 25 and 98 %. As a result of this study, it was revealed that attachment of branched PEG chains had an impressive influence on stability toward proteolytic enzymes than the attachment of linear PEG chains had (Monfardini, Schiavon et al. 1995).

Mori et al. investigated steric hindrance activity and pharmacokinetic effects of dioleoyl N-(monomethoxy polyethylcneglycol succinyl)phosphatidylethanolamine (PEG-PE) coated liposomes with different PEG chain lengths (750 Da, 2 kDa and 5 kDa). Blood circulation time and steric barrier activity were found to be directly proportional to the chain length of PEG. However, immunoliposomes that are conjugated with PEG_{5kDa}-PE showed reduced target binding in mice due to its extremely strong steric hindrance activity. As a result of this study, the most appropriate PEG-PE was found as PEG_{2kDa}-PE that showed high and compatible target binding to that of ganglioside GM (monosialogangliosidc) (Mori, Klibanov et al. 1991).

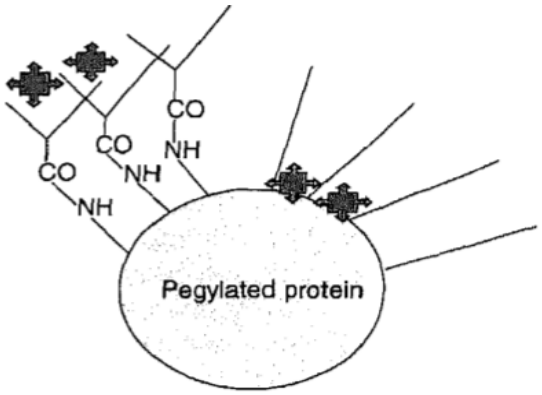

Figure 2.3. Steric hindrance of branched and linear PEG
(Source: Molineux, 2002)

PEGylation may also alter the biodistribution profile of the drug molecules because of reduced kidney excretion and this leads to significant passive targeting that is mostly seen in cancerous or inflamed tissues due to enhanced permeability and retention (EPR) effect (Caliceti and Veronese 2003; Hamidi, Azadi et al. 2006). As a result of, leaky hypervascular structure of these types of tissues and increased production of vascular permeability enhancing factors, polymers accumulate at neoplastic tissue and remain inside due to the lack of lymphatic drainage (Caliceti and Veronese 2003; Duncan 2003; Hamidi, Azadi et al. 2006; Knop, Hoogenboom et al. 2010). Enhanced permeability and retention (EPR) effect is represented in the Figure 2.4.

Tan et al. reported that significant amount of PEGylated methionininase (PEG-rMETase) accumulated in the tumor tissues of mice when intravenously administrated and tumor/blood retention ratio was determined as 1/6 in contrast to 1/10 for natural methionininase (Tan, Sun et al. 1998).

Gabizon and Martin revealed that PEGylated liposomes had less cellular uptake by the cells of reticuloendothelial system (RES) and had a reduced tendency to leak drug while in blood stream (Gabizon and Martin 1997). As an example for that, Hong et al. investigated the effects of PEG (2 kDa) attachment on the efficacy of liposomal doxorubicin and pharmacokinetic properties with C-26 syngeneic tumor model in BALB/c mice. Modified liposomes had twice longer blood circulation times and twice less tumor accumulation efficiency than that of unmodified liposomes. At a dose of 10 mg/kg, there was no difference between the PEG modified and unmodified liposomal groups. As a result of this study, it was revealed that PEGylation of liposomes has no

beneficial effects on the efficacy of liposomal doxorubicin while increased pharmacokinetic properties in the C-26 tumor model (Hong, Huang et al. 1999).

In contrast of previous study, PEG containing liposomal doxorubicin (Doxil) has improved tumor accumulation and is a commercial product in drug delivery market. Doxil has prolonged blood circulation time, higher tumor/blood ratio and improved therapeutic activity compared to free doxorubicin. Gabizon et al. investigated the pharmacokinetic effects and accumulation in tumor tissue of Doxil and compared with unmodified form clinically. Slow plasma clearance (0.1 liter/h for Doxil versus 45 liters/h for free DOX), small volume of distribution (4 liters for Doxil versus 254 liters for free DOX) and longer half-life. Tumor accumulation of the drug increased 4- to 16-fold compared to unmodified drug and urinary excretion of drug and metabolites also reduced significantly. As a result of this study, it was revealed that pharmacokinetics of doxorubicin dramatically improved and tumor accumulation that was related to longevity in circulation was enhanced (Gabizon, Catane et al. 1994).

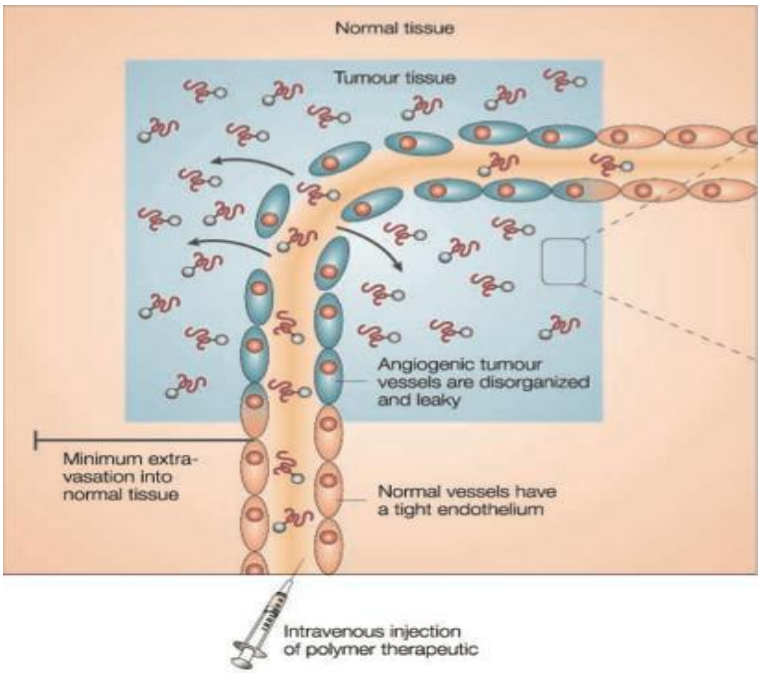

Figure 2.4. The enhanced permeability and retention (EPR) effect (Source: Duncan, 2003)

2.1.2 Limitations of PEGylation

Besides the advantages of PEG, there are several potential drawbacks including the formation of bifunctional polymer chains via chemical synthesis, poor cell

recognition- uptake, decrease in conjugate activity and non-biodegradability (Bailon, Palleroni et al. 2001; Caliceti and Veronese 2003; Veronese and Pasut 2005; Bouladjine, Al-Kattan et al. 2009; Knop, Hoogenboom et al. 2010).

PEG is a synthetic polymer and obtained by chemical synthesis. Therefore, the batch of polymer may consist of molecules having different molecular weights and results in a certain degree of (< 1.2) and this leads to a population of molecules that might have different biological properties such as half-life, renal clearance time, immunogenicity and tissue distribution (Veronese and Pasut 2005; Bouladjine, Al-Kattan et al. 2009).

Another disadvantage of PEG that arises from nature of chemical synthesis is the formation of bifunctional polymer chains. Diol ended molecules are always present at the end of the synthesis. There are generally between 1-10% depending upon molecular weight of polymer. High diol ended molecule concentration leads to undesirable cross- reactions and also non-uniform biomolecule-PEG conjugates (Veronese 2001; Ryan, Mantovani et al. 2008). Especially, polymer batches that have molecular weight above 5 kDa are composed of monofunctional and bifunctional polymer chains (Ryan, Mantovani et al. 2008).

PEGylation reduces the uptake into parenchymal cells due to steric hindrance of polymer chain and masking of recognition sites and charges (Caliceti and Veronese 2003; Kunath, Merdan et al. 2003; Eto, Gao et al. 2005; Torchilin 2007). Kunath et al. reported that conjugation of PEI (Polyethyleneimine) with a tripeptide sequence arginine-glycine-aspartic acid (RGD) without a PEG spacer resulted in improved transfection efficiency in integrin-expressing Mewo cells at low N/P ratios. However, RGD-PEG-PEI complexes showed reasonable transfection efficiency and decreased targeting due to shielding PEI and RGD ligand (Kunath, Merdan et al. 2003; Eto, Gao et al. 2005).

Zhang et al. investigated the surface modified with PEG or folic acid superparamagnetic magnetite nanoparticles in terms of cell uptake and pharmacological properties. PEG- surface modified superparamagnetic magnetite nanoparticles showed decreased cellular uptake compared to that of unmodified nanoparticles by mouse macrophage (RAW 264.7) due to steric hindrance effect of PEG moieties and folic acid modification had no effect on cellular uptake. On the contrary, PEG and folic acid surface modifications increased the cellular uptake of superparamagnetic magnetite nanoparticles by human breast cancer cells (BT20). As a result of this study, PEG

showed reduced cellular recognition by macrophages and increased cellular uptake by breast cancer cells. Therefore, it was concluded that, PEG surface modification can be used to facilitate the superparamagnetic magnetite nanoparticle uptake by specifically cancer cells for cancer therapy and diagnosis (Zhang, Kohler et al. 2002).

Molino et al. reported that PEGylation of E2 protein nanocapsules reduced cellular uptake by human monocyte derived macrophages and MDA-MB-231 breast cancer cells. In addition to this, the authors also indicated that increased chain length of PEG resulted in decreased cellular uptake by the mentioned cells (Molino, Bilotkach et al. 2012).

Decrease in the biomolecule activity compared to unconjugated molecule is also a problem in PEGylation reaction. Bailon et al. reported that PEGylation with branched 40 kDa PEG of interferon α- 2a influenced negatively receptor/ligand interactions and antiviral activity decreased to 7% of the native protein. However, antitumor activity increased and immunogenicity reduced, conversely (Bailon, Palleroni et al. 2001).

Non-biodegradable structure is one of the most prominent disadvantages of PEG due to possible cellular toxicity, renal excretion and liver accumulation. Knop et al. indicated that oligomers with a molar mass below 400 Da had toxic effects as a result of oxidation reactions into acidic metabolites while the toxicity significantly decreases with increasing molecular weights and also they may deposit in the kidney vacuoles (Bailon, Palleroni et al. 2001; Knop, Hoogenboom et al. 2010). On the other hand, higher molecular weight polymer chains that exceed renal clearance threshold may accumulate in liver and lead to macromolecular syndrome. In the determination of kidney excretion threshold, not only molecular weight, but also hydrodynamic radius of the molecule is important and PEG molecules above 20- 60 kDa molar mass and approximately 3.5 nm hydrodynamic radius reported as problematic (Veronese and Pasut 2005; Bouladjine, Al-Kattan et al. 2009; Knop, Hoogenboom et al. 2010). Branched and multi-arm PEGs are generally proposed as a solution to overcome this drawback of PEG.

2.2 Types of PEG Architectures

The most used PEG structure is linear, especially monomethoxyPEG or dihydroxyPEG (Bailon, Palleroni et al. 2001) However, with the advances in the

polymer chemistry area, novel polymeric architectures are being explored such as graft polymers and block copolymers (Duncan 2003).

Different structures of PEGs provide different pharmacokinetic properties to the systems they are attached to (Bailon, Palleroni et al. 2001; Veronese 2001). It has also revealed that the attachment of branched PEGs to a molecule can provide better shielding of the conjugate surface than the attachment of linear PEGs due to its umbrella-like shape. As a result of this, enhancement in biological half- life, reduced immunogenicity and protection against enzymes are provided to the molecules that are conjugated with branched PEGs (Monfardini, Schiavon et al. 1995; Ryan, Mantovani et al. 2008; Bays, Tao et al. 2009; Ryan, Wang et al. 2009; Sayers, Mantovani et al. 2009; Gunasekaran, Nguyen et al. 2011).

Bailon et al. reported that monoPEGylated with 40 kDa branched PEG interferon α-2a demonstrated better pharmacological properties in terms of blood circulation time and *in vivo* tumor activity. Although biological activity of the PEGylated interferon α-2a reduced to 7% of its original activity, prolonged blood circulation and exposure time resulted in compensation of reduced biological activity (Bailon, Palleroni et al. 2001).

Comb-type polymers have been recently indicated in the literature as potential alternatives to linear and branched PEGs for improving the pharmacokinetic properties of conjugates (Sayers, Mantovani et al. 2009; Gunasekaran, Nguyen et al. 2011). Comb-type PEGs consist of a polymethacrylate or polyacrylate backbone and a number of linear PEG chains that are grafted to the backbone (Figure 2.5) (Sayers, Mantovani et al. 2009). This inventory structure of comb-type PEG provides *in vivo* hydrolytic susceptibility and degradation, thus avoiding accumulation in liver and allowing usage of higher molecular weight polymers (Sayers, Mantovani et al. 2009).

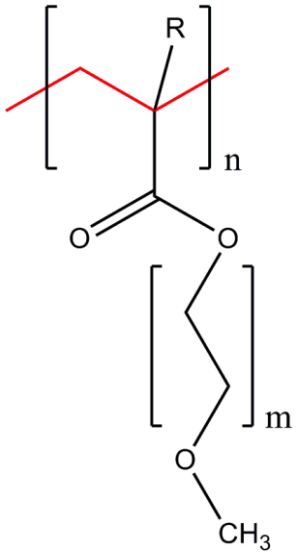

R=CH_3 or H

Figure 2.5. Chemical structure of comb-type PEG

Moreover, comb-type PEG can be synthesized by controlled radical polymerization techniques (CRP) such as ATRP (Atom Transfer Radical Polymerization), TMM-LRP (Transition Metal- Mediated Living Radical Polymerization) and RAFT (Reversible Addition Fragmentation Chain Transfer) polymerization. These methods allow tight control over the molecular weight; provide defined macromolecular architectures and end-group functionalities. (Ryan, Wang et al. 2009; Gunasekaran, Nguyen et al. 2011).

Reversible Addition Fragmentation Chain Transfer (RAFT) polymerization is an amenable technique for generating polymers to synthesize complex polymeric structures with narrow polydispersity (PDI) and varying functionalities at the chain ends for biomedical applications (Heredia, Nguyen et al. 2008; Chang, Bays et al. 2009; Pissuwan, Boyer et al. 2010). RAFT polymerization demonstrates good tolerance to a wide range of functional groups in monomers, solvents and initiators and controlled by a chain transfer agent that contains thiocarbonylthio moiety (CTA) (Moad, Rizzardo et al. 2009; Willcock and O'reilly 2010; Bulmus 2011).

2.2.1 Comb-Type PEG Conjugates

Heredia et al. demonstrated an efficient methodology to synthesize comb-type poly(polyethylene glycol methyl ether acrylate) p(PEG-A) with a defined end-group functionality via reversible addition fragmentation chain-transfer (RAFT) and conjugate it with siRNA to potentially induce similar pharmacological effects of PEG. For conjugation of siRNA with pPEG-A an efficient (88.3 ± 6.5 conjugation yield) method that enables the reversible release of siRNA from polymer chain under reductive conditions such as intracellular environment was developed. In a subsequent study, Gunasekaran et al. investigated the stability of pPEG-A-siRNA conjugates by preparing conjugates with two different molecular weights that were low molecular weight (LMWC)- 6000 g/mol and high molecular weight (HMWC)- 17400 g/mol. It was reported that both siRNA-p(PEG-A) had increased stability in serum and ribonuclease resistance. They had less degradation (16% degradation at 72 h for HMWC) compared to unmodified siRNA and thiol-modified siRNA, 10 and 48 h, respectively. Additionally, it was revealed that siRNA- p(PEG-A) conjugates showed less degradation in 50% serum when compared the literature degradation values (Kim, Jeong et al. 2006) of naked siRNA and siRNA-linear PEG (Mn:5000 g/mol) due to umbrella-like shape of the polymer providing greater protection to siRNA. Moreover, HMWC showed more resistance to ribonuclease than LMWC and naked siRNA because of greater steric hindrance of higher molecular weight polymer. As a result of both studies RAFT-synthesized comb-type p(PEG-A) conjugation with siRNA found to be effective (Heredia, Nguyen et al. 2008; Gunasekaran, Nguyen et al. 2011).

Gao et al. reported significant enhancements in pharmacological properties of myoglobin-comb type poly(oligo(ethylene glycol) methyl ether methacrylate) p(PEG-MA) conjugates and green fluorescence protein (GFP)- p(PEG-MA) conjugates compared to native proteins (Gao, Liu et al. 2009; Gao, Liu et al. 2010). The blood circulation half-life, terminal elimination half-life and clearance rate increased from 0.05 h, 3h and 1.43 ml/h to 2 h, 18 h and 0.035 ml/h for myoglobin and p(PEG-MA) conjugate, respectively (Gao, Liu et al. 2009) from 0.1, 4h, 7 ml/h to 2h, 26 h and 0.5 ml/h for GFP and p(PEG-MA) conjugate respectively in nude mice (BALB/c nu/nu) (Gao, Liu et al. 2010). The tumor accumulation of GFP native protein and GFP- p(PEG-MA) conjugate was also investigated. GFP- p(PEG-MA) conjugate in tumor tissue was

50 times greater than that of unmodified GFP at 24 h and tumor/blood ratio of the conjugate increased from 0.1 at 30 min to 2.1 at 72 h. The result indicated tumor accumulation via EPR effect (Gao, Liu et al. 2010). As a result of both studies, the authors proposed protein conjugation technology with p(PEG-MA) as a successful candidate for improving the efficacy of protein and peptide drugs and targeting agents that are for cancer imaging and therapy (Gao, Liu et al. 2009; Gao, Liu et al. 2010).

Sayers et al. investigated conjugation of salmon calcitonin with comb-type α-aldehyde functionalized p(PEG-MA) with the molecular masses between 6.5 and 109 kDa and found that polymer conjugation did not interfere with biological activity of protein (Sayers, Mantovani et al. 2009). Ryan et al. also investigated cytotoxicity, bioactivity, stability against liver homogenate, serum and intestinal enzymes and plasma half- life of both comb-type p(PEG-MA)-salmon calcitonin (sCT- PolyPEG$^{®}_{6.5\ kDa}$) and linear PEG (5 kDa)- salmon calcitonin conjugates (sCT- $PEG_{5\ kDa}$). No significant cytotoxity of both types of conjugates were observed and biological activity of conjugates were 85% and 92% of the unmodified sCT activity for sCT- PolyPEG$^{®}_{6.5kDa}$ and sCT- PEG_{5kDa}, respectively. sCT- PolyPEG$^{®}_{6.5kDa}$ and sCT- $PEG_{5\ kDa}$ were found to be 8.5 and 1.9-fold resistant to liver homogenates and retained their 56% and 21% of the biological activity against intestinal enzymes, respectively. The plasma half-life of linear and comb-type conjugates were 83.3 ± 24.5 min and 631.9 ± 341.9 min, respectively whereas that of sCT was 41.8 ± 12.4 min. Consequently, both types of conjugates were non-toxic and retained their bioactivity after conjugation. However, comb-type conjugate was more resistant to proteolytic enzymes and liver metabolism and provided enhanced plasma half-life to the protein compared to linear one because of its umbrella-like shape and steric hindrance effect (Ryan, Wang et al. 2009). Additionally, Ryan et al. also investigated the effect of comb-type PEG molecular weight (6.5 kDa- 9 kDa- 23 kDa- 40 kDa) on the stability and plasma half-life of conjugated sCT. Increasing molecular weights resulted in greater stability of polymer conjugates against intestinal enzymes. The degradation half-life of sCT-P (40 kDa) conjugate was found to be 11 times longer than that of sCT-P (6.5 kDa) conjugate. The plasma half-life was 41.8 ± 12.4 min, 631.9 ± 341.9 min, 668.3 ± 347.7 min and 1425.6 ± 257.0 min for free sCT, sCT-P (6.5 kDa), sCT-P (23 kDa) and sCT-P (40 kDa), respectively, which indicated linear relationship between molecular weight of polymers and plasma half-life of conjugates (Ryan, Frias et al. 2011). Consequently, p(PEG-MA)- salmon calcitonin was proposed to be a potential biotherapeutic agent because of

its enhanced pharmacological properties and Generally Regarded As Safe (GRAS) status (Ryan, Wang et al. 2009; Sayers, Mantovani et al. 2009; Ryan, Frias et al. 2011).

In addition to biomolecule conjugates, comb-type PEG has also been used onto the nanoparticles and micelles to improve pharmacological properties and hydrophilicity. Deshpande et al. investigated the effect of copolymer structure on the characteristics of complexes with phosphorothioate antisense oligonucleotide (ISIS 5132) and a diblock copolymer (DMAEMA-PEG), a brush-type copolymer (DMAEMA-OEGMA) and a comb-type copolymer (DMAEMA-stat-p(PEG-MA) (Figure 2.6) in comparison with DMAEMA as a control (Deshpande, Garnett et al. 2002). As a result of the study, it was revealed that all the copolymers demonstrated good binding affinity while comb-type copolymer exhibited the highest. Additionally, different copolymer architectures allowed access to a range of oligonucleotide complexes. DMAEMA-OEGMA and DMAEMA-PEG formed compact complexes, whereas the comb-type copolymer (DMAEMA-stat-p(PEG-MA) formed soluble complexes because of PEG hydrophilic branches that prevented efficient micellization and displayed the lowest transfection efficacy (Deshpande, Garnett et al. 2002).

The influence of these copolymer architectures on cellular interaction and uptake of DNA complexes was investigated by in a subsequent study of Deshpande et al. and it was revealed that comb-type copolymer DMAEMA-stat-p(PEG-MA) displayed less cellular interaction and uptake than DMAEMA-OEGMA and DMAEMA-PEG due to prevented self-assembled into micelle-like constructs (Deshpande, Davies et al. 2004). As a result of these studies, different copolymer architecture induced different conjugate (oligonucleotide-copolymer) complexes and cellular uptake profiles. Comb-type copolymer DMAEMA-stat-p(PEG-MA) was not the most appropriate candidate for DNA complexes because of more hydrophilic structures (Deshpande, Garnett et al. 2002; Deshpande, Davies et al. 2004).

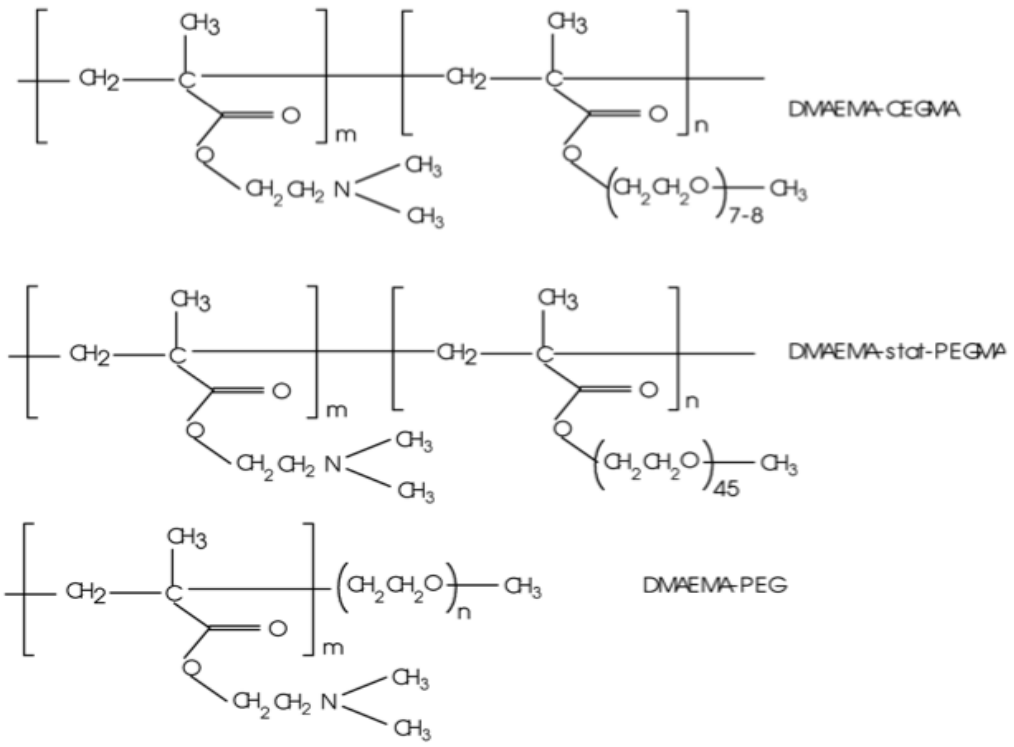

Figure 2.6. Structures of tertiary amine methacrylate polymers
(Source: Deshpande et al. 2002)

Tedja et al. reported that surface modification of TiO_2 nanoparticles with oligoethylene glycol monomer (OEGMA- M_n: 475 g/mol) and poly(oligoethylene glycol) methyl ether methacrylate) (p(PEG-MA)) with various chain lengths resulted in decrease in cellular uptake by A549 and H1299 cell line compared to that of unmodified and only linker (silane) modified nanoparticles due to the stability of particle aggregates and gravitational settling rate difference of nanoparticles. Additionally, modification of TiO_2 nanoparticles with OEGMA and p(PEG-MA) caused a significant decrease in protein adsorption in the range of 58 and 98 kDa, reduced cytotoxicity and improvement of biocompatibility (Tedja 2012).

CHAPTER 3

MATERIALS AND METHODS

3.1 Materials

Oligo(ethylene glycol) methyl ether methacrylate OEGMA (number-average molecular weight M_n=475 g/mol) and 4-cyano-4-(phenylcarbonothioylthio) pentanoic acid (CPADB) were purchased from Aldrich. O-[2-(3- Mercaptopropionylamino) ethyl]-O-methylpolyethylene glycol 20,000 (Mn= 20 000 g/mol, PDI<1.08) was bought from Fluka and thiol-PEG, mPEG-SH (Mn= 10 000 g/mol, PDI<1.08 PEG 10K) was purchased from Nanocs. The polymerization initiator, 2,2-azoisobutyronitrile (AIBN), was crystallized twice from methanol prior to use. Diethyl ether, acetonitrile, N,N-dimethylformamide (DMF), tris(2-carboxyethyl) phosphine hydrochloride (TCEP), hexylamine (HEA) and triethylamine (TEA) were bought from Sigma. Dialysis membranes MWCO 1000 and 3500 were purchased Spectrum® Laboratories. N'N-dimethylacetamide (DMAc) was obtained from VWR BDH Prolabo and $CDCl_3$ was purchased from Merck.

Cell culture media, RPMI-1640 and DMEM, were purchased from Biological Industries. Fetal bovine serum (FBS) was obtained from Gibco and Trypsin-EDTA was bought from Biological Industries. 3-(4,5-dimethylthiazol-2-yl)-2,5-diphenyl tetrazolium bromide (MTT), nocodazole, cytochalasin D, dimethyl sulfoxide (DMSO), phosphate buffer saline (PBS) and gentamicin were purchased from Sigma. Oregon Green® 488 maleimide, and DAPI dilactate dyes were bought from Invitrogen Molecular Probes. Lactate Dehydrogenase (LDH) assay was obtained from Promega.

BEAS-2B and A549 cells were kindly provided by Prof. Dr. Serdar ÖZÇELİK and Biotechnology and Bioengineering Research and Application Center, Izmir Institute of Technology, Izmir, Turkey, respectively.

Nuclear Magnetic Resonance spectra were taken using Varian VNMRJ 400 spectrometer at Izmir Institute of Technology, Izmir. Shimadzu modular system comprising a RID-10A refractive-index detector and Malvern BIYOM ViscoTek system comprising a light scattering detector were used for gel permeation

chromatography applications. Dynamic Light Scattering analyses were performed by using Malvern Zetasizer Nano ZS. NanoMagnetics Instruments Solver Pro 7 from NT-MDT was used for Atomic Force Microscopy analyses. UV-Vis spectroscopy analyses were performed by using Thermo Scientific Evolution 201 and Varioskan Flash (Thermo Electron Corporation) microplate reader. BD FACSCanto^{TM}, BD Biosciences was used for flow cytometry analyses and Olympus BX71 fluorescence microscope was used for intracellular distribution analyses.

3.2 Methods

3.2.1 Synthesis of Poly(Polyethylene glycol) Methyl Ether Methacrylate p(PEG-MA)

Comb-type PEG, poly(polyethylene glycol methyl ether methacrylate) (p(PEG-MA)) was synthesized according to the literature with some modifications (Heredia, Nguyen et al. 2008; Gunasekaran, Nguyen et al. 2011).

CPADB, AIBN and oligo(ethylene glycol) methyl ether acrylate (OEGMA) monomer (M_n= 475 g/mol) were dissolved in acetonitrile. [OEGMA]/[CPADB]/[AIBN] mol ratio was adjusted as 50/1/0.25. Monomer concentration was 1 M. The solution was purged with N_2 at 4^{o}C for 30 minutes to remove oxygen and then immersed into an oil bath at 65^{o}C. The polymerization reaction was performed for 1 hour 40 minutes and 3 hour 45 minutes to obtain polymers having a M_n of 10,000 g/mol and 20, 000 g/mol, respectively. Polymerization reaction scheme for synthesis of poly(ethylene glycol) methyl ether methacrylate p(PEG-MA) is shown in the Figure 3.1.

Purification step was needed after synthesis to remove excess OEGMA monomer, CPADB and AIBN. Acetonitrile was evaporated under vacuum and the higher molecular weight polymer (M_n= 20,000 g/mol) was precipitated in cold diethyl ether followed by centrifugation, while lower molecular weight polymer (M_n= 10,000 g/mol) was dialyzed against ultrapure water for 5 days using a dialysis membrane with a MWCO of 3500 and finally freeze-dried.

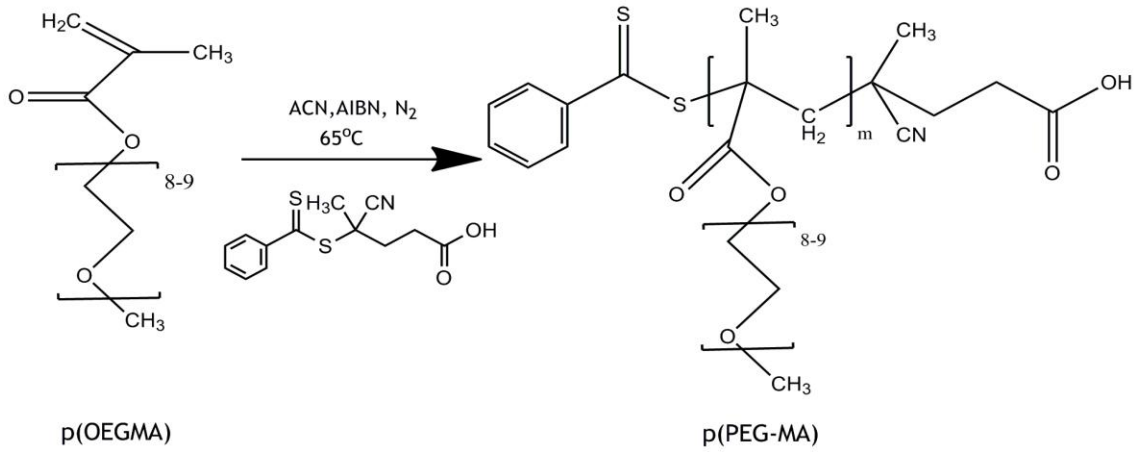

Figure 3.1.Polymerization reaction scheme for synthesis of poly(polyethylene glycol) methyl ether methacrylate p(PEG-MA).

3.2.2 Physicochemical Characterization of Polymers

3.2.2.1 Nuclear Magnetic Resonance (NMR) Analysis

^{1}H Nuclear Magnetic Resonance (NMR) spectroscopy was used to determine the chemical structure, theoretical molecular weights and purity of polymers. NMR samples were dissolved in deuterated chloroform ($CdCl_3$) at 8 mg/ml concentration and ^{1}H NMR spectra were taken using Varian VNMRJ 400 spectrometer with 8 scan number at Izmir Institute of Technology, Izmir. ACD/SpecManager® software was used to analyze NMR spectra.

3.2.2.2 Gel Permeation Chromatography (GPC) Analysis

Gel Permeation Chromatography was used to obtain molecular weight of polymers. A Shimadzu modular system with a RID-10A refractive-index detector and a Malvern BIYOM ViscoTek system with a light scattering detector were used separately to characterize molecular weight and molecular weight distribution of polymers. While Shimadzu modular system included SIL-10AD auto injector, PSS Gram 30 A◦ and 100 A◦ (10 μM, 8x300 mm) guard column, Malvern BIYOM ViscoTek system included Viscotek GPCmax auto injector, Viscotek TDA light scattering detectors.

GPC samples were dissolved in N,N-Dimethylacetamide (DMAc) for Shimadzu system and ultra-pure water for Malvern system at 2 mg/ml concentration. Then, samples were filtered by using 0.45μm syringe type membrane filter. N,N-Dimethylacetamide (DMAc) containing 0,05 % w/v LiBr (1 ml/min) and PBS (0.02 M Sodium Phosphate, 0.15 M NaCl, 0.05% NaN_3) (0.8 ml/min) were used as mobile phase in Shimadzu and Malvern GPC systems, respectively.

3.2.2.3 Dynamic Light Scattering (DLS) Analysis

The hydrodynamic size of the polymers is an important property for the cell uptake (Chithrani, Ghazani et al. 2006). Dynamic light scattering method is used to determine the hydrodynamic size of particles (Kersey, Merkel et al. 2012).

Polymer solutions (0.05 mM) were prepared in 7 different media: water, phosphate buffer saline (PBS) at pH 7.4, PBS containing 10% fetal bovine serum (FBS), cell culture medium RPMI-1640, cell culture medium DMEM, RPMI-1640 containing 10% FBS and DMEM containing 10% FBS and filtered using 0.22 μm filter. The measurements were replicated 3 times with 3 repeats for each polymer solution using Zetasizer Nano ZS (Malvern, UK) (measurement range 0.3 nm – 10.0 microns; light source He-Ne laser 633 nm Max 5mW; Power 100 VA) in Malvern disposable polystyrene low volume cuvettes at room temperature. Refractive index and viscosity values of dispersants are given in Table 3.1.

Table 3.1. Refractive index and viscosity values of different dispersants.

Dispersant	Refractive Index	Viscosity (cP)	Reference
Water	1.333	0.880	(Abilez, Benharash et al. 2006; Dieguez 2009)
PBS	1.338	0.899	(Abilez, Benharash et al. 2006)
PBS+10% FBS	1.338	0.899	(Abilez, Benharash et al. 2006)
RPMI	1.330	1.010	(Yunus and Rahman 1988)
RPMI+10% FBS	1.330	1.100	(Yunus and Rahman 1988)
DMEM	1.345	1.010	(Dardik, Chen et al. 2005)
DMEM+10% FBS	1.520	1.100	(Gauggel, Derreza-Greeven et al. 2012)

3.2.3 End Group Modifications

3.2.3.1 Removal of RAFT End-Group and Deactivation of Thiol End-Group

Living end group (reactive thiocarbonylthio group) of RAFT synthesized polymers may be a significant source of cellular toxicity. It is possible to remove thiocarbonylthio groups by modification of polymers after polymerization. Aminolysis reaction is one of the most widely used methods that is performed in the presence of amines to remove ω-end group (Pissuwan, Boyer et al. 2010) and yields polymers with thiol end-groups (Barner-Kowollik 2008).

In this study, the RAFT end-group of comb-type polymers, p(PEG-MA), was removed by aminolysis (Figure 3.2) and the thiol end-group formed upon aminolysis was simultaneously deactivated by addition of a PEG-methacrylate (OEGMA) monomeric unit through Michael addition (Figure 3.3). Similarly, the thiol-end-group of linear polymers, PEG, was directly deactivated by addition of OEGMA monomeric unit.

Briefly, the RAFT-group ended comb-type polymer p(PEG-MA), OEGMA monomer, HEA and TEA were dissolved in acetonitrile. [p(PEG-MA)]/[OEGMA]/[HEA]/[TEA] mol ratio was adjusted to be 1/5/10/10 while polymer concentration was 4 mM. The reaction was performed under N_2 at room temperature for 2 hours. Acetonitrile was evaporated under vacuum and the solution was precipitated in cold diethyl ether followed by centrifugation. Purified polymers were dried under vacuum followed by ^{1}H NMR analysis.

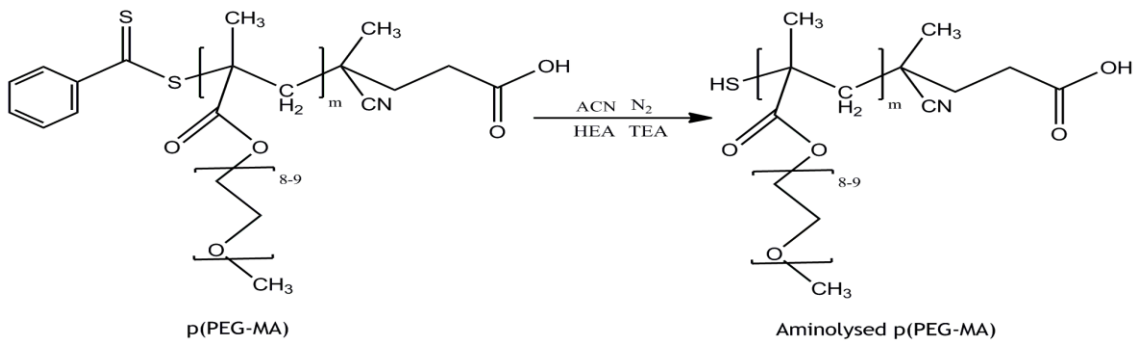

Figure 3.2.Removal of RAFT end-group of comb-type polymers, p(PEG-MA) via aminolysis reaction.

For the deactivation of thiol end-group of linear polymers, PEG was reacted with OEGMA in the presence of tris(2-carboxyethyl) phosphine hydrochloride (TCEP) to break disulphide bonds. Polymer was dissolved in phosphate buffer (pH: 7.1).TCEP and OEGMA monomer were then added to the polymer solution. [PEG]/[OEGMA]/ [TCEP] ratio and polymer concentration were adjusted to be 1/20/20 and 10 mM, respectively. Nitrogen was purged for 30 minutes. The reaction was stirred for 20 hours at room temperature. Fresh TCEP (0.2 M) was then added to the reaction mixture and the reaction was further continued for another 4 hours at room temperature. Polymer solution was dialysed against ultrapure water for 4 days using dialysis tubing with a MWCO of 3500 Da and finally lyophilized.

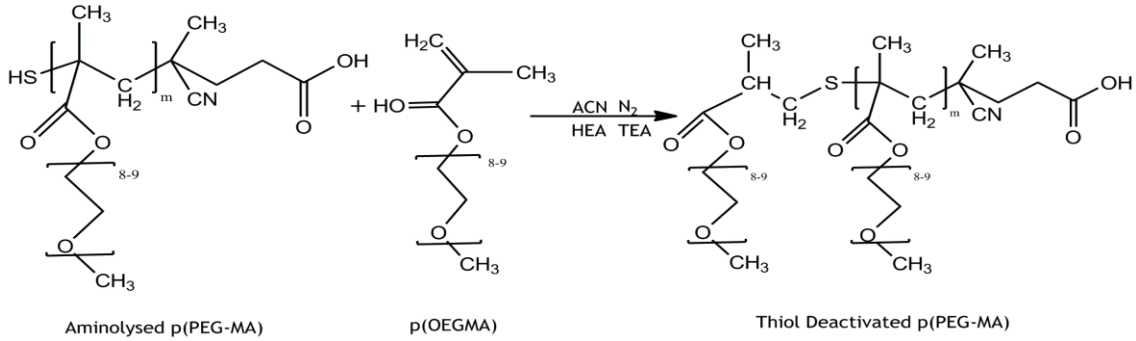

Figure 3.3. Deactivation of thiol end-group of comb-type polymers (p(PEG-MA)) by addition of OEGMA monomeric unit.

3.2.3.3 Fluorescent Dye Labelling

Comb-type and linear polymers were labeled with a thiol-reactive dye, Oregon Green maleimide 488®. Fluorescent labeling of thiol-terminated comb-type polymer, p(PEG-MA) and thiol-terminated linear polymer, PEG, was performed according to the manufacturer's protocol (Thiol Reactive Probes Manuel, Molecular Probes- Invitrogen). Briefly, dye (100 mM) was dissolved in DMF. Polymer (0.1 M) was dissolved separately in phosphate buffer (at pH 7.1) and reacted with TCEP (0.02 M) for 5 minutes. Dye solution in DMF was added drop wise to the polymer solution under stirring. The final concentration of dye in the reaction mixture was 0.5 M. Nitrogen was purged into the reaction solution for 30 minutes. Reaction was continued for 2 hours at room temperature followed by addition of fresh TCEP (0.01 M). Nitrogen was purged for another 30 minutes. The reaction solution was shaken overnight at room

temperature. The resulting solution was dialysed against ultrapure water for 5 days using dialysis tubing with a MWCO of 3500 Da and then freeze-dried. The fluorescent labeling degree of 33 μM polymers was verified by UV-Vis spectroscopy (Thermo Scientific Evolution 201 Spectrophotometer) in the range between 350 nm and 550 nm using quartz cuvette and calculated using absorbance values at 491 nm and extinction coefficient of the dye that is 81000 $M^{-1}cu^{-1}$ according to Equation 3.1.

$$n_{\frac{Dye}{Polymer}} = \frac{A_x * M_W}{C * \varepsilon} \quad (3.1)$$

Where A_x, ε, M_w and C are the absorbance values of the dye at the absorption maximum wavelength, the molar extinction coefficient of the dye or reagent at the absorption maximum wavelength, the molecular weight and concentration of fluorescently-labeled polymer, respectively.

3.2.4 Cell Culture Experiments

BEAS-2B (Human bronchial epithelium) and A549 (Human lung adenocarcinoma epithelial cell line) cells were cultured using DMEM and RPMI- 1640 medium, respectively, supplemented with 10% fetal bovine serum (FBS) and 0.1% gentamicin as an antibiotic at 37^{o}C and 5% carbon dioxide in a humidified atmosphere. Subculture was performed when the cells had 80-90% confluence using 40 μl/cm^2 trypsin-EDTA that contained 0.5% trypsin and 0.2 % EDTA.

3.2.4.1 Determining the Effect of Polymers on Cell Viability via MTT Assay

3-(4,5-dimethylthiazol-2-yl)-2,5-diphenyl tetrazolium bromide (MTT) assay is a colorimetric assay that is used to determine cell viability via measuring the activity of cellular enzymes that reduce the tetrazolium dye to its insoluble formazan giving a purple color (Deshpande, Garnett et al. 2002; Venkataraman, Ong et al. 2011).

A549 and BEAS- 2B cells were seeded a day prior to sample exposure at a concentration of 10^4 cells/well in a 96 well- plate and incubated overnight at 37 °C and 5% CO_2 in a humidified atmosphere. Polymers were sterilized by ethanol addition and dissolved in PBS and dilutions of 25 μM, 50 μM, 100 μM and 200 μM were prepared. Varying concentrations of sterile polymer solutions were transferred to wells. The PBS content of each well was adjusted to be 0.5% (v/v). The final volume of each well was 200 μl. The cells were incubated at 37 °C and 5% CO_2 in a humidified atmosphere for 24 or 72 h. After the incubation period, 3-(4,5-dimethylthiazol-2-yl)-2,5-diphenyl tetrazolium bromide (MTT) dye (5 mg/ml) was added to each well by adjusting the final concentration of dye to be 10% (v/v) and the plates were incubated at 37^{o}C for 4 hours. At the end of the incubation period, plates were centrifuged at 1800 rpm for 10 minutes, supernatants were removed and pellets were dissolved using DMSO. Cell viability was detected by spectrophotometric analysis at 570 and 690 nm (Varioskan Flash, Thermo Electron Corporation, Finland). Calibration curve was prepared using the absorbance values of varying cell concentrations between 5.10^2 and 5.10^5 cells per well and the viable cell number was calculated with the help of the calibration curve. Percent cell viability was calculated relative to the absorbance of positive control that was cells without any treatment using calibration curve.

3.2.4.2 Determining Membrane Integrity via Lactate Dehydrogenase (LDH) Assay

Release of intracellular enzymes upon treatment of cells with the non-cytotoxic concentration range of polymers, can be ascribed to an increase in cell membrane permeability as opposed to general lysis due to cell death and it is called polymer induced enzyme leakage. The integrity of cell membrane was evaluated by LDH assay after incubation of cells with the linear and comb-type polymers (Mager, Eiriksdottir et al. 2010; Benfer and Kissel 2012).

A549 and BEAS-2B cells were seeded a day prior to sample exposure at a concentration of 10^4 cells/well in a 96 well- plate and incubated overnight at 37 °C and 5% CO_2 in a humidified atmosphere. Spontaneous LDH release, maximum LDH release, culture medium background and volume correction experimental controls were prepared. Polymers were sterilized by ethanol addition and dissolved in PBS and

dilutions of 25 μM, 50 μM, 100 μM and 200 μM were prepared. Varying concentrations of sterile polymer solutions were transferred to wells. The PBS content of each well was adjusted to be 0.5% (v/v). The final volume of each well was 200 μl. The cells were incubated at 37 °C and 5% CO_2 in a humidified atmosphere for 24 or 72h.

At the end of the incubation period, LDH assay was applied according to the manufacturer's protocol (CytoTox 96, Non-Radioactive Cytotoxicity Assay Manuel, Promega) and membrane integrity was detected by spectrophotometric analysis at 490 nm (Varioskan Flash, Thermo Electron Corporation, Finland. Total LDH release (%) values were calculated according to Equation 3.2:

$$\Delta_{\%\ \text{LDH Release}} = \left[\frac{A_X - A_{\text{Spontaneous}}}{A_{\text{Max}}}\right] * 100 \qquad (3.2)$$

Where, A_x, A_{max}, $A_{\text{Spontaneous}}$ are the absorbance values of experimental wells, maximum LDH release control wells and spontaneous LDH release control wells, respectively.

3.2.4.3 Cell Uptake of Polymers

Cellular uptake of comb-type and linear polymers were determined via flow cytometry analyses by using fluorescent-labeled polymers and endocytosis inhibitor that are nocodazole and cytochalasin D (Mager, Eiriksdottir et al. 2010; Mager, Langel et al. 2012).

Briefly, A549 and BEAS-2B cells were seeded a day prior to sample exposure at a concentration of 10^5 cells/well in a 12 well- plate and incubated overnight at 37 °C and 5% CO_2 in a humidified atmosphere. Polymers were dissolved in ultrapure water and dilutions of 12.5 μM and 25 μM were prepared. The experimental set that was used for determining endocytosis inhibition was exposed to 20 μM nocodazole (dissolved in DMSO at a concentration of 16.6 mM) and 20 μM cytochalasin D (dissolved in DMSO at a concentration of 19.7 mM) for 30 minutes before the addition of fluorescent-labeled polymers. The DMSO content of wells was adjusted to be 0.5% (v/v). Varying concentrations of sterile polymer solutions were transferred to wells. The ultra-pure water content of each well was adjusted to be 0.5% (v/v). The final volume of each well

was 2 ml. The cells were incubated either 4^{o}C or 37 °C for either 1 or 3 h and each experiment performed in triplicate.

At the end of the incubation period, medium was removed and wells were washed with cold PBS twice. The cells were harvested by trypsinization and centrifuged for 5 minutes. Supernatant was removed and pellet was resuspended in 200 µl cold PBS. Data from 10000 events per sample was collected and analyzed using by using FacsDiva V.5.0.3 software of flow cytometry (BD FACSCantoTM, BD Biosciences, San Jose, USA) that was equipped by Oregon green solid state 488 laser and 530/ 30-filter configuration. Cell uptake (%) values were calculated according to Equation 3.3 and then normalized via multiplication with normalization coefficients in Table 4.3.

$$\text{Cell Uptake (\%)} = \frac{\text{FITC-H mean}_{P3} * \text{Total Event}_{P3}}{\text{FITC-H mean}_{P1} * \text{Total Event}_{P1}} * 100 \qquad (3.3)$$

3.2.4.4 Intracellular Distribution of Polymers

Intracellular localization of comb-type and linear polymers were determined via fluorescent microscopy by using fluorescent organelle-specific dyes. DAPI (4', 6-Diamidino-2-Phenylindole, Dilactate) were used to stain nucleus (Wang, Liang et al. 2011; Benfer and Kissel 2012).

Briefly, A549 and BEAS-2B cells were grown on coverslips inside 6 well-plates a day prior to sample exposure at a concentration of 2.10^{4} cells/well and incubated overnight at 37 °C and 5% CO_2 in a humidified atmosphere. Polymers were dissolved in ultrapure water and 50 µM polymer solutions were transferred to wells. The ultra-pure water content of each well was adjusted to be 0.5% (v/v). The final volume of each well was 2 ml. The cells were incubated at 37 °C for 1 h and each experiment performed in triplicate.

At the end of the incubation period, medium was removed and wells were washed with PBS three times and cells were fixed by using 2% paraformaldehyde containing PBS for 10 minutes at 37^{o}C (Wang, Liang et al. 2011). Wells were washed with PBS three times to remove excess fixation solution. Then, the stock DAPI solution was diluted to 150 nM and 750 µl of the diluted solution was transferred onto coverslips. After the incubation for 2 minutes at dark, the wells were rinsed with PBS

several times and excess buffer was drained from coverslip. Coverslips were mounted and necessary microscopy settings were applied. The excitation and emission wavelengths were 496-524 nm and 358-461 nm for Oregon Green Maleimide 488® and DAPI, respectively.

CHAPTER 4

RESULTS AND DISCUSSION

4.1 Synthesis of Poly(Polyethylene Glycol) Methyl Ether Methacrylate (p(PEG-MA))

Comb-type PEG, poly(polyethylene glycol methyl ether methacrylate) (p(PEG-MA)) at two different molecular weights was synthesized via reversible addition fragmentation chain transfer (RAFT) polymerization by using oligo(ethylene glycol) methyl ether methacrylate (OEGMA) (M_n:475 g/mol) as monomer, 4-cyano- 4-(thiobenzoylthio) pentanoic acid (CDTB) as a RAFT agent and AIBN as a radical initiator. There are also several literature studies that applied similar reaction methodology to synthesize comb-type PEG polymers (Heredia, Nguyen et al. 2008; Gunasekaran, Nguyen et al. 2011).

Molecular weights of polymers were determined via Gel Permeation Chromatography (GPC) and Nuclear Magnetic Resonance (NMR) spectroscopy. Molecular weight distribution (polydispersity index (PDI)) of purified polymers was investigated by GPC.

4.2 Characterization of Poly(Polyethylene Glycol) Methyl Ether Methacrylate (p(PEG-MA))

4.2.1 Chemical Structure and Molecular Weight Characterization

Chemical structure of synthesized polymers was determined via ^{1}H-NMR spectroscopy (Figure 4.1 and 4.2). The signal between 4.0 and 4.4 ppm and at 7.4, 7.5 and 7.9 ppm belong to 2 protons of methylene group of oligo(ethylene glycol) side chains and 5 protons of the RAFT agent, respectively. Other characteristic peaks that belong to protons in the polymer are presented in Figure 4.1 and 4.2.

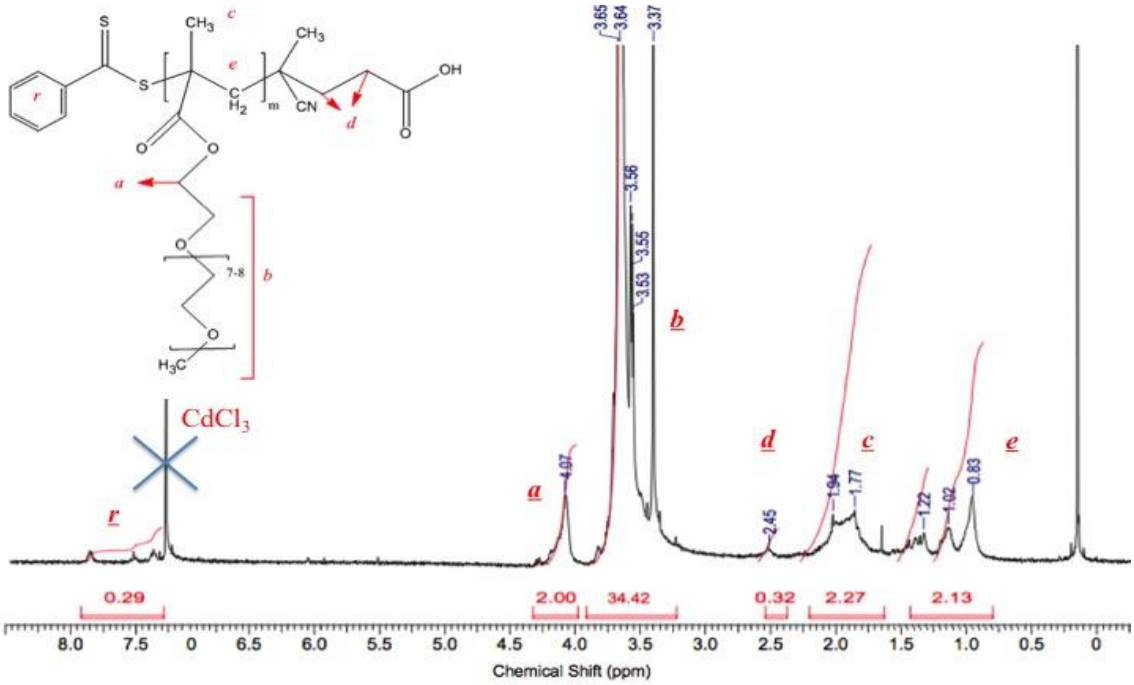

Figure 4.1. ^{1}H-NMR spectrum of purified p(PEG-MA)- (10K) synthesized using a [OEGMA]/[CPADB]/[AIBN] mol ratio of 50/1/0.25.

The molecular weight of synthesized polymers was calculated via ^{1}H-NMR spectroscopy assuming that each polymeric chain possesses a RAFT end-group. The proportion of the integral of methylene protons (2 H at 4.0- 4.4 ppm) of oligo(ethylene glycol) side chains and the integral of the RAFT agent protons (5 H at 7.3- 7.9 ppm) (Figure 4.1 and 4.2) were used for calculation of molecular weight. The equation of NMR-molecular weight calculation via NMR spectroscopy is given in Equation 4.1:

$$M_N^{NMR} = \left[\frac{\int_{4.0\ ppm}^{4.4ppm} / 2}{\int_{7.3\ ppm}^{7.9\ ppm} / 5} * M_W^{OEGMA} \right] + M_W^{RAFT} \qquad (4.1)$$

Where M_W^{OEGMA} and M_W^{RAFT} are the molecular mass of OEGMA monomer and RAFT agent, respectively.

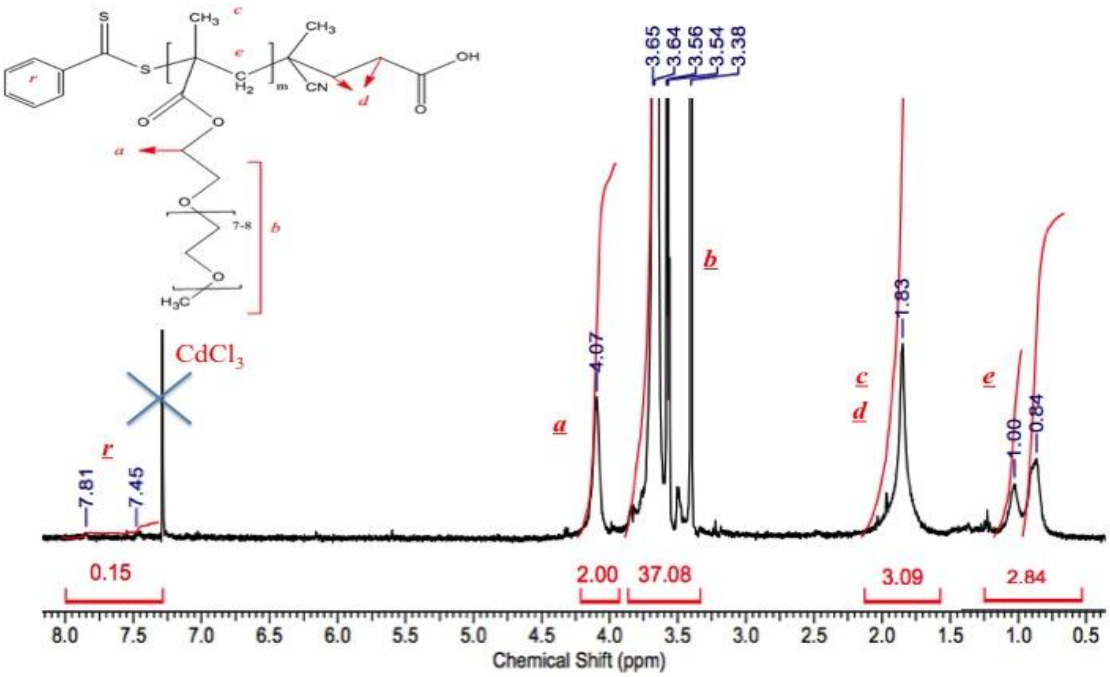

Figure 4.2. ^{1}H-NMR spectrum of purified p(PEG-MA)- (20K) synthesized using a [OEGMA]/[CPADB]/[AIBN] mol ratio of 50/1/0.25.

The number average molecular weight (M_n) and molecular weight distribution of polymers were also characterized using gel permeation chromatography (GPC). M_n values obtained by GPC were found in a good agreement with the M_n values obtained by ^{1}H- NMR data and Equation 4.1. However, the values obtained by GPC were always higher than the M_n^{NMR} values. This was attributed to the assumption of each polymeric chain possesses a RAFT end-group. Additionally, the low the polydispersity index (PDI) (< 1.2) values implied narrow molecular weight distribution of polymers and thus, RAFT controlled polymerization mechanism.

Table 4.1. Properties of comb-type p(PEG-MA) polymers synthesized throughout the study

Polymer No	**Polymer Type**	**M_n^{NMR} (g/mol)**	**M_n^{GPC} (g/mol)**	**PDI**
1	10K	9300	11360	1.11
2	10K	8400	9700	1.12
3	20K	16100	20300	1.18

4.2.2 Hydrodynamic Size of Polymers

The hydrodynamic size of polymers is one of the most important parameters affecting the biological interactions of polymers (Armstrong, Wenby et al. 2004). The hydrodynamic size of comb-type and linear PEG polymers in various dispersants was investigated via Dynamic Light Scattering (DLS) Experiments were replicated 3 times with 3 repeats and statistical analyses were performed via Student's *t* test. The results are given in the Table 4.2 and Appendix A (Figure A.6).

Table 4.2. Mean number average diameter of polymers determined by Dynamic Light Scattering (DLS) (nm).

	Water	**PBS**	**10% FBS included PBS**	**RPMI**	**DMEM**	**10% FBS included RPMI**	**10% FBS included DMEM**
C10K	2,84±1,20	3,72±1,02	6,29±0,05	4,04±1,14	3,86±0,54	7,13±0,19	7,31±0,52
C20K	4,21±0,41	4,08±0,22	6,66±0,12	3,97±0,1	3,96±0,1	6,78±0,68	7,54±0,43
L10K	6,49±0,90	6,19±0,68	6,94±0,27	6,19±0,82	6,43±0,36	6,99±1,56	7,35±1,19
L20K	7,32±1,62	7,43±1,69	7,49±0,42	7,24±0,52	7,83±0,34	7,52±0,52	8,09±0,85

The hydrodynamic diameter of comb-type polymers was found to be significantly ($p<0.05$) smaller than linear polymers of equivalent molecular weights when water was used as dispersant. This difference may arise from the umbrella-like shape of comb-type polymers that promises a more compact structure when compared with linear PEG polymers having equivalent molecular weights. Molecular weight difference did not seem to have a significant effect on the hydrodynamic diameter of polymers in the range studied. In the case of PBS and cell culture medium as dispersants, no significant hydrodynamic diameter change occurred compared to the diameters in water.

In the case of serum usage, the presence of serum affected the hydrodynamic diameter of comb-type and linear PEG in a different way. The hydrodynamic diameters of comb-type PEG polymers increased when 10% serum was included in PBS and cell culture media. In contrast, the hydrodynamic diameters of linear PEG polymers

remained the same. PEG is known as one of the most excellent protein-repellent polymers (Sheth and Leckband 1997), therefore no interactions between serum components and linear PEG were expected to occur. However, it is also known that oligomeric PEG chains can bind proteins and PEG chain length and conformation are important factors in protein adsorption (Sheth and Leckband 1997; Efremova, Sheth et al. 2001). As a result, comb-type structure may be triggering protein- binding due to its hydrophobic backbone leading to hydrophobic interactions with serum proteins.

Finally, no significant hydrodynamic size differences between linear and comb-type PEG polymers were observed when the polymers were in cell culture media with FBS ($p>0.05$).

4.3 End Group Modifications

Reactive thiocarbonylthio end-group of RAFT synthesized polymers was indicated as a source of cytotoxicity (Pissuwan, Boyer et al. 2010) and instability (Boyer, Granville et al. 2009). Therefore, before investigating the effect of comb-type polymers on the cellular metabolism, the reactive thiocarbonylthio end-group of the polymers was removed. Removal of the cytotoxic living end group of the polymers results in the formation of reactive thiol end-group that is able to conjugate bioactive compounds such as fluorescent dyes.

In this study, modification of the reactive thiocarbonylthio end-group of RAFT synthesized polymers was performed via aminolysis reaction yielding polymers with reactive thiol end group. Linear PEG polymers that have already possessed a thiol end-group and aminolysed comb-type polymers were both reacted with OEGMA monomer before using in cellular metabolism experiments or conjugated with a fluorescent molecule before using in cellular uptake and intracellular distribution experiments.

4.3.1 Removal of RAFT End-Group of Comb-Type Polymers and Deactivation of Thiol End-Group

End group cleavage is an important step in the evaluation of effects of RAFT-synthesized polymers with cell metabolism because residual RAFT agent functionality

in polymers can be a problem due to its inherent reactivity and the possibility of decomposition (Willcock and O'reilly 2010). There are a number of methods available to remove thiocarbonylthio groups via the reduction with nucleophiles and ionic reducing agents. Aminolysis is a well-established and versatile method that is based on the reaction of thiocarbonythio group with excess primary or secondary amines acting as nucleophiles yielding polymers with thiol end-groups (Barner-Kowollik 2008; Boyer, Granville et al. 2009; Willcock and O'reilly 2010). There are several literature studies that reported aminolysis reaction to remove thiocarbonylthio group of RAFT-synthesized polymers (Qiu and Winnik 2006; Roth, Kessler et al. 2008; Boyer, Granville et al. 2009).

In this study, RAFT-synthesized comb-type p(PEG-MA) polymers were aminolysed in the presence of excess amines to cleave thiocarbonythio end-group. Cleaved polymers were immediately purified via diethyl ether precipitation. End-group modification of polymer was verified by NMR spectroscopy revealing the end-group between 7.3 and 7.9 ppm via (Figure 4.3). Visual comparison of the color of the polymer solutions before and after aminolysis also confirmed success of removal process since the pink color of the RAFT group disappeared leading to a colorless polymer solution. Molecular weights of aminolysed polymers were also checked via Gel Permeation Chromatography (GPC) to determine if any changes occurred due to the oxidation of thiol end-groups in the presence of trace of oxygen yielding disulphide coupled polymer chains (Willcock and O'reilly 2010).

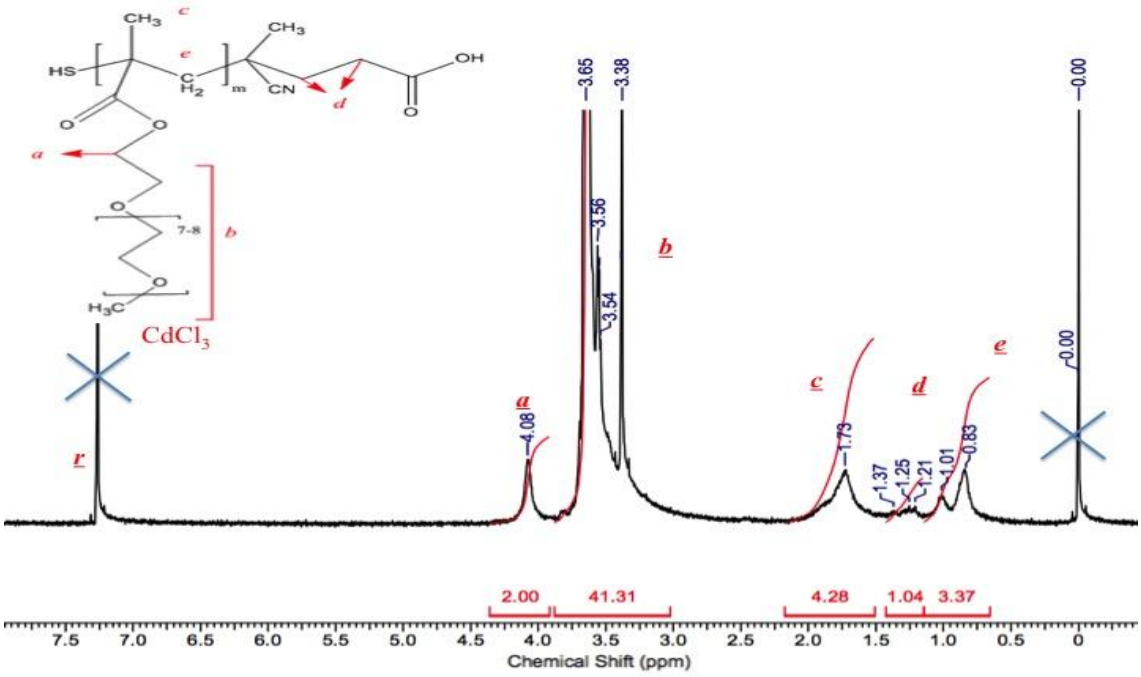

Figure 4.3. [1]H-NMR spectrum of RAFT end-group removed comb-type 20K p(PEG-MA) polymer after removal of the RAFT end-group.

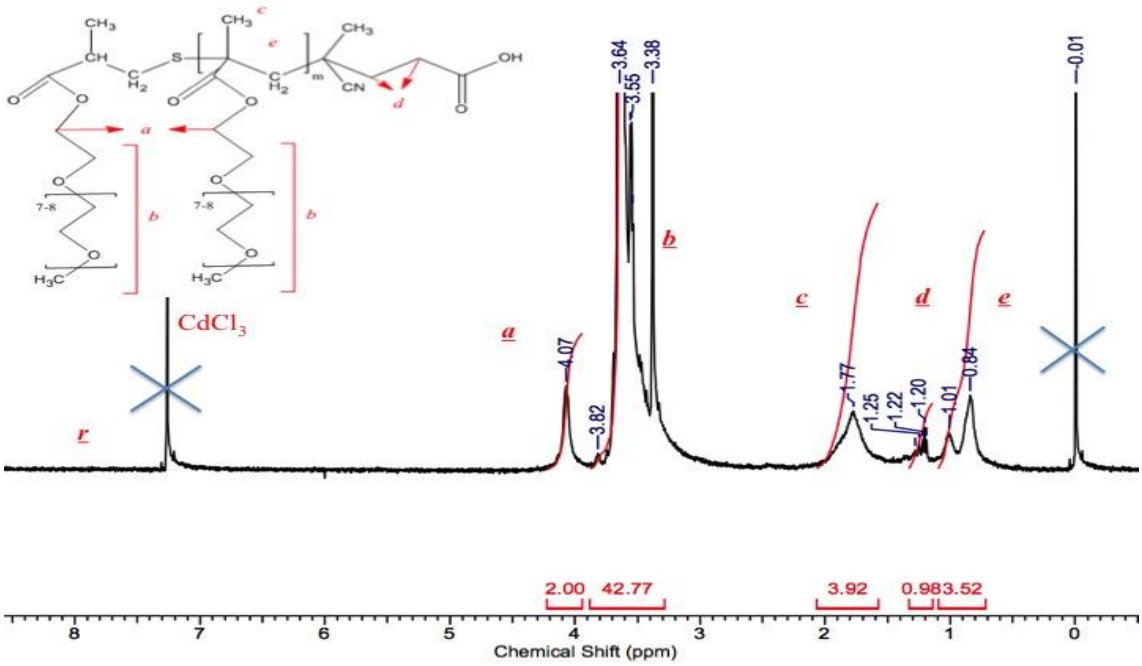

Figure 4.4. [1]H-NMR spectrum of thiol-deactivated comb-type 20K p(PEG-MA) polymer.

Deactivation of thiol end- group formed after cleavage of the RAFT end-group is necessary to minimize polymer unwanted reactivity and possible toxic effects. Monomer addition is one of the most widely used methods to mask the toxicity of

reactive end-groups while the original polymer chemical structure is being protected without any other group addition (Barner-Kowollik and Perrier 2008). In this study, thiol-ended polymers formed upon aminolysis were simultaneously deactivated by addition of a PEG-methacrylate (OEGMA) monomeric unit through Michael addition. The verification of end-group deactivation was performed via ^{1}H-NMR spectroscopy (Figure 4.4.).

4.3.2 Fluorescent Dye Labelling

Determination of *in vitro* cellular uptake and intracellular distribution of polymers requires labeling of polymers. Labeling of polymers often relies on covalent conjugation of a fluorescent probe to polymer of interest. Fluorescent probes allow high fluorescent labeling degrees (dye/polymer) and stable images in fluorescence microscopy (Watson, Jones et al. 2005; Scales, Convertine et al. 2006). Oregon green maleimide® is one of the green fluorescent probes which can be easily covalently coupled to thiol groups of aminolysed comb-type polymers and thiol-reactive linear polymers (Thiol Reactive Probes Manuel, Molecular Probes- Invitrogen).

Molecules react with functionalized fluorophores at different rates yielding polymer- fluorophore conjugates having varying degree of fluorophore labeling. Thus the number of fluorescence molecules per polymer chain is usually variable and represents a labeling distribution (Vira, Mekhedov et al. 2010). Quantification of polymer labeling degree was essential study since accurate quantification and comparison of cellular uptake of different polymers crucially depends on the labeling degree of polymers. In this study, labeling degree of fluorescently labeled polymers was determined from UV-Vis spectra of polymers taken in the range between 350 and 550 nm. The UV-Vis spectra are represented in Figure 4.5.

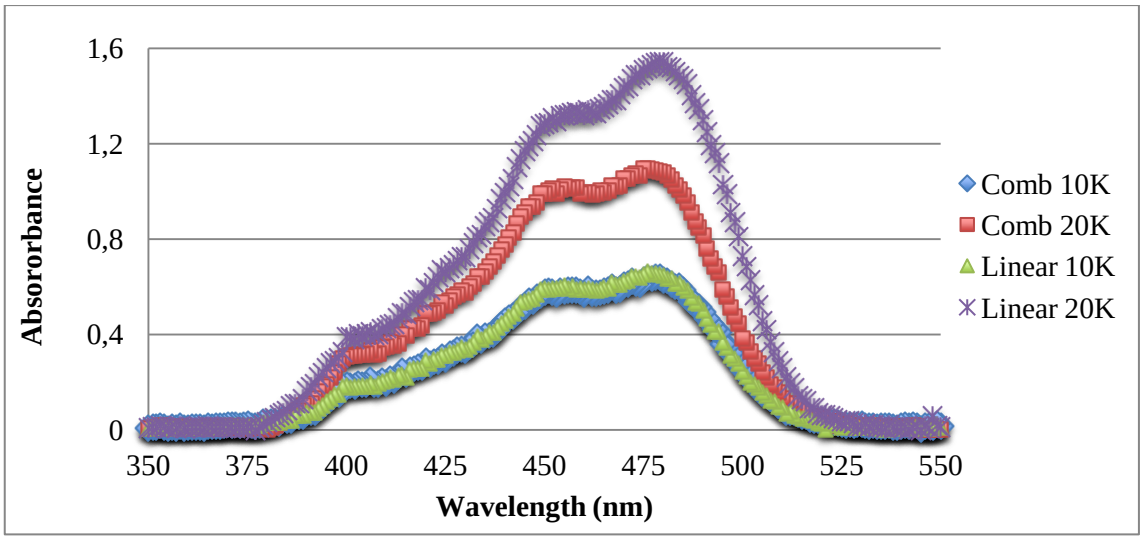

Figure 4.5. The UV-Vis spectra of Oregon Green Maleimide® labeled polymers at 33 μM polymer concentration.

The degree of labeling was calculated by determining the polymer and fluorophore molar concentrations of conjugates based on the absorbance measurements at 491 nm and the molar extinction coefficient of fluorophore reported by the manufacturer ($\varepsilon_{491\ nm}$ = 81000 $M^{-1}cu^{-1}$) with the help of Equation 3.1. The labeling degree of polymers is given in Table 4.3:

Table 4.3. The fluorescence labeling degree of comb-type and linear PEG polymers.

Polymer	M_n^{GPC} (g/mol)	OG/Polymer Ratio (mol/mol)	OG/Polymer Ratio (μg/mg)	Normalization Coefficient
Comb-type 10K	10530	0.153	6.73	1.180
Comb-type 20K	20300	0.321	7.34	0.542
Linear 10K	10000	0.174	8.06	1.000
Linear 20K	20000	0.467	10.83	0.373

4.3 Effect of Polymers on Cell Viability

The BEAS-2B (Human bronchial epithelium) and A549 (Human lung adenocarcinoma epithelial cell line) cell lines were used for investigating the effect of

comb-type and linear polymers on cell viability. In order to evaluate the cytotoxicity of the polymers, a well-known method, MTT was used. ANOVA test was utilized to determine statistical inference of obtained data.

A calibration curve relating absorbance value difference ($A_{570nm} - A_{690nm}$) and cell number was first established for both cell lines (Figure 4.6). The R^2 vales close to 1 suggested that the established equations can be used to calculate cell viabilities accurately.

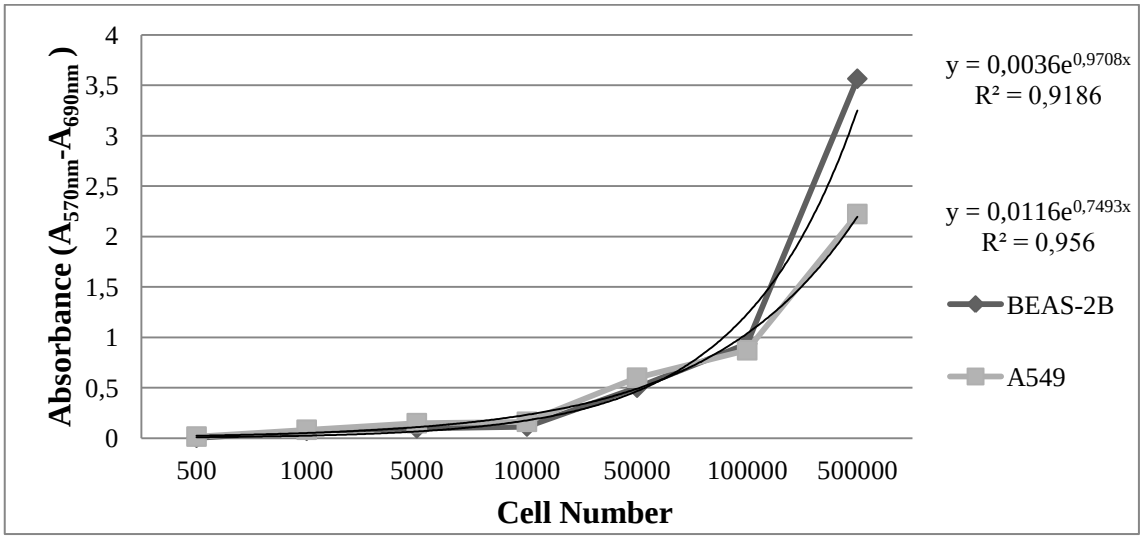

Figure 4.6. Cell number- absorbance calibration curve obtained from MTT assays of BEAS-2B and A549 cell lines.

Figures 4.7 and 4.8 show the cell viability of A549 cell line as a function of polymer dose and type for 24 and 72 hours of incubation, respectively. The dose dependent decrease in cell viability was clearly seen from both graphs. There was no statistically significant ($p>0.05$) difference between the effects of both types of polymers for 24 h of incubation. However, there was a significant decrease in the cell viability when A549 cells were incubated with linear 20K and comb-type 20K polymers at 200 μM concentration for 72 h. Nevertheless, the cell viability was still higher than 50 % ($p<0.05$).

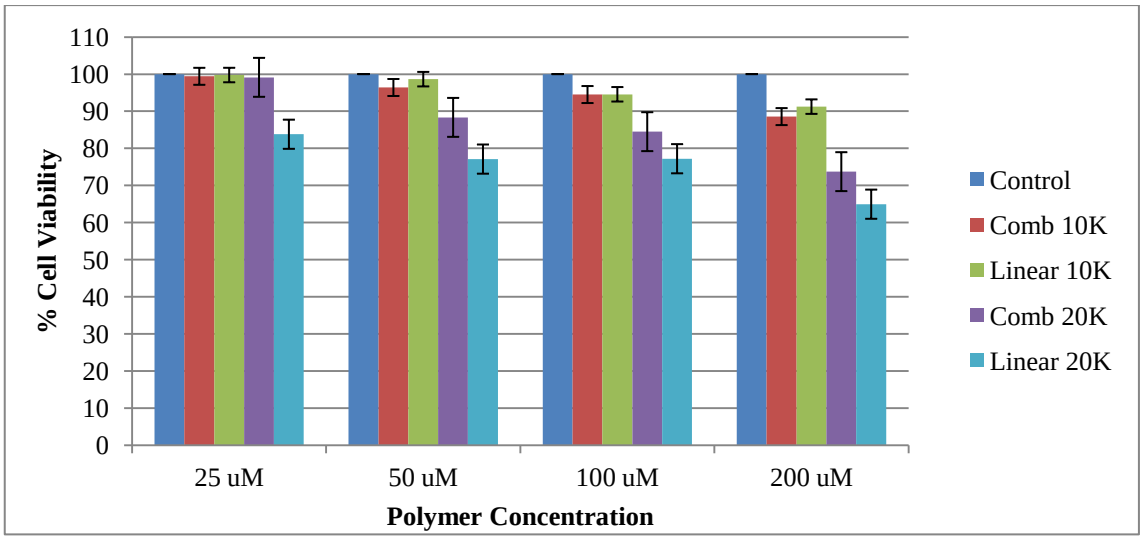

Figure 4.7. The percent cell viability of A549 cell line after incubation with polymers for 24 hours.

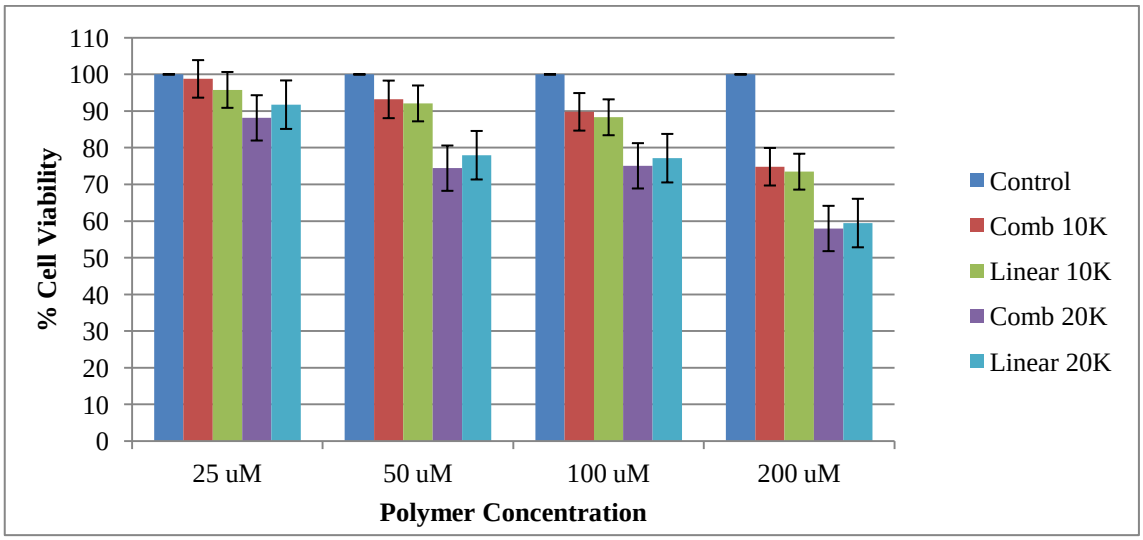

Figure 4.8. The percent cell viability of A549 cell line after incubation with polymers for 72 hours.

Figures 4.9 and 4.10 show the cell viability of BEAS-2B cell line as a function of polymer dose and type for 24 and 72 hours of incubation, respectively. The dose dependent decrease in cell viability was clearly seen from both graphs. There was no statistically significant ($p>0.05$) difference between the effects of both types of polymers for 24 h of incubation. However, there was a significant decrease in the cell viability when BEAS-2B cells were incubated with linear 20K at 100 and 200 μM concentrations for 72 h. Nevertheless, the cell viability was still higher than 60 % ($p<0.05$).

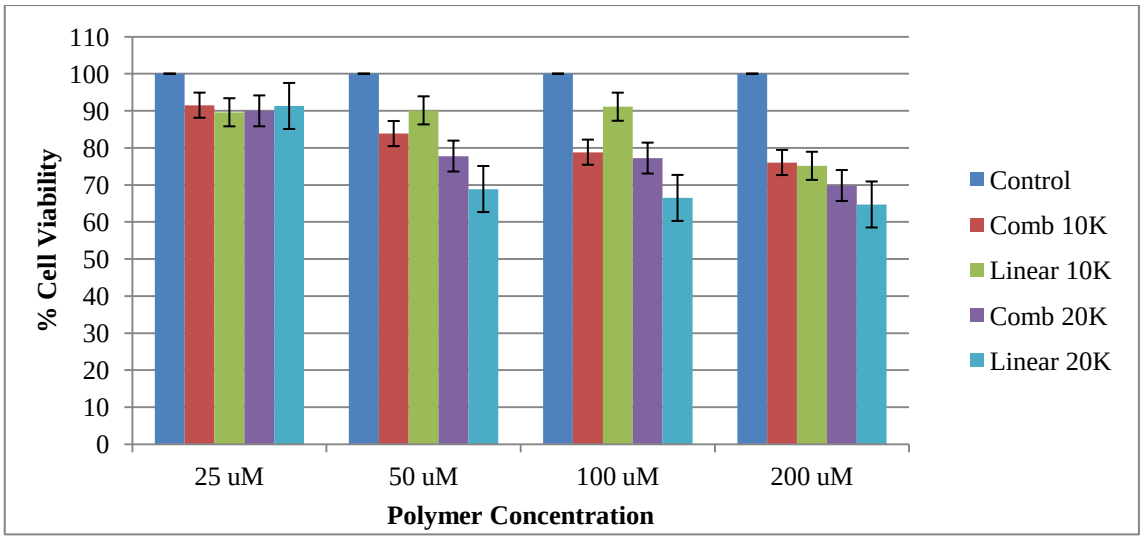

Figure 4.9. The percent cell viability of BEAS-2B cell line after incubation with polymers for 24 hours.

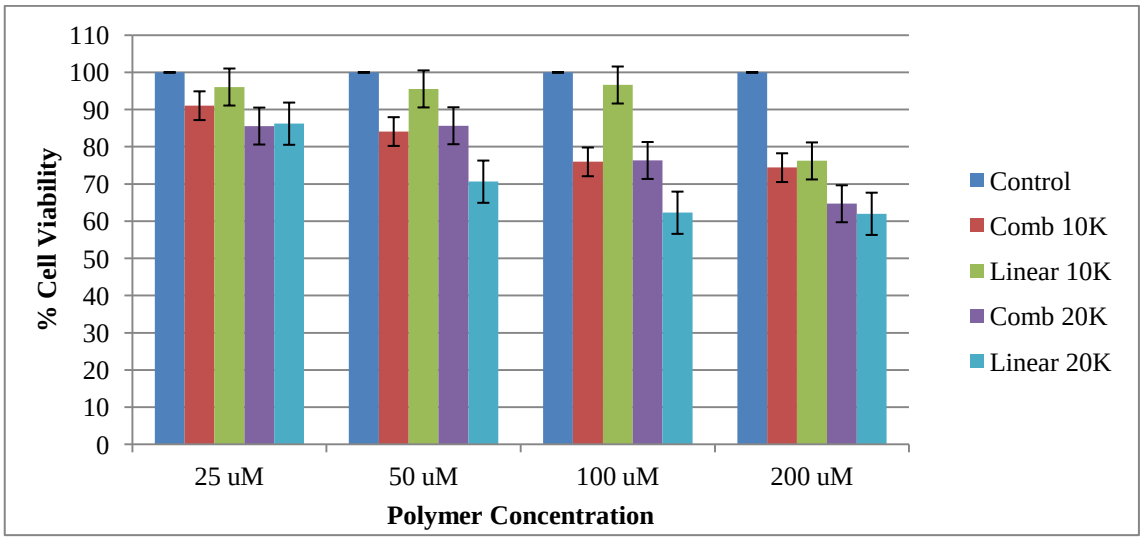

Figure 4.10. The percent cell viability of BEAS-2B cell line after incubation with polymers for 72 hours.

These results are consistent with literature. Comb-type PEG, linear PEG and their conjugates with salmon calcitonin were also demonstrated to be non-toxic on HT29-MTX-E12 (E12) and Caco-2 cell lines (Ryan, Wang et al. 2009). Incubation of E12 and Caco-2 cells with comb-type PEG (6.5 kDa) at 1 mg/ml concentration resulted in 83% and 89% cell viability, respectively. It was also revealed that linear PEG polymers at different molecular weight (5kDa and 1.1 kDa) have no significant effects on viability of (E12) and Caco-2 cell lines (Ryan, Wang et al. 2009).

Chang et al. investigated cytotoxicity of RAFT-synthesized p(PEG-A) on NIH 3T3 cells. Significant cytotoxicity ($p<0.05$ ANOVA test) was observed when cells were

incubated with RAFT end-group ended p(PEG-A) due to the instable nature of the RAFT end-group. After removing the RAFT end-group via aminolysis and capping, cell viabilities were significantly increased from 50% to 75% suggesting that the thiol chain end was a significant source of toxicity and cytotoxicity can be reduced by deactivation of the free thiols (Chang, Bays et al. 2009).

4.4. Effect of Polymers on Membrane Integrity

Measuring the leakage of lactate dehydrogenase (LDH) enzyme from cells upon exposure to various agents at non-cytotoxic concentration range is a common way to test the membrane permeability differences (Mager, Eiriksdottir et al. 2010; Benfer and Kissel 2012).

Figure 4.11 shows the LDH release (%) of A549 cell line as a function of polymer dose and type for 24 and 72 hours of incubation. It can be seen that polymers caused a dose dependent LDH release. Comb-type and linear 20K polymers at 200 µM caused a significant increase in LDH release ($p<0.05$ ANOVA test) after 72 h of incubation. This result was consistent with the MTT results as comb-type and linear 20K polymers at 200 µM concentration showed significant cytotoxic effects on A549 cells.

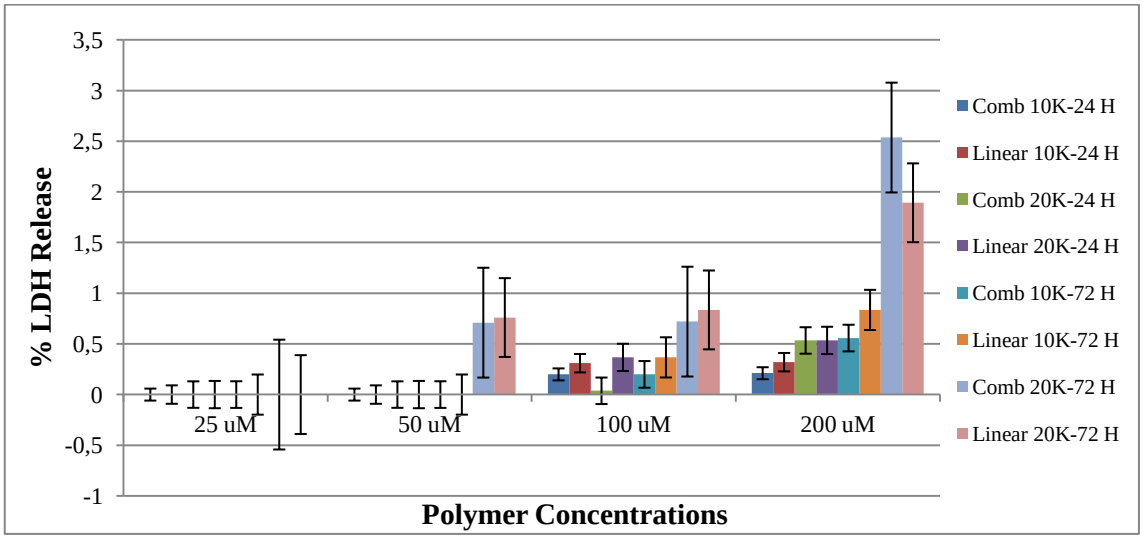

Figure 4.11. The percent LDH release of A549 cells after incubation with polymers for 24 or 72 h.

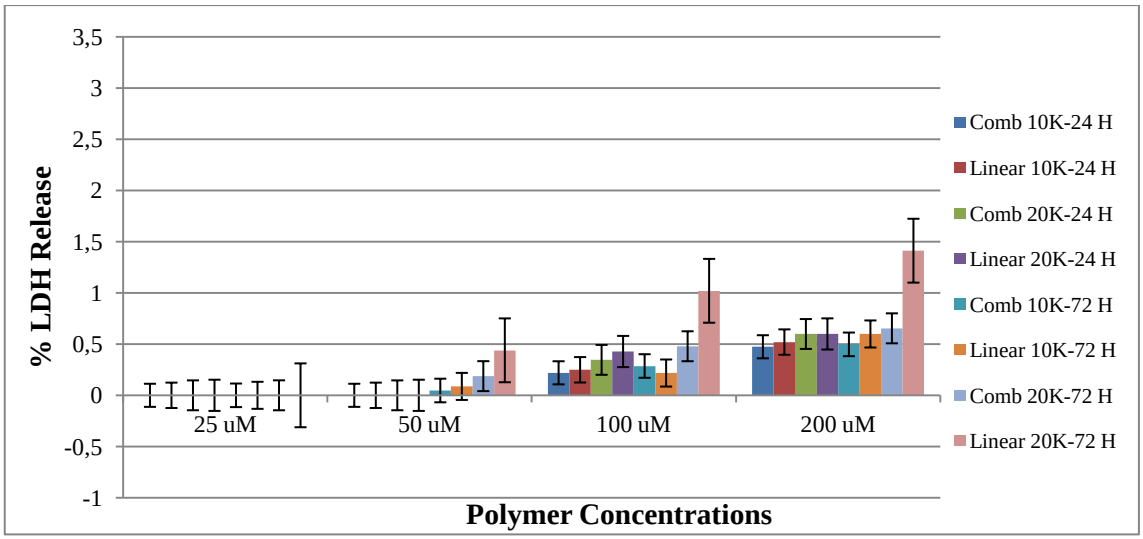

Figure 4.12. The percent LDH release of BEAS-2B cells after incubation with polymers for 24 or 72 h.

Figure 4.12 shows the LDH release (%) of BEAS-2B cell line as a function of polymer dose and type for 24 and 72 hours of incubation. Similar to A549 cell line, polymers caused dose dependent LDH release increase. Linear 20K polymers at 100 and 200 μM caused a significant increase in LDH release ($p<0.05$), consistent with cytotoxicity data. There was no significant difference between the effects of both types of polymer on cell membrane integrity. Nevertheless, the LDH release caused by polymers was relatively very small (only less than 2.5 % for A549 cells and 1.5 % for BEAS-2B cells, which indicates that none of the polymers disrupts significantly the cell membrane integrity.

The LDH release results are consistent with the literature studies. Pissuwan et al. reported that LDH release increased only between 0.4% -1% of the positive control after exposure of CHO-K1, NIH3T3 and Raw264.7 cell lines with RAFT-synthesized p(PEG-A) for 24 hours at 500 μM (Pissuwan, Boyer et al. 2010). Hong et al. investigated the effect of linear PEG (M_n: 16300 g/mol, PDI: 1.22) on membrane permeability and conclude that PEG do not induce hole formation or enlarge the size of preexisting damages in membrane (Hong, Leroueil et al. 2006).

4.5. Cell Uptake of Polymers

Cellular uptake of comb-type and linear polymers was determined via flow cytometry analyses. The energy dependency of cellular uptake was investigated by incubating cells with polymers at either 37^{o}C or 4^{o}C. Separately, cells were also incubated with polymers at varying concentrations for varying incubation times to determine the effect of these parameters on cell uptake. In order to assess the effect of transport inhibitors on cellular uptake of polymers, cells were incubated with polymers in the presence of the transport inhibitors. In all these experiments, the levels of polymer uptake were presented as a mean fluorescence percentage with respect to control cells calculated according to Equation 3.3.

4.5.1 Energy Dependence of Polymer Uptake

In order to determine whether polymer uptake was an active or passive process, cells were incubated with polymers at 37^{o}C or 4^{o}C for 1h. It is known that lowered incubation temperatures inhibit active cell uptake processes (Iacopetta and Morgan 1983; Khalil, Kogure et al. 2006). In preliminary experiments, it was determined that an incubation period of 3h was sufficient for cells to take up polymers at 37^{o}C.

As expected, exposure of polymers at 4^{o}C resulted in the reduction of cellular polymer uptake by cells due to the inhibition of endocytosis for all polymer types in both cell lines (Figure 4.13 and Figure 4.14). This cellular uptake profile revealed that both linear and comb-type polymers at different molecular weights are internalized via energy-dependent mechanisms.

Similar results were reported in literature for linear PEG internalization mechanism. The uptake of PEG polymers was found to be diminished completely at 4°C (Yu, Zhao et al. 2004).

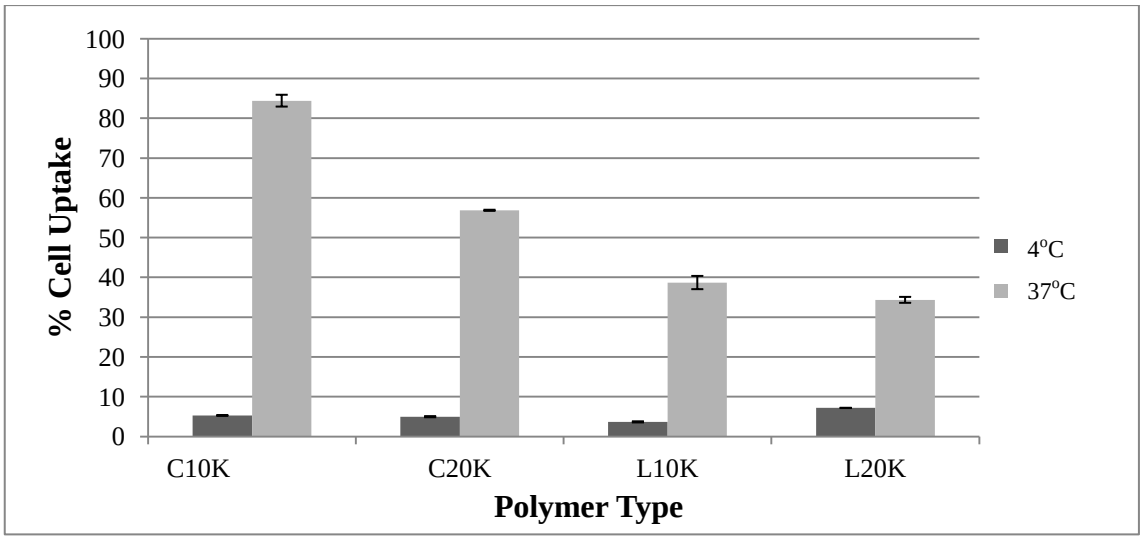

Figure 4.13. Polymer uptake profile of A549 cells at 37°C and 4°C. The polymer concentration and incubation time are 12.5 μM and 1h, respectively.

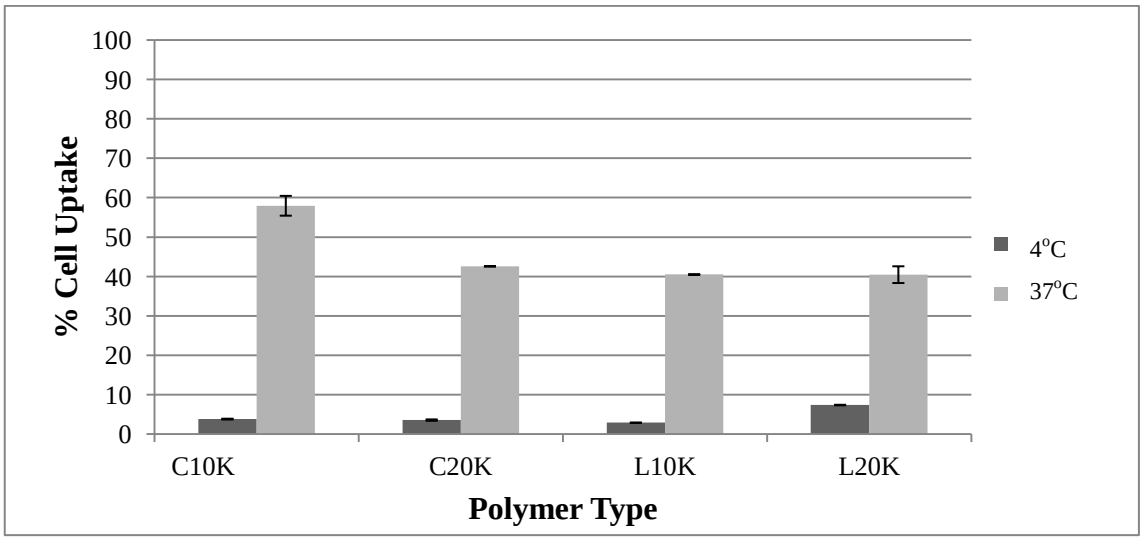

Figure 4.14. Polymer uptake profile of BEAS-2B cells at 37°C and 4°C. The polymer concentration and incubation time are 12.5 μM and 1h, respectively.

Interestingly, comb-type polymers were found to be taken up more by A549 cells at 37°C regardless of molecular weight when compared with the linear type. In case of BEAS-2B cells, comb-type 10K polymers were internalized more than the linear 10K polymers while the uptake of 20K polymers was not dependent on the polymer architecture.

4.5.2 The Effect of Polymer Concentration and Incubation Time on Cellular Uptake of Polymers

Cellular uptake of both types of polymers increased in a dose-dependent manner in both cell lines as it can be seen from Figures 4.15 and 4.16. Percent cell uptake values of all polymers at 25 μM were significantly different from the values at 12.5 μM. Additionally, for A549 cells, longer incubation times resulted in higher uptake of linear PEGs while incubation time did not have a similar effect on the uptake of comb-type polymers, suggesting that the uptake of linear PEG is slower than the uptake of comb-type PEGs. For BEAS-2B cells, cell uptake values after 3h of incubation were significantly higher than the values after 1h for both polymers. Again, it was noted that the uptake of comb-type PEG at 12.5 μM concentration was higher than the uptake of its linear counterpart at the same concentration.

In literature, it was reported that PEG polymers accumulated in the macrophages in a time-and dose-dependent fashion (Yu, Zhao et al. 2004). It was also showed that comb-type PEG containing micelles, $PMMA_{48}$-b-$P(PEGMEMA)_{75,}$ were taken up by cells with increasing micelle concentrations and incubation durations (Kim, Pourgholami et al. 2011).

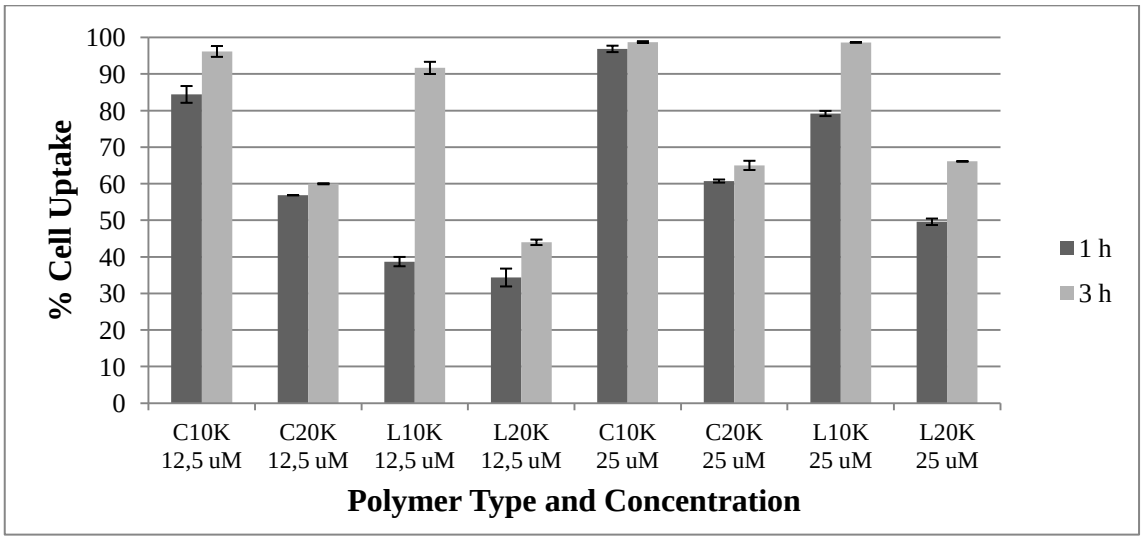

Figure 4.15. Polymer uptake profile of A549 cell line at 12.5 and 25 μM for 1h and 3h

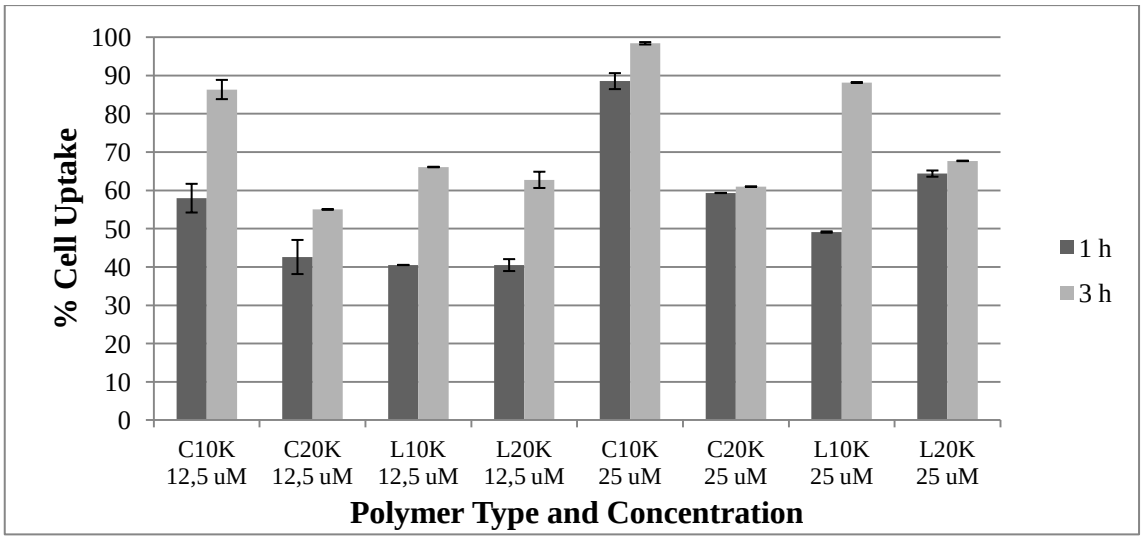

Figure 4.16. Polymer uptake profile of BEAS-2B cell line at 12.5 and 25 μM for 1h and 3h.

In the literature, one of the main disadvantages of linear PEG usage is stated to be low cellular internalization (Kunath, Merdan et al. 2003). However, comb-type 10K PEGs were found to be taken up significantly higher than linear PEGs at the same molecular weight.

According to Figures 4.15 and 4.16, it was concluded that A549 cell line takes up more polymer than BEAS-2B cell line at the same conditions. This may be due to cancerogenic character of A549 cell line. The difference in uptake rates and amounts of different polymers may be attributed to the differences in chemical structure and hydrodynamic conformation of polymers.

4.5.3 The Effect of Transport Inhibitors on Cellular Uptake of Polymers

Certain cell treatments can inhibit internalization via endocytosis, which is generally useful in determining the uptake pathways. The cytoskeleton plays an important role in multiple cellular activities including endocytosis. The role of two major constituents of the cytoskeleton that are microtubules and actin filaments were investigated in polymer uptake. Nocodazole and cytochalasin D as transport inhibitors were utilized to investigate uptake pathways (Khalil, Kogure et al. 2006; Saha, Kim et al. 2013).

Cytochalasin D is a well-known actin-disrupting agent and used for investigating the role of the actin filaments in polymer uptake (Khalil, Kogure et al. 2006; Mager, Eiriksdottir et al. 2010; Al Soraj, He et al. 2012). Nocodazole is a microtubule depolymerization inhibitor and used in order to assess the influence of microtubules on polymer internalization by A549 and BEAS-2B cell lines (dos Santos, Varela et al. 2011).

4.5.3.1 Cellular Toxicity of Transport Inhibitors

Transport inhibitors may have cytotoxic effects on cells while inhibiting cellular uptake pathways. It is therefore essential to investigate the cellular toxicity of each transport inhibitors to determine the inhibitor concentration that can be used in further experiments at their working concentrations prior to cellular uptake experiments with polymers.

The toxic concentrations of each transport inhibitor for several cell lines have been given in literature. It was reported that microtubule structure of human airway epithelia cells depolymerized after treatment with 33 μM nocodazole for 30 minutes. It was also reported that incubation of A549 cells with 10 μg/ml cytochalasin D for 1h blocked actin polymerization (Odrljin, Haidaris et al. 2001). Additionally, the combination of 33 μM nocodazole and 25 μg/ml cytochalasin D was found to trigger complete inhibition of endocytosis (Yi, Harson et al. 2001). It was also reported that incubating A549 cells with 5 μg/ml cytochalasin A and 20 μM nocodazole for 30 minutes inhibited actin polymerization and the depolymerization of microtubules (dos Santos, Varela et al. 2011). However, the cytotoxic effects of 20 μM nocodazole and 5 μg/ml cytochalasin A were found to be approximately 97% and 75%, respectively (dos Santos, Varela et al. 2011). In summary, literature reports indicate that optimization of incubation conditions is essential to determine the right concentration of transport inhibitors and the incubation time that would promise inhibition of endocytosis without severe side effects on cellular viability.

Consequently, prior to experiments with polymers viability of cells was assessed after 3 h of exposure to each inhibitor. Results shown in Figure 4.17 indicated a dose-dependent toxicity of nocodazole. However, even after incubation with 60 μM nocodazole, cellular viability was still greater than 90 % and 80 % for A549 and BEAS-

2B, respectively. Based on these results, a nocodazole concentration of 20 μM was selected for transport inhibition experiments.

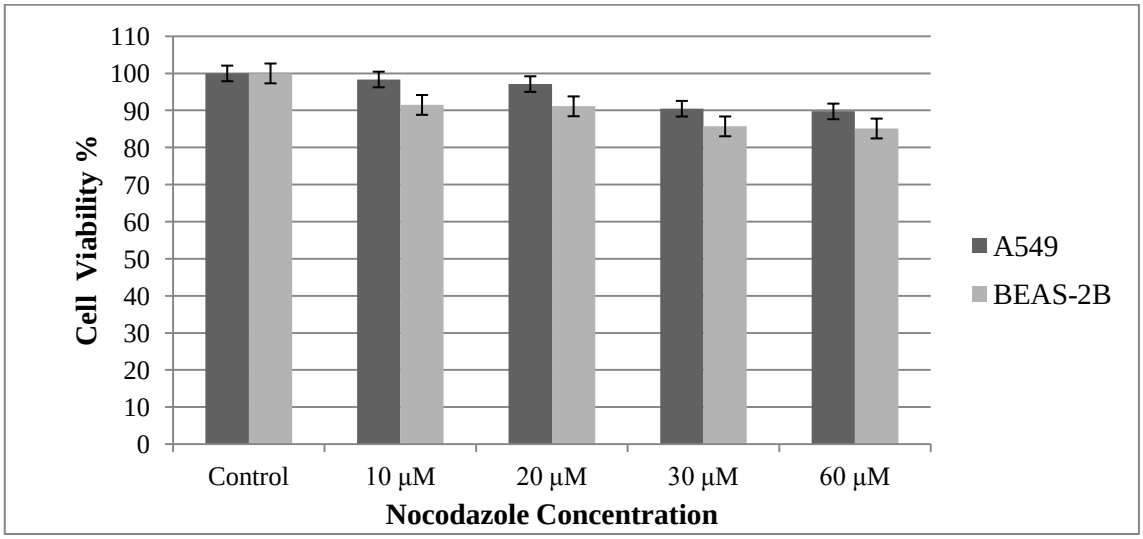

Figure 4.17. Viability of A549 and BEAS-2B cells after exposure to varying concentrations of nocodazole for 3 hours.

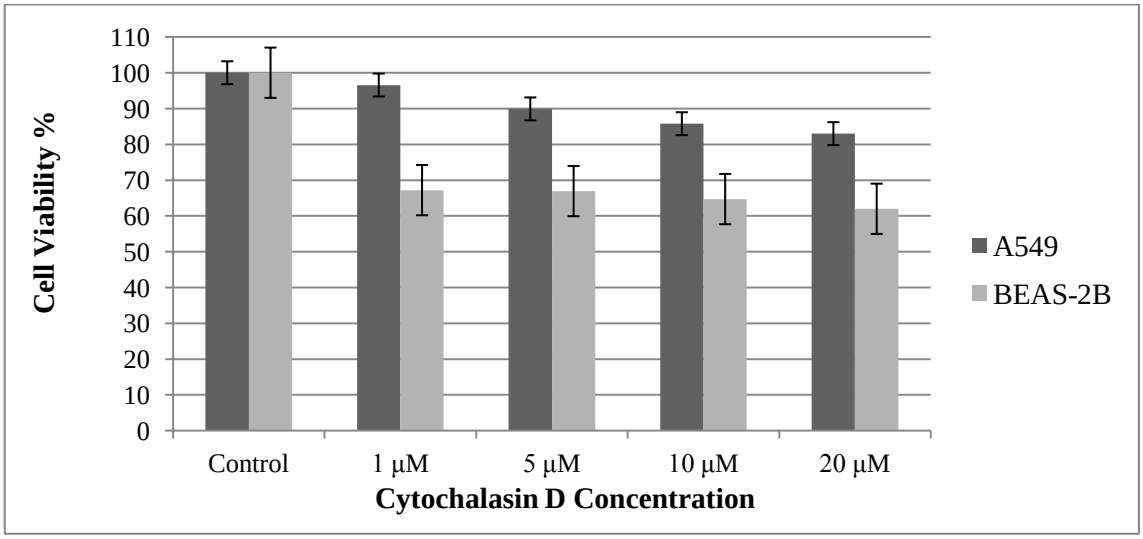

Figure 4.18. Viability of A549 and BEAS-2B cells after exposure to varying concentrations of cytochalasin D for 3 hours.

According to Figure 4.18, cytochalasin D was found to have more cytotoxic effect especially on BEAS-2B cell line compared to nocodazole. A cytochalasin D concentration of 10 μM was selected for transport inhibition experiments.

The viability of both cells in the presence of both inhibitors was also determined via MTT assay. The result of this experiment is shown in Figure 4.19. In the presence of the both types of inhibitors, cell viability reduced to 61% of the control for both of the

cell lines. Since cell viability was still greater than 50% and very close each other in both cell lines, it was 20 μM nocodazole and 10 μM cytochalasin D were decided to be used in further experiments.

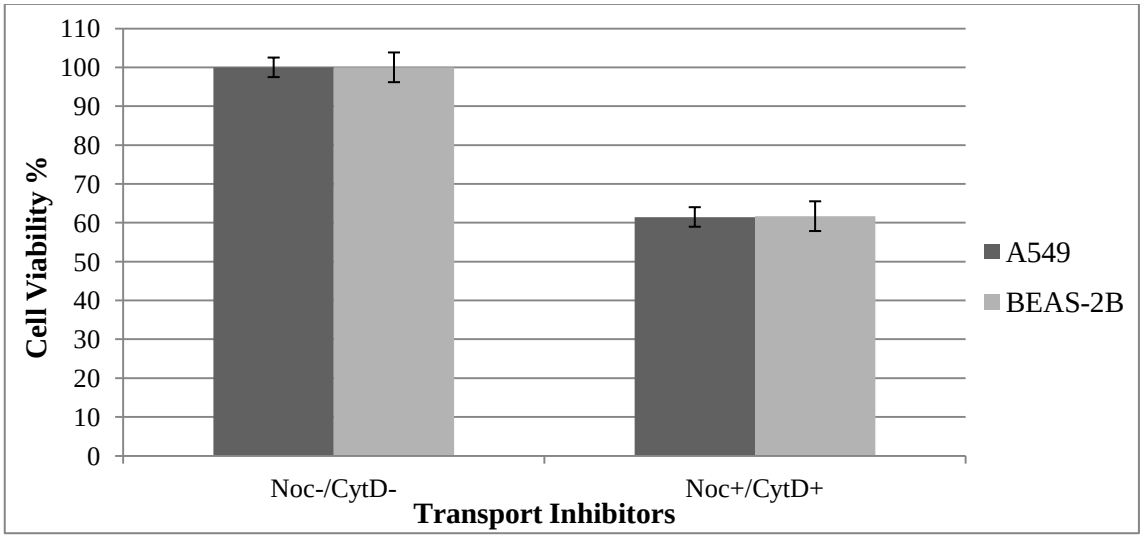

Figure 4.19. Viability of A549 and BEAS-2B cells after exposure to 20 μM nocodazole and 10 μM cytochalasin D for 3 hours.

4.5.3.2 Cell Uptake Pathway of Polymers

Effect of transport inhibitors on cellular uptake of polymers was determined via flow cytometry. The comb- type 10K polymer uptake results after treatment with inhibitors are shown in Figure 4.20 for A549 and BEAS-2B cells. Nocodazole had no significant effect on internalization of comb-type 10K polymer by A549 cells ($p>0.05$), while it displayed a significant reduction in the uptake by BEAS-2B cells ($p<0.05$). In contrast, Cytochalasin D caused a substantial decrease ($p<0.05$) in polymer uptake in 1 h by A549 cells while it showed no significant effect on the uptake by BEAS-2B cells ($p>0.05$).

In the presence of both types of inhibitors, A549 cells displayed lowered polymer uptake indicating the importance of both pathways (actin and microtubule-dependent) on cellular uptake mechanism.

In BEAS-2B cells, the polymer uptake in 1 h was found to increase in the presence of both types of inhibitors when compared with the uptake in the presence of nocodazole only. Additionally, the uptake in the presence of both inhibitors was almost

the same with the uptake in the presence of cytochalasin D only. Combination of both results may indicate that blocking one pathway (i.e. microtubule-dependent) may activate other endocytic pathways.

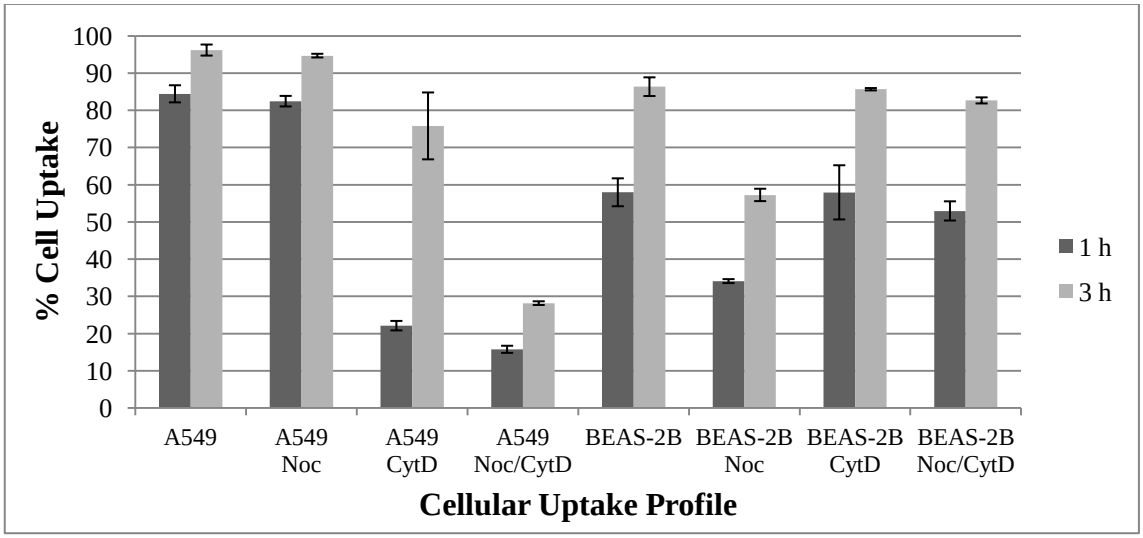

Figure 4.20. Uptake of comb-type 10K PEG by A549 and BEAS-2B cells. Polymer concentration is 12.5 μM after 1h or 3h.

Similar results were obtained with the comb-type 20K polymers in both cells when cells were incubated in the presence of Noc only, CytD only or both inhibitors (Figure 4.21).

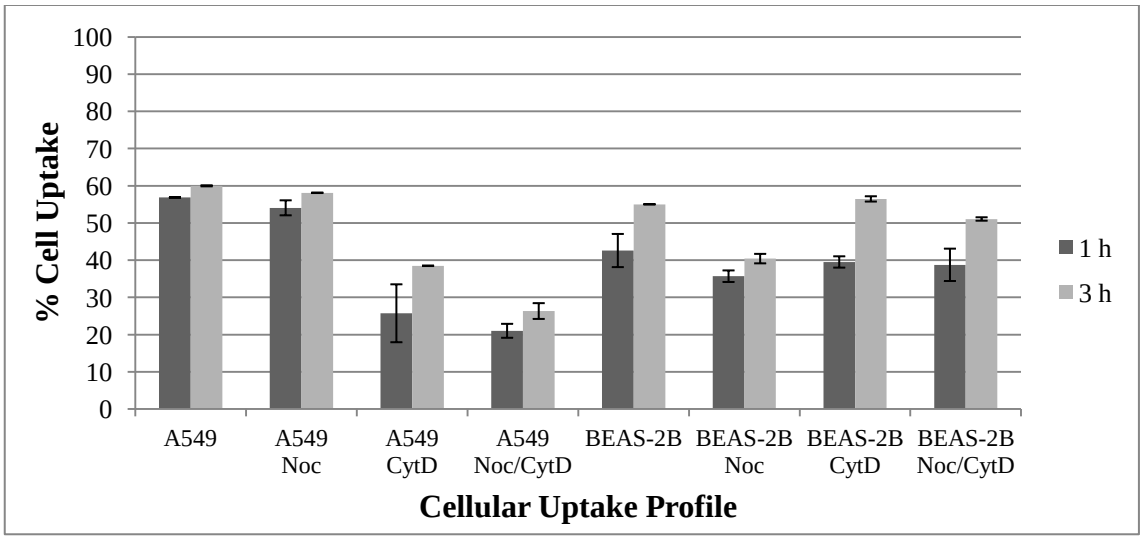

Figure 4.21. Uptake of comb-type 20K PEG by A549 and BEAS-2B cells. Polymer concentration is 12.5 μM after 1h or 3h.

As a result of the cellular uptake experiments with transport inhibitors, it was concluded that comb-types polymers are internalized by A549 cells mainly via actin-dependent pathway, although it seemed that inhibition of microtubule dependent pathway blocks the polymer uptake when actin-dependent pathway is inhibited. Overall, these results suggest that comb-type PEGs (both 10K and 20K) are internalized by mainly actin-dependent pathways, however when this pathway is inhibited microtubule-dependent pathway takes role in the internalization of polymers. In contrast, in BEAS-2B cells, the main uptake mechanism of comb-type polymers is microtubule-dependent. However, other endocytic pathways start taking role in internalization process when microtubule-dependent pathway is inhibited. As a result, comb-type PEG polymers possess different uptake mechanisms in normal and cancer cells.

The linear PEG (10K and 20K) uptake results are given in Figures 4.22 and 4.23. According to data, linear 10K and 20K polymers are internalized by A549 cells via different pathways. Linear 20K PEG is taken up by cells by both actin and microtubule-dependent pathways. In case of linear 10K, actin- dependent pathway appears to be the main uptake mechanism. However, when actin-dependent and microtubule-dependent pathways are both inhibited, linear 10K PEG uptake by A549 cells becomes less, suggesting that actin-dependent pathway takes role in the uptake process when microtubule dependent pathway is inhibited.

BEAS-2B cells take up both linear 10K and 20K PEG mainly via microtubule-dependent pathway. On the other hand, when both microtubule and actin-dependents are blocked, other endocytic pathways appear to be involved in the uptake process of linear PEGs.

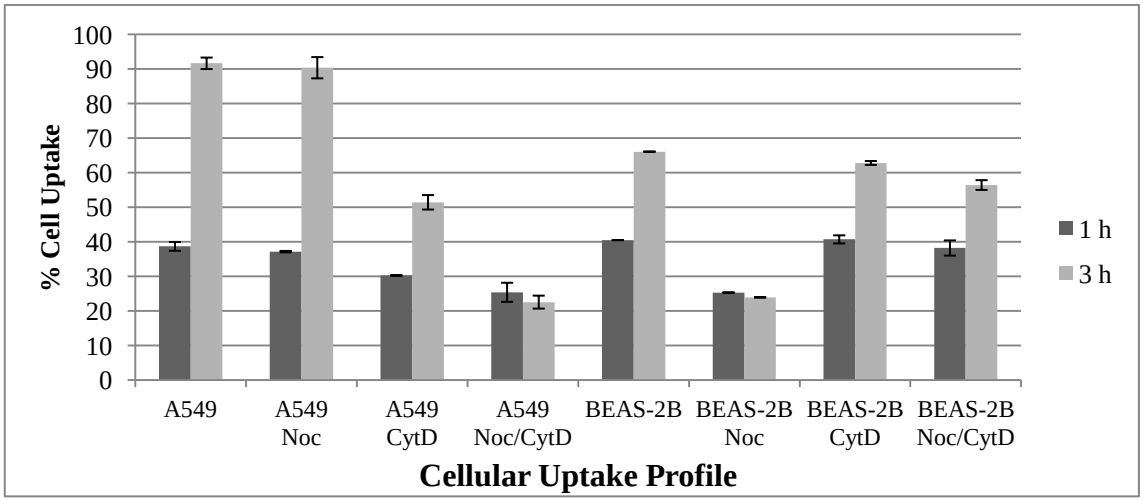

Figure 4.22. Uptake of linear 10K PEG by A549 and BEAS-2B cells. Polymer concentration is 12.5 μM after 1h or 3h.

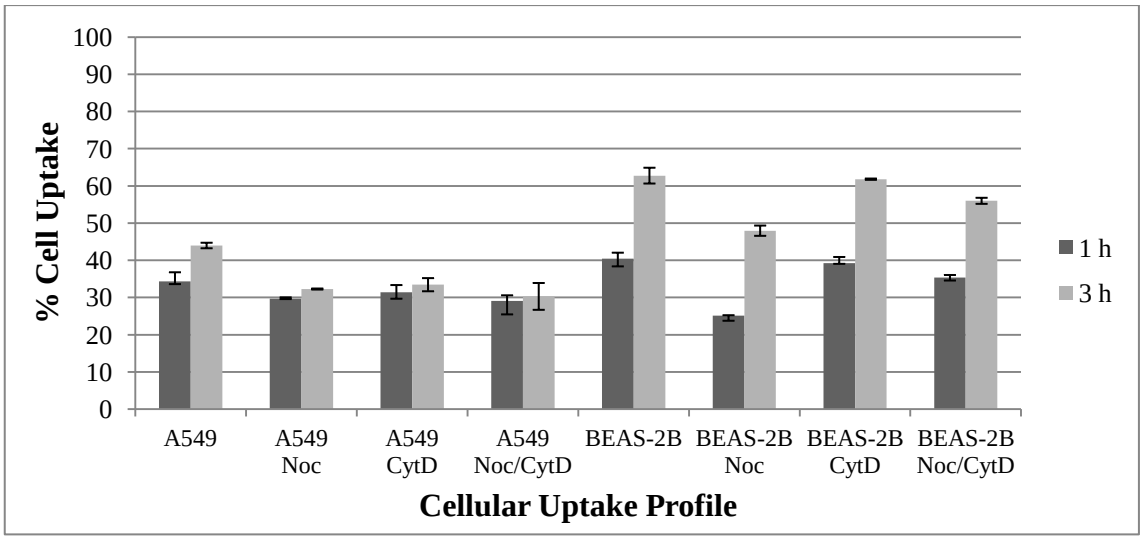

Figure 4. 23. Uptake of linear 20K PEG by A549 and BEAS-2B cells. Polymer concentration is 12.5 μM after 1h or 3h.

4.6. Intracellular Localization of Polymers

The intracellular distribution of polymers was determined via fluorescence microscopy. Polymers were labeled with Oregon Green. Nucleus was stained selectively by DAPI (4',6-Diamidino-2-Phenylindole Dilactate) a blue fluorescent dye. The images of A549 and BEAS-2B cells after incubation with polymers are shown in Figures 4.24 – 4.31.

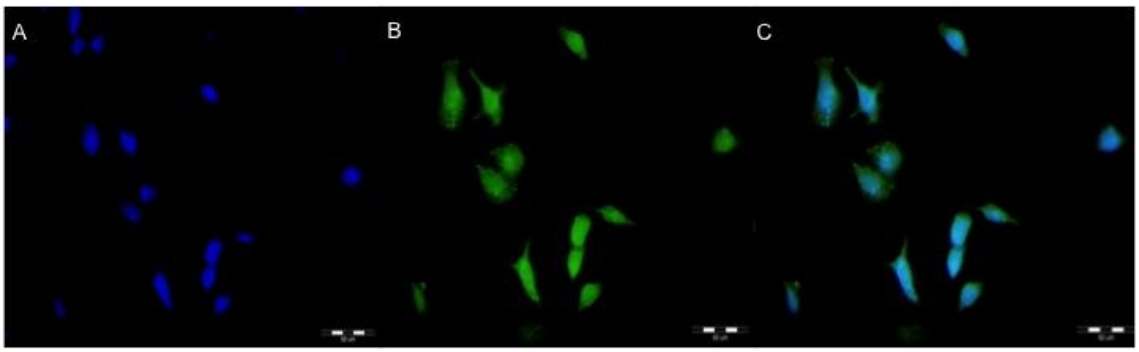

Figure 4.24. Fluorescence micrographs of A549 cells after incubation with Oregon green labeled comb-type 10K PEG at 40X magnification a) Nucleus staining by DAPI b) Oregon green stained comb-type 10K polymers c) Merge of a and b. Scale bar is 50 μm.

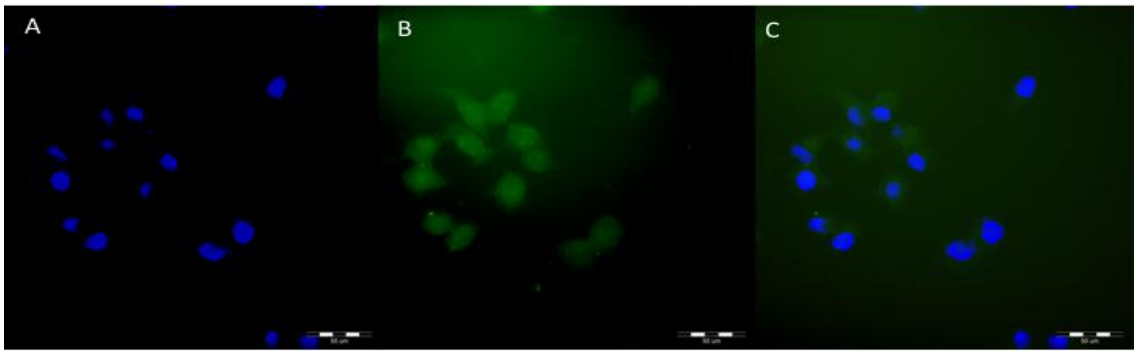

Figure 4.25. Fluorescence micrographs of A549 cells after incubation with Oregon green labeled comb-type 20K PEG at 40X magnification a) Nucleus staining by DAPI b) Oregon green stained comb-type 10K polymers c) Merge of a and b. Scale bar is 50 μm.

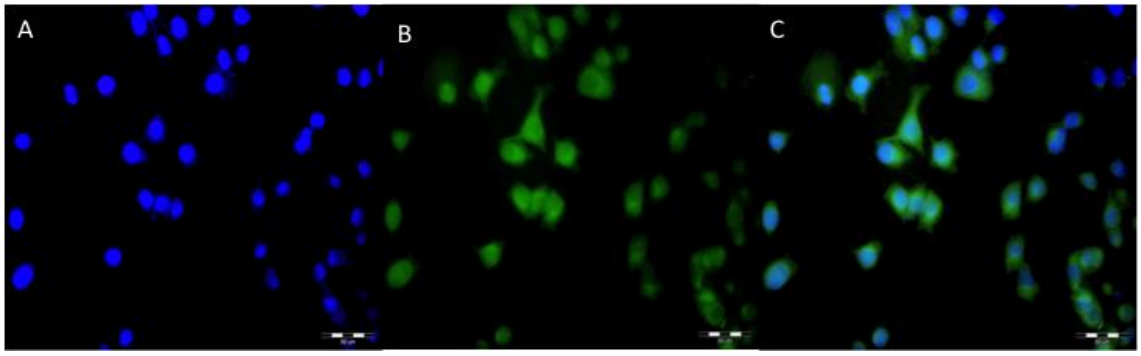

Figure 4.26. Fluorescence micrographs of A549 cells after incubation with Oregon green labeled linear 10K PEG at 40X magnification a) Nucleus staining by DAPI b) Oregon green stained comb-type 10K polymers c) Merge of a and b. Scale bar is 50 μm.

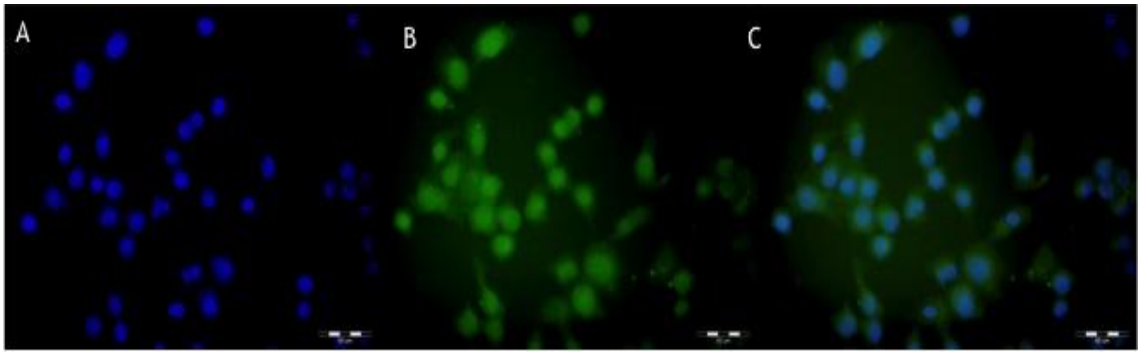

Figure 4.27. Fluorescence micrographs of A549 cells after incubation with Oregon green labeled comb-type 10K PEG at 40X magnification a) Nucleus staining by DAPI b) Oregon green stained comb-type 10K polymers c) Merge of a and b. Scale bar is 50 μm.

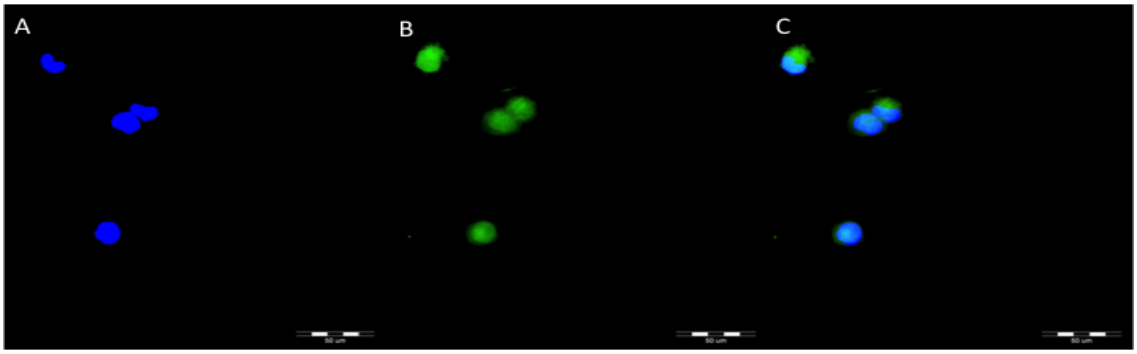

Figure 4.28. Fluorescence micrographs of BEAS-2B cells after incubation with Oregon green labeled comb-type 10K PEG at 40X magnification a) Nucleus staining by DAPI b) Oregon green stained comb-type 10K polymers c) Merge of a and b. Scale bar is 100 μm.

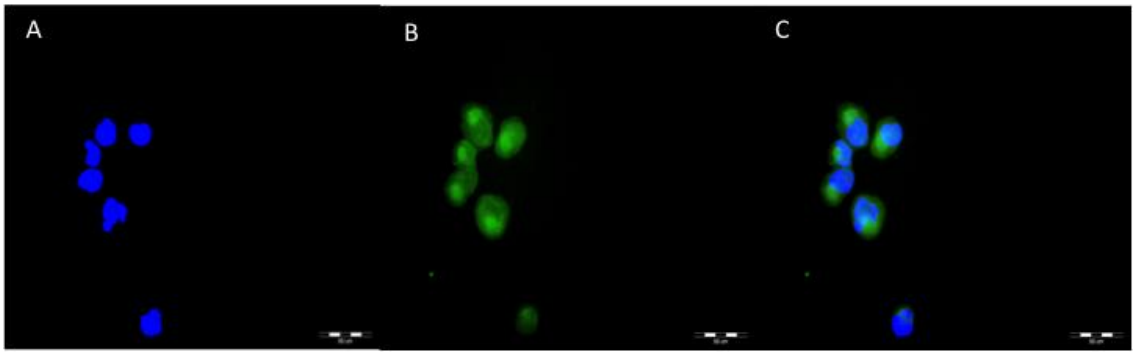

Figure 4.29. Fluorescence micrographs of BEAS-2B cells after incubation with Oregon green labeled comb-type 20K PEG at 40X magnification a) Nucleus staining by DAPI b) Oregon green stained comb-type 10K polymers c) Merge of a and b. Scale bar is 100 μm.

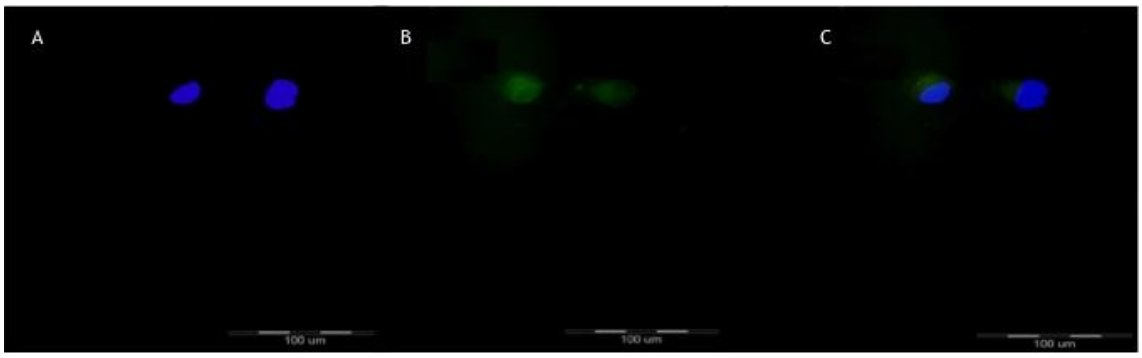

Figure 4.30. Fluorescence micrographs of BEAS-2B cells after incubation with Oregon green labeled linear 10K PEG at 40X magnification a) Nucleus staining by DAPI b) Oregon green stained comb-type 10K polymers c) Merge of a and b. Scale bar is 100 μm.

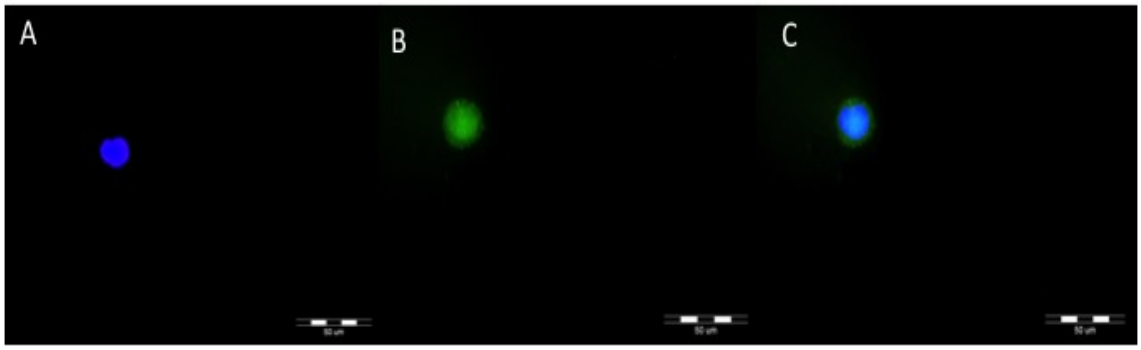

Figure 4.31. Fluorescence micrographs of BEAS-2B cells after incubation with Oregon green labeled linear 20K PEG at 40X magnification a) Nucleus staining by DAPI b) Oregon green stained comb-type 10K polymers c) Merge of a and b. Scale bar is 100 μm.

According to the fluorescence microscopic analysis, green-labeled linear and comb-type PEGs were localized in cytoplasm predominantly. However, comb-type 10K polymer mainly demonstrated punctual distribution pattern due to accumulation in endocytic vesicles.

CHAPTER 5

CONCLUSION

The aim of this thesis was to investigate interactions of *in vitro* cultured cells with comb-type PEG, poly(polyethylene glycol) methyl ether methacrylate (p(PEG-MA)), and compare to linear PEG counterparts.

Comb-type poly(ethylene glycol) methyl ether methacrylate p(PEG-MA) polymers having molecular weights of 10,000 g/mol and 20,000 g/mol were synthesized via reversible addition fragmentation chain transfer (RAFT) polymerization. Linear PEG counterparts at the same molecular weights were purchased. The molecular weight range of the polymers was deliberately chosen below the *in vivo* renal clearance threshold for soluble polymers (<20,000 g/mol) considering the potential use of these polymers as polymer therapeutics.

Characterization of both types of polymers was performed via Nuclear Magnetic Resonance Spectroscopy (NMR), Gel Permeation Chromatography (GPC) and Dynamic Light Scattering (DLS). The results obtained from GPC measurements and NMR spectroscopy proved the successful synthesis of comb-type PEG polymers at defined molecular weight and narrow polydispersity (<1.2) under the synthesis conditions. DLS experiments showed that the comb-type polymers have smaller hydrodynamic diameters when compared with linear PEG counterparts. Comb-type polymers also displayed increased diameters after incubation in serum containing cell culture media while linear PEG counterparts did not suggesting the presence of possible interactions of comb-type polymers with serum proteins.

Human lung adenocarcinoma epithelial cell line (A549) and its non-cancerous counterpart- human bronchial epithelium cell line (BEAS-2B)- were used as model cell lines for developing a comperative study.

In vitro cytotoxicity of polymers on cytotoxicity was determined via MTT assay. Both types of polymers showed dose dependent toxicity. However, the lowest cell viability observed with comb-type PEG at 200 μM concentration for 72 h was only 57% of the untreated cells.

The effect of polymers on cell membrane integrity was determined via LDH assay. Both types of polymers enhanced membrane permeability of both cell lines in a dose-dependent manner, supporting MTT assay results. Nevertheless, LDH release differences were below 2% of control cells, which can be considered insignificant.

The cellular uptake of PEG polymers was determined via flow cytometry analyses. It was revealed that both linear and comb-type polymers at different molecular weights were internalized via energy-dependent mechanisms. Cellular uptake of polymers increases in a dose and incubation time dependent manner in both cell lines.

The amount of internalized polymer was depended on hydrodynamic volume and internalization mechanism properties and also consistent in each cell line. Comb-type 10K polymer was taken most due to its smallest hydrodynamic volume while comb-type 20K polymers have lower internalization even it has very close hydrodynamic volume to comb-type 10K polymer. Therefore, comb-type PEG polymers were also found to overcome the low cellular internalization problem of linear PEGs at equivalent molecular weight. Therefore, comb-type PEG polymers offer an alternative PEG with better cellular uptake properties.

The dependence of internalization mechanism of polymers on cytoskeleton components was tried to estimate by using transport inhibitors that are nocodazole (microtubule blocker) and cytochalasin D (actin blocker). Comb-type and linear PEG polymers were internalized via microtubule dependent mechanisms in BEAS-2B cell lines. In contrast, comb-type polymers are internalized by A549 cells mainly via actin-dependent pathway. Therefore, comb-type PEG polymers possess different uptake mechanisms in normal and cancer cells that may provide a potential for selective targeting strategies. Linear 10K polymers demonstrated actin dependent internalization pathway in A549 cell line whereas only microtubule dependent in BEAS-2B cell line similar to comb-type PEG internalization. However, as the hydrodynamic size increases in FBS included RPMI cell culture medium; both types of inhibitors began to have significant effects on uptake of Linear 20K in A549 cell line. Therefore, the internalization mechanism of PEG polymers was found to depend on hydrodynamic size of polymers.

Linear and comb-type PEG were found to be localized in endocytic vesicles and cytosol.

As conclusion, comb-type PEGs offers an alternative to linear PEG with better cellular uptake properties and different uptake mechanisms by normal and cancer cells that may provide a potential for selective targeting strategies.

Overall, this study provides preliminary data for comparison of linear and comb-type PEG in terms of physicochemical properties and interactions with both normal and cancerogenic cell lines.

The follows suggestions can be made for future studies;

1. The cellular uptake of PEG polymers may be investigated in more detail with different types of transport inhibitors such as genestein (caveolae mediated endocytosis inhibitor), wortmannin (macropinocytosis inhibitor) and chlorpromazine (clathrin mediated endocystosis inhibitors (Khalil, Kogure et al. 2006).

2. The intracellular distribution of PEG polymers may be investigated in more detail using additional organelle-specific dyes.

REFERENCES

Abilez, O., P. Benharash, et al. (2006). "A novel culture system shows that stem cells can be grown in 3D and under physiologic pulsatile conditions for tissue engineering of vascular grafts." Journal of Surgical Research **132**(2): 170-178.

Al Soraj, M., L. He, et al. (2012). "siRNA and pharmacological inhibition of endocytic pathways to characterize the differential role of macropinocytosis and the actin cytoskeleton on cellular uptake of dextran and cationic cell penetrating peptides octaarginine (R8) and HIV-Tat." J Control Release **161**(1): 132-141.

Armstrong, J. K., R. B. Wenby, et al. (2004). "The hydrodynamic radii of macromolecules and their effect on red blood cell aggregation." Biophys J **87**(6): 4259-4270.

Bailon, P., A. Palleroni, et al. (2001). "Rational design of a potent, long-lasting form of interferon: a 40 kDa branched polyethylene glycol-conjugated interferon alpha-2a for the treatment of hepatitis C." Bioconjug Chem **12**(2): 195-202.

Barner-Kowollik, C. (2008). Handbook of RAFT Polymerization. Darmstadt, Germany, WILEY-VCH.

Barner-Kowollik, C. and S. Perrier (2008). "The future of reversible addition fragmentation chain transfer polymerization." Journal of Polymer Science Part a-Polymer Chemistry **46**(17): 5715-5723.

Bays, E., L. Tao, et al. (2009). "Synthesis of semitelechelic maleimide poly(PEGA) for protein conjugation by RAFT polymerization." Biomacromolecules **10**(7): 1777-1781.

Benfer, M. and T. Kissel (2012). "Cellular uptake mechanism and knockdown activity of siRNA-loaded biodegradable DEAPA-PVA-g-PLGA nanoparticles." European Journal of Pharmaceutics and Biopharmaceutics **80**(2): 247-256.

Bouladjine, A., A. Al-Kattan, et al. (2009). "New advances in nanocrystalline apatite colloids intended for cellular drug delivery." Langmuir **25**(20): 12256-12265.

Boyer, C., A. Granville, et al. (2009). "Modification of RAFT-Polymers via Thiol-Ene Reactions: A General Route to Functional Polymers and New Architectures." Journal of Polymer Science Part a-Polymer Chemistry **47**(15): 3773-3794.

Bulmus, V. (2011). "RAFT polymerization mediated bioconjugation strategies." Polymer Chemistry **2**(7): 1463-1472.

Caliceti, P., O. Schiavon, et al. (2001). "Immunological properties of uricase conjugated to neutral soluble polymers." Bioconjug Chem **12**(4): 515-522.

Caliceti, P. and F. M. Veronese (2003). "Pharmacokinetic and biodistribution properties of poly(ethylene glycol)-protein conjugates." Advanced Drug Delivery Reviews **55**(10): 1261-1277.

Chang, C. W., E. Bays, et al. (2009). "Differences in cytotoxicity of poly(PEGA)s synthesized by reversible addition-fragmentation chain transfer polymerization." Chemical Communications(24): 3580-3582.

Charrois, G. J. and T. M. Allen (2004). "Drug release rate influences the pharmacokinetics, biodistribution, therapeutic activity, and toxicity of pegylated liposomal doxorubicin formulations in murine breast cancer." Biochim Biophys Acta **1663**(1-2): 167-177.

Chithrani, B. D., A. A. Ghazani, et al. (2006). "Determining the size and shape dependence of gold nanoparticle uptake into mammalian cells." Nano Lett **6**(4): 662-668.

Curran, M. and P. McCormack (2008). "Methoxy Polyethylene Glycol-Epoetin Beta." Drugs **68**(8): 1139-1156.

Dardik, A., L. L. Chen, et al. (2005). "Differential effects of orbital and laminar shear stress on endothelial cells." Journal of Vascular Surgery **41**(5): 869-880.

Deshpande, M. C., M. C. Davies, et al. (2004). "The effect of poly(ethylene glycol) molecular architecture on cellular interaction and uptake of DNA complexes." J Control Release **97**(1): 143-156.

Deshpande, M. C., M. C. Garnett, et al. (2002). "Influence of polymer architecture on the structure of complexes formed by PEG-tertiary amine methacrylate copolymers and phosphorothioate oligonucleotide." Journal of Controlled Release **81**(1-2): 185-199.

Dieguez, L. D., N.; Mir, M.; Martinez, E.; Moreno, M.; Samitier, J. (2009). "Effect of the Refractive Index of Buffer Solutions in Evanescent Optical Biosensors." Sensor Letters **7**(5): 851-855.

dos Santos, T., J. Varela, et al. (2011). "Effects of Transport Inhibitors on the Cellular Uptake of Carboxylated Polystyrene Nanoparticles in Different Cell Lines." Plos One **6**(9).

Doss, S. and B. Schiller (2010). "Peginesatide: a potential erythropoiesis stimulating agent for the treatment of anemia of chronic renal failure." Nephrol Nurs J **37**(6): 617-626.

Duncan, R. (2003). "The dawning era of polymer therapeutics." Nature Reviews Drug Discovery **2**(5): 347-360.

Efremova, N. V., S. R. Sheth, et al. (2001). "Protein-Induced Changes in Poly(ethylene glycol) Brushes: Molecular Weight and Temperature Dependence." Langmuir **17**(24): 7628-7636.

Eto, Y., J. Q. Gao, et al. (2005). "PEGylated adenovirus vectors containing RGD peptides on the tip of PEG show high transduction efficiency and antibody evasion ability." J Gene Med **7**(5): 604-612.

Gabizon, A., R. Catane, et al. (1994). "Prolonged circulation time and enhanced accumulation in malignant exudates of doxorubicin encapsulated in polyethylene-glycol coated liposomes." Cancer Res **54**(4): 987-992.

Gabizon, A. and F. Martin (1997). "Polyethylene glycol-coated (pegylated) liposomal doxorubicin. Rationale for use in solid tumours." Drugs **54 Suppl 4**: 15-21.

Gao, W., W. Liu, et al. (2010). "In situ growth of a PEG-like polymer from the C terminus of an intein fusion protein improves pharmacokinetics and tumor accumulation." Proc Natl Acad Sci U S A **107**(38): 16432-16437.

Gao, W., W. Liu, et al. (2009). "In situ growth of a stoichiometric PEG-like conjugate at a protein's N-terminus with significantly improved pharmacokinetics." Proc Natl Acad Sci U S A **106**(36): 15231-15236.

Gauggel, S., C. Derreza-Greeven, et al. (2012). "Characterization of biologically available wood combustion particles in cell culture medium." Altex-Alternatives to Animal Experimentation **29**(2): 183-200.

Gunasekaran, K., T. H. Nguyen, et al. (2011). "Conjugation of siRNA with Comb-Type PEG Enhances Serum Stability and Gene Silencing Efficiency." Macromolecular Rapid Communications **32**(8): 654-659.

Hamidi, M., A. Azadi, et al. (2006). "Pharmacokinetic consequences of pegylation." Drug Delivery **13**(6): 399-409.

Heredia, K. L., T. H. Nguyen, et al. (2008). "Reversible siRNA-polymer conjugates by RAFT polymerization." Chemical Communications(28): 3245-3247.

Hong, R. L., C. J. Huang, et al. (1999). "Direct comparison of liposomal doxorubicin with or without polyethylene glycol coating in C-26 tumor-bearing mice: is surface coating with polyethylene glycol beneficial?" Clin Cancer Res **5**(11): 3645-3652.

Hong, S. P., P. R. Leroueil, et al. (2006). "Interaction of polycationic polymers with supported lipid bilayers and cells: Nanoscale hole formation and enhanced membrane permeability." Bioconjugate Chemistry **17**(3): 728-734.

Iacopetta, B. J. and E. H. Morgan (1983). "The kinetics of transferrin endocytosis and iron uptake from transferrin in rabbit reticulocytes." J Biol Chem **258**(15): 9108-9115.

Jokerst, J. V., T. Lobovkina, et al. (2011). "Nanoparticle PEGylation for imaging and therapy." Nanomedicine (Lond) **6**(4): 715-728.

Kaul, G. and M. Amiji (2004). "Biodistribution and targeting potential of poly(ethylene glycol)-modified gelatin nanoparticles in subcutaneous murine tumor model." J Drug Target **12**(9-10): 585-591.

Kersey, F. R., T. J. Merkel, et al. (2012). "Effect of aspect ratio and deformability on nanoparticle extravasation through nanopores." Langmuir **28**(23): 8773-8781.

Khalil, I. A., K. Kogure, et al. (2006). "Uptake pathways and subsequent intracellular trafficking in nonviral gene delivery." Pharmacol Rev **58**(1): 32-45.

Kim, S. H., J. H. Jeong, et al. (2006). "PEG conjugated VEGF siRNA for anti-angiogenic gene therapy." Journal of Controlled Release **116**(2): 123-129.

Kim, Y., M. H. Pourgholami, et al. (2011). "An Optimized RGD-Decorated Micellar Drug Delivery System for Albendazole for the Treatment of Ovarian Cancer: From RAFT Polymer Synthesis to Cellular Uptake." Macromolecular Bioscience **11**(2): 219-233.

Knop, K., R. Hoogenboom, et al. (2010). "Poly(ethylene glycol) in Drug Delivery: Pros and Cons as Well as Potential Alternatives." Angewandte Chemie-International Edition **49**(36): 6288-6308.

Kunath, K., T. Merdan, et al. (2003). "Integrin targeting using RGD-PEI conjugates for in vitro gene transfer." J Gene Med **5**(7): 588-599.

Lee, L. S., C. Conover, et al. (1999). "Prolonged circulating lives of single-chain Fv proteins conjugated with polyethylene glycol: a comparison of conjugation chemistries and compounds." Bioconjug Chem **10**(6): 973-981.

Mager, I., E. Eiriksdottir, et al. (2010). "Assessing the uptake kinetics and internalization mechanisms of cell-penetrating peptides using a quenched fluorescence assay." Biochimica Et Biophysica Acta-Biomembranes **1798**(3): 338-343.

Mager, I., K. Langel, et al. (2012). "The role of endocytosis on the uptake kinetics of luciferin-conjugated cell-penetrating peptides." Biochimica Et Biophysica Acta-Biomembranes **1818**(3): 502-511.

Moad, G., E. Rizzardo, et al. (2009). "Living Radical Polymerization by the RAFT Process - A Second Update." Australian Journal of Chemistry **62**(11): 1402-1472.

Molineux, G. (2002). "Pegylation: engineering improved pharmaceuticals for enhanced therapy." Cancer Treat Rev **28 Suppl A**: 13-16.

Molino, N. M., K. Bilotkach, et al. (2012). "Complement activation and cell uptake responses toward polymer-functionalized protein nanocapsules." Biomacromolecules **13**(4): 974-981.

Monfardini, C., O. Schiavon, et al. (1995). "A branched monomethoxypoly(ethylene glycol) for protein modification." Bioconjug Chem **6**(1): 62-69.

Mori, A., A. L. Klibanov, et al. (1991). "Influence of the steric barrier activity of amphipathic poly(ethyleneglycol) and ganglioside GM1 on the circulation time of liposomes and on the target binding of immunoliposomes in vivo." FEBS Lett **284**(2): 263-266.

Odrljin, T. M., C. G. Haidaris, et al. (2001). "Integrin alphavbeta3-mediated endocytosis of immobilized fibrinogen by A549 lung alveolar epithelial cells." Am J Respir Cell Mol Biol **24**(1): 12-21.

Ozcan, I., F. Segura-Sanchez, et al. (2010). "Pegylation of poly(gamma-benzyl-L-glutamate) nanoparticles is efficient for avoiding mononuclear phagocyte system capture in rats." Int J Nanomedicine **5**: 1103-1111.

Pissuwan, D., C. Boyer, et al. (2010). "In vitro cytotoxicity of RAFT polymers." Biomacromolecules **11**(2): 412-420.

Qiu, X.-P. and F. M. Winnik (2006). "Facile and Efficient One-Pot Transformation of RAFT Polymer End Groups via a Mild Aminolysis/Michael Addition Sequence." Macromolecular Rapid Communications **27**(19): 1648-1653.

Roth, P. J., D. Kessler, et al. (2008). "A Method for Obtaining Defined End Groups of Polymethacrylates Prepared by the RAFT Process during Aminolysis." Macromolecules **41**(22): 8316-8319.

Ryan, S. M., J. M. Frias, et al. (2011). "PK/PD modelling of comb-shaped PEGylated salmon calcitonin conjugates of differing molecular weights." J Control Release **149**(2): 126-132.

Ryan, S. M., G. Mantovani, et al. (2008). "Advances in PEGylation of important biotech molecules: delivery aspects." Expert Opin Drug Deliv **5**(4): 371-383.

Ryan, S. M., X. Wang, et al. (2009). "Conjugation of salmon calcitonin to a combed-shaped end functionalized poly(poly(ethylene glycol) methyl ether methacrylate) yields a bioactive stable conjugate." J Control Release **135**(1): 51-59.

Saha, K., S. T. Kim, et al. (2013). "Surface functionality of nanoparticles determines cellular uptake mechanisms in mammalian cells." Small **9**(2): 300-305.

Sayers, C. T., G. Mantovani, et al. (2009). "Site-specific N-terminus conjugation of poly(mPEG(1100)) methacrylates to salmon calcitonin: synthesis and preliminary biological evaluation." Soft Matter **5**(16): 3038-3046.

Scales, C. W., A. J. Convertine, et al. (2006). "Fluorescent labeling of RAFT-generated poly(N-isopropylacrylamide) via a facile maleimide-thiol coupling reaction." Biomacromolecules **7**(5): 1389-1392.

Schlesinger, N., U. Yasothan, et al. (2011). "Pegloticase." Nat Rev Drug Discov **10**(1): 17-18.

Schreiber, S., M. Khaliq-Kareemi, et al. (2007). "Maintenance therapy with certolizumab pegol for Crohn's disease." N Engl J Med **357**(3): 239-250.

Sheth, S. R. and D. Leckband (1997). "Measurements of attractive forces between proteins and end-grafted poly(ethylene glycol) chains." Proceedings of the National Academy of Sciences of the United States of America **94**(16): 8399-8404.

Stewart, S., H. Jablonowski, et al. (1998). "Randomized comparative trial of pegylated liposomal doxorubicin versus bleomycin and vincristine in the treatment of AIDS-related Kaposi's sarcoma. International Pegylated Liposomal Doxorubicin Study Group." J Clin Oncol **16**(2): 683-691.

Tan, Y., X. Sun, et al. (1998). "Polyethylene glycol conjugation of recombinant methioninase for cancer therapy." Protein Expr Purif **12**(1): 45-52.

Tedja, R. S., A.H.; Whittaker, M.R.; Lim, M.; Marquis, C.; Boyer, C.; Davis, T.P.; Amala, R. (2012). "Effect of TiO2 nanoparticle surface functionalization on protein adsorption, cellular uptake and cytotoxicity: the attachment of PEG comb polymers using catalytic chain transfer and thiol–ene chemistry." Polymer Chemistry **3**: 2743-2751.

Torchilin, V. P. (2007). "Targeted pharmaceutical nanocarriers for cancer therapy and imaging." AAPS J **9**(2): E128-147.

Turecek, P. L., M. J. Bossard, et al. (2012). "BAX 855, a PEGylated rFVIII product with prolonged half-life. Development, functional and structural characterisation." Hamostaseologie **32 Suppl 1**: S29-38.

Venkataraman, S., W. L. Ong, et al. (2011). "The role of PEG architecture and molecular weight in the gene transfection performance of PEGylated poly(dimethylaminoethyl methacrylate) based cationic polymers." Biomaterials **32**(9): 2369-2378.

Veronese, F. M. (2001). "Peptide and protein PEGylation: a review of problems and solutions." Biomaterials **22**(5): 405-417.

Veronese, F. M. and G. Pasut (2005). "PEGylation, successful approach to drug delivery." Drug Discovery Today **10**(21): 1451-1458.

Vicent, M. J. and R. Duncan (2006). "Polymer conjugates: nanosized medicines for treating cancer." Trends Biotechnol **24**(1): 39-47.

Vira, S., E. Mekhedov, et al. (2010). "Fluorescent-labeled antibodies: Balancing functionality and degree of labeling." Anal Biochem **402**(2): 146-150.

Wang, Q. L., B. Liang, et al. (2011). "2-Deoxy-D-Glucose Treatment of Endothelial Cells Induces Autophagy by Reactive Oxygen Species-Mediated Activation of the AMP-Activated Protein Kinase." Plos One **6**(2).

Watson, P., A. T. Jones, et al. (2005). "Intracellular trafficking pathways and drug delivery: fluorescence imaging of living and fixed cells." Adv Drug Deliv Rev **57**(1): 43-61.

Werle, M. and A. Bernkop-Schnurch (2006). "Strategies to improve plasma half life time of peptide and protein drugs." Amino Acids **30**(4): 351-367.

Willcock, H. and R. K. O'reilly (2010). "End group removal and modification of RAFT polymers." Polymer Chemistry **1**(2): 149-157.

Woodburn, K. W., C. P. Holmes, et al. (2012). "Absorption, distribution, metabolism and excretion of peginesatide, a novel erythropoiesis-stimulating agent, in rats." Xenobiotica **42**(7): 660-670.

Yi, S. M. P., R. E. Harson, et al. (2001). "Lectin binding and endocytosis at the apical surface of human airway epithelia." Gene Therapy **8**(24): 1826-1832.

Yu, D., Y. Zhao, et al. (2004). "Cellular penetration and localization of polyethylene glycol." ACR Meeting Abstracts **45**.

Yunus, W. M. B. and A. B. Rahman (1988). "Refractive-Index of Solutions at High-Concentrations." Applied Optics **27**(16): 3341-3343.

Zhang, Y., N. Kohler, et al. (2002). "Surface modification of superparamagnetic magnetite nanoparticles and their intracellular uptake." Biomaterials **23**(7): 1553-1561.

APPENDICES

APPENDIX A

POLYMER CHARACTERIZATION

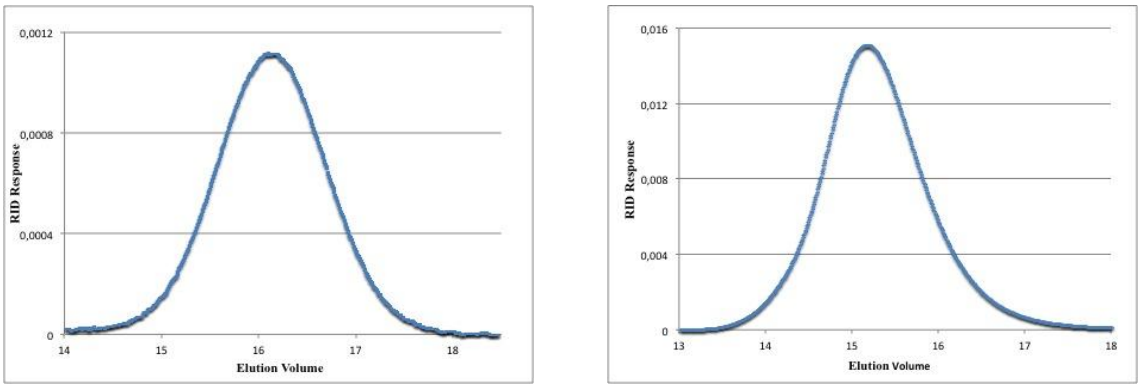

Figure A.1. GPC chromatograms of 10K and 20K p(PEG-MA) (a) Elugram of 10K p(PEG-MA) (Mn = 10 530 g/mol, PDI =1.11) b) Elugram of p(PEG-A) (Mn = 20 300 g/mol PDI = 1.176).

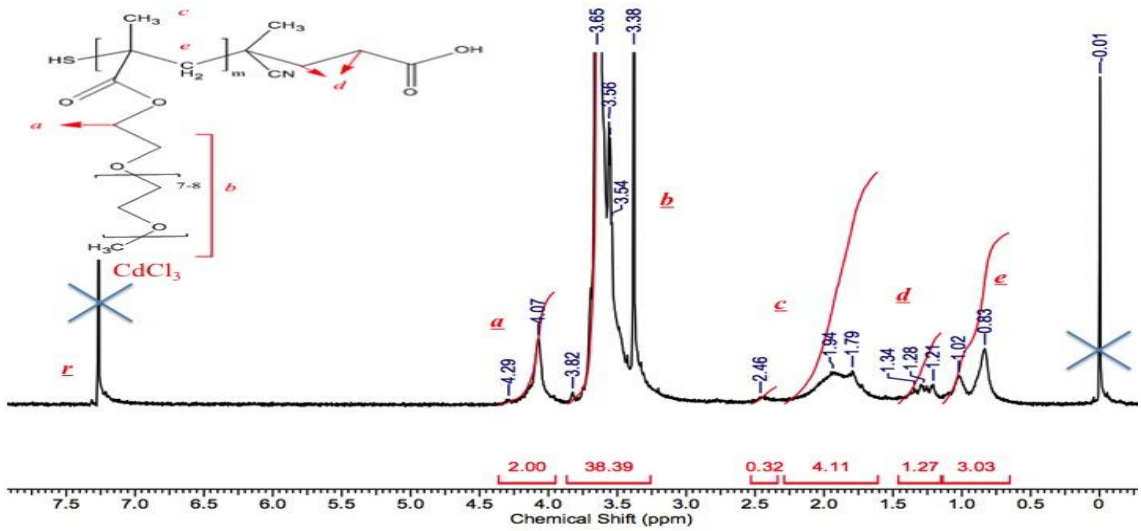

Figure A.2. ^{1}H-NMR spectrum of RAFT end-group removed comb-type 10K p(PEG-MA) polymers.

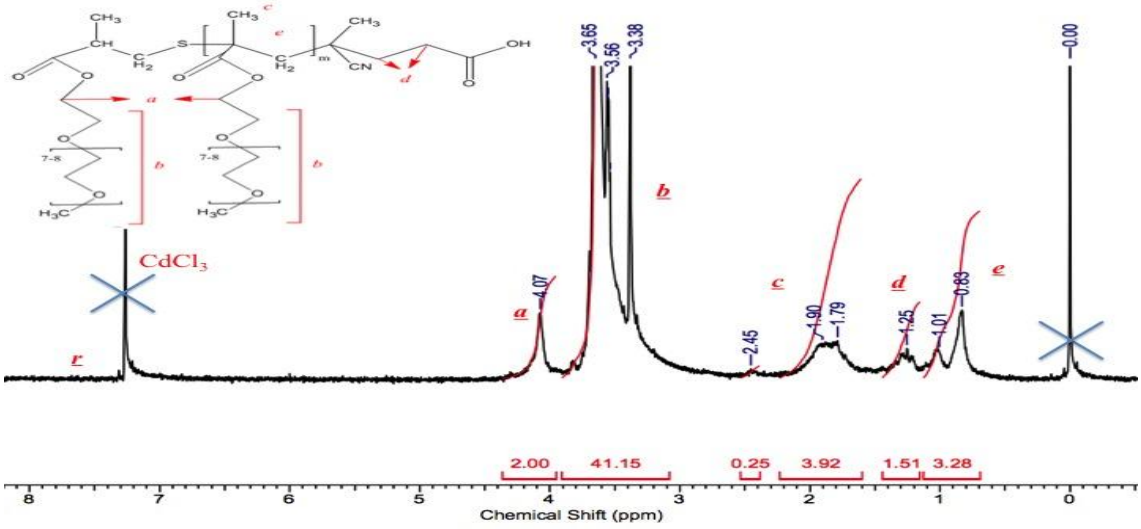

Figure A.3. [1]H-NMR spectrum of thiol-deactivated comb-type 10K p(PEG-MA) polymers.

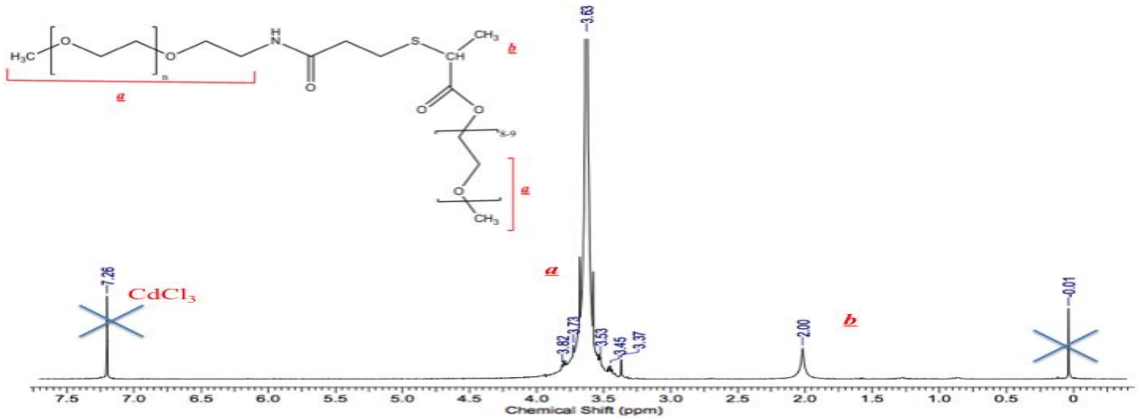

Figure A.4. [1]H-NMR spectrum of thiol-deactivated linear 10K p(PEG-MA) polymers.

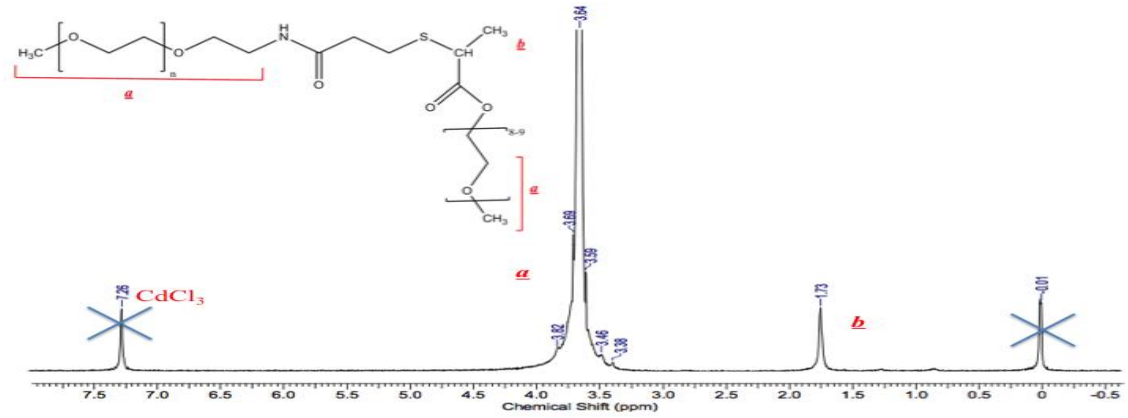

Figure A.5. [1]H-NMR spectrum of thiol-deactivated linear 20K p(PEG-MA) polymers.

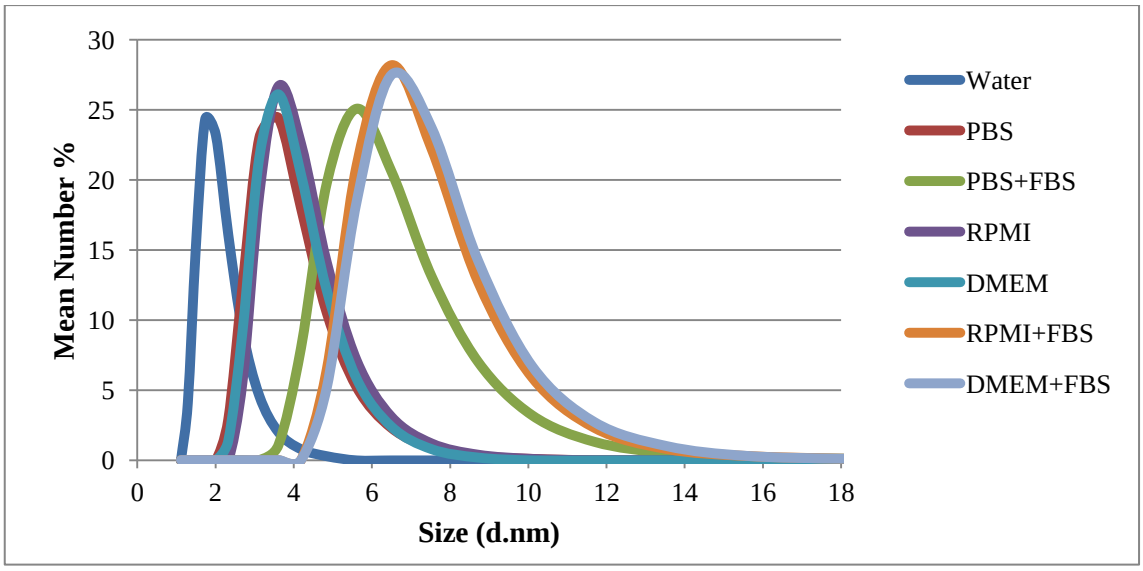

Figure A.6. Hydrodynamic diameter (D_h) of Comb 10K polymer obtained by DLS method in water, PBS, PBS containing 10% FBS, RPMI, DMEM, RPMI 1640 containing 10% FBS, and DMEM containing 10% FBS.

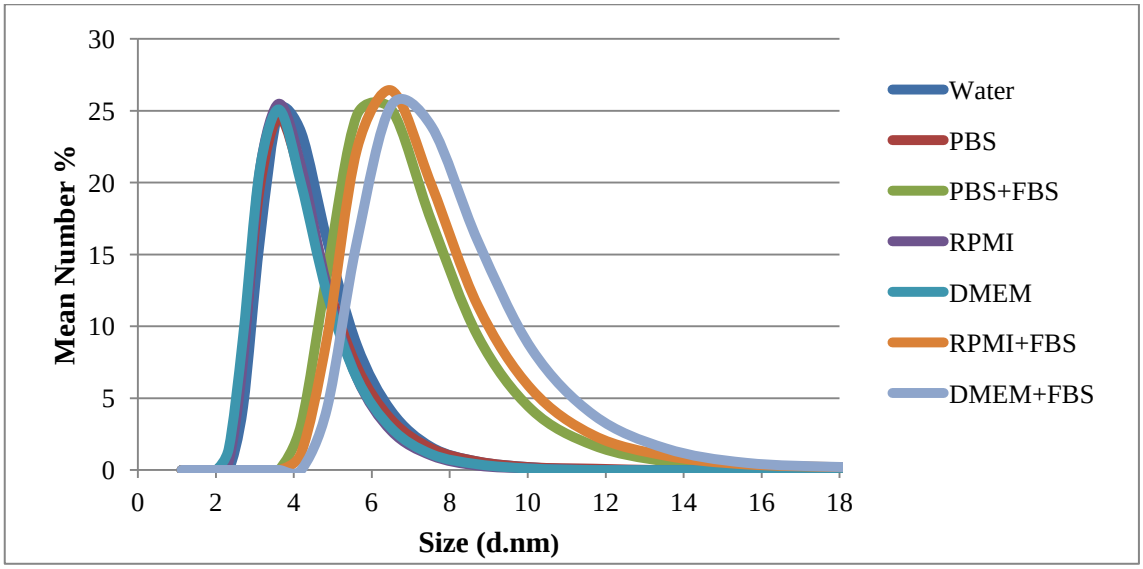

Figure A.7. Hydrodynamic diameter (D_h) of Comb 20K polymer obtained by DLS method in water, PBS, PBS containing 10% FBS, RPMI, DMEM, RPMI 1640 containing 10% FBS, and DMEM containing 10% FBS.

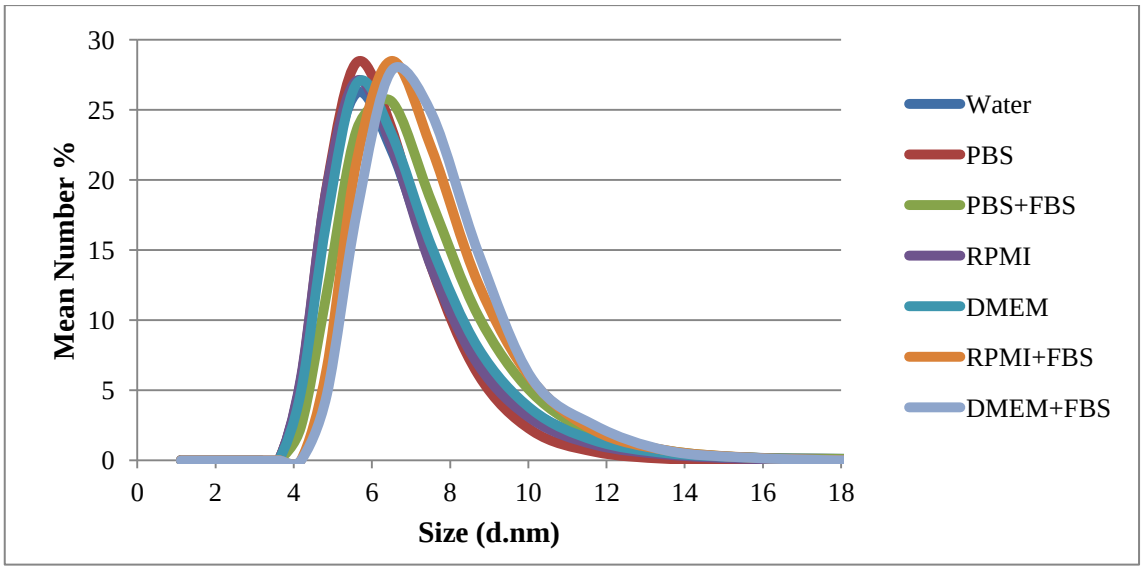

Figure A.8. Hydrodynamic diameter (D_h) of Linear 10K polymer obtained by DLS method in water, PBS, PBS containing 10% FBS, RPMI, DMEM, RPMI 1640 containing 10% FBS, and DMEM containing 10% FBS.

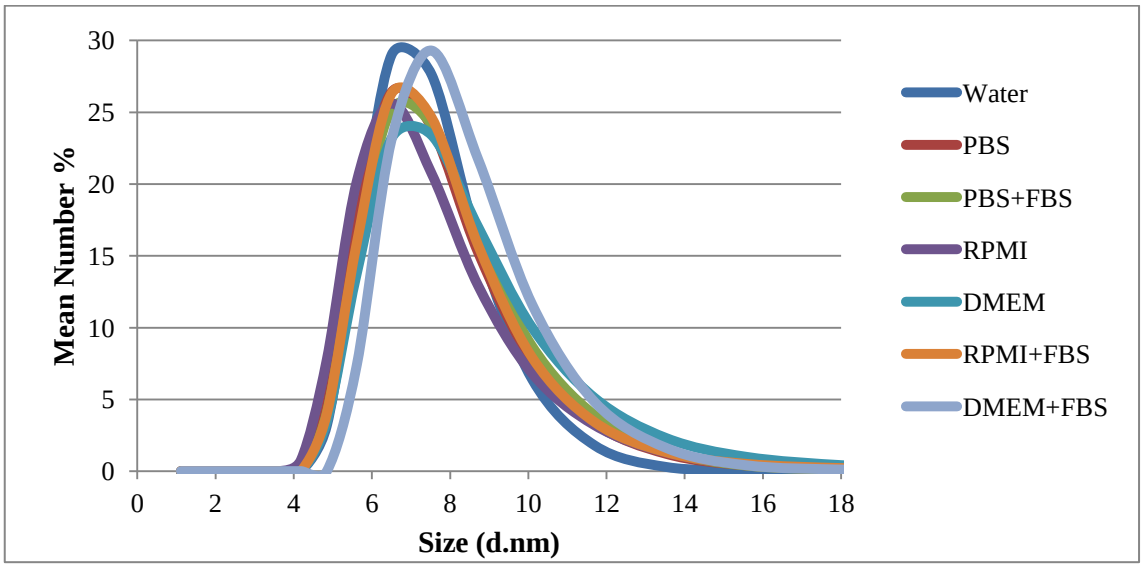

Figure A.9. Hydrodynamic diameter (D_h) of Linear 20K polymer obtained by DLS method in water, PBS, PBS containing 10% FBS, RPMI, DMEM, RPMI 1640 containing 10% FBS, and DMEM containing 10% FBS.

APPENDIX B

CELL VIABILITY AND MEMBRANE INTEGRITY ANALYSES

Table B.1. The percent cell viability results of A549 cell line after incubation with polymers for 24 hours.

Polymer	Control	25 µM	50 µM	100 µM	200 µM
Comb-type 10K	100 ± 3,1	99,4± 1,2	96,4± 2,40	94,5± 3,20	85,5± 3,2
Linear 10K	100± 3,1	99,7± 1,3	98,6± 1,30	94,5± 2,40	91,2± 2,1
Comb-type 20K	100± 3,1	99,1± 0,9	83,3± 10,4	84,5± 11,7	73,7± 9,8
Linear 20K	100± 3,1	83,8± 8,2	77,1± 8,70	77,2± 7,40	64,9± 7,6

Table B.2. The percent cell viability results of A549 cell line after incubation with polymers for 72 hours.

Polymer	Control	25 µM	50 µM	100 µM	200 µM
Comb-type 10K	100 ± 2,7	98,8± 4,50	93,2± 9,70	89,8± 9,30	74,8± 9,10
Linear 10K	100± 2,7	95,8± 7,10	93,1± 8,10	88,3± 8,90	73,5± 9,00
Comb-type 20K	100± 2,7	88,1± 11,2	74,4± 11,4	75,1± 12,1	56,9± 13,7
Linear 20K	100± 2,7	91,7± 14,3	78,0± 12,1	77,1± 13,6	59,4± 14,3

Table B.3. The percent cell viability results of BEAS-2B cell line after incubation with polymers for 24 hours.

Polymer	Control	25 µM	50 µM	100 µM	200 µM
Comb-type 10K	100 ± 4,2	91,5± 2,4	78,8± 5,40	94,5± 4,10	76,0± 4,60
Linear 10K	100± 4,2	89,6± 2,7	98,6± 6,20	91,1± 4,40	75,1± 5,10
Comb-type 20K	100± 4,2	90,0± 3,2	83,3± 6,10	77,2± 6,20	69,8± 6,70
Linear 20K	100± 4,2	91,3± 10,2	77,1± 11,2	66,5± 13,2	64,7± 13,6

Table B.4. The percent cell viability results of BEAS-2B cell line after incubation with polymers for 72 hours.

Polymer	Control	25 µM	50 µM	100 µM	200 µM
Comb-type 10K	100 ± 3,7	91,0± 6,40	84,1± 8,6	76,0± 8,10	74,4±7,90
Linear 10K	100± 3,7	96,1± 11,0	95,6± 9,4	96,6± 7,80	76,2± 10,2
Comb-type 20K	100± 3,7	85,6± 10,4	85,7± 9,8	76,3± 9,30	64,7± 10,7
Linear 20K	100± 3,7	86,2± 13,4	70,6± 9,9	62,2± 10,1	62,0±11,4

Table B.5. The percent % LDH release of A549 cell line after incubation with polymers for 24 hours.

Polymer	Control	25 µM	50 µM	100 µM	200 µM
Comb-type 10K	0 ± 0,08	0± 0,22	0± 0,31	0,25± 0,21	0,27± 0,19
Linear 10K	0± 0,08	0± 0,34	0± 0,37	0,30± 0,27	0,34± 0,23
Comb-type 20K	0± 0,08	0± 0,42	0± 0,45	0,13± 0,45	0,52± 0,61
Linear 20K	0± 0,08	0± 0,47	0± 0,49	0,64± 0,51	0,57± 0,59

Table B.6. The percent % LDH release of A549 cell line after incubation with polymers for 72 hours.

Polymer	Control	25 µM	50 µM	100 µM	200 µM
Comb-type 10K	0 ± 0,12	0± 0,47	0± 0,37	0,24± 0,41	0,54± 0,35
Linear 10K	0± 0,12	0± 0,64	0± 0,41	0,37± 0,46	0,78± 0,47
Comb-type 20K	0± 0,12	0± 1,23	0,63± 1,17	0,73± 1,02	2,52± 1,13
Linear 20K	0± 0,12	0± 0,89	0,77± 0,94	0,87± 0,83	1,87± 0,89

Table B.7. The percent % LDH release of BEAS-2B cell line after incubation with polymers for 24 hours.

Polymer	Control	25 µM	50 µM	100 µM	200 µM
Comb-type 10K	0 ± 0,11	0± 0,17	0± 0,19	0,23± 0,34	0,48± 0,22
Linear 10K	0± 0,11	0± 0,22	0± 0,27	0,26± 0,37	0,51± 0,26
Comb-type 20K	0± 0,11	0± 0,31	0± 0,39	0,34± 0,41	0,56± 0,35
Linear 20K	0± 0,11	0± 0,37	0± 0,44	0,41± 0,40	0,57± 0,37

Table B.8. The percent % LDH release of BEAS-2B cell line after incubation with polymers for 72 hours.

Polymer	**Control**	**25 µM**	**50 µM**	**100 µM**	**200 µM**
Comb-type 10K	0 ± 0,17	0± 0,19	0,12± 0,17	0,34± 0,29	0,53± 0,27
Linear 10K	0± 0,17	0± 0,27	0,17± 0,19	0,21± 0,31	0,62± 0,31
Comb-type 20K	0± 0,17	0± 0,31	0,24± 0,25	0,48± 0,32	0,69± 0,22
Linear 20K	0± 0,17	0± 0,64	0,41± 0,72	1,02± 0,71	1,39± 0,67

APPENDIX C

CELL UPTAKE ANALYSIS

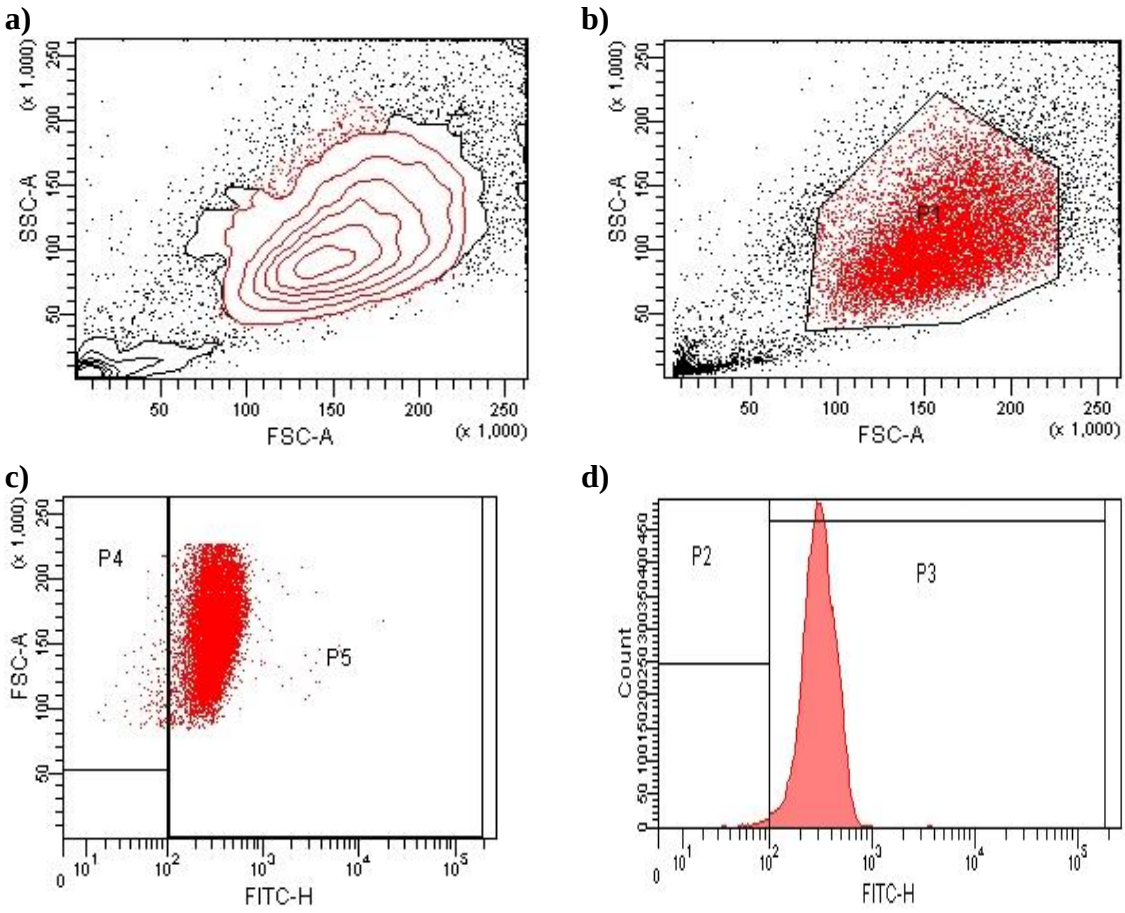

e)

Population	#Events	%Parent	FITC-H Mean	FITC-H SD
P1	10,514	75.7	324	238
P2	115	1.1	72	20
P3	10,399	98.9	326	238
P4	123	1.2	73	20
P5	10,362	98.6	327	238

g) $$\text{Cell Uptake (\%)} = \frac{\text{FITC-H mean}_{P3} * \text{Total Event}_{P3}}{\text{FITC-H mean}_{P1} * \text{Total Event}_{P1}} * 100$$

Figure C.1. Uptake of 25 μM comb-type 10K polymer by A549 cells after incubation for 3hours. a) Contour plot b) Scatter diagram c) Dot plot d) Histogram f) Statistical analyses g) Cell uptake equation.